Development of Condition Monitoring Method for Power Cables by Means of Partial Discharge and Water Tree Detections

（部分放電と水トリーの検出による電力ケーブルの状態モニタリング手法の開発）

July, 2019

Doctor of Philosophy (Engineering)

Nhet Ra
(ニアト ラ)

Toyohashi University of Technology

Abstract

Development of Condition Monitoring Method for Power Cables by Means of Partial Discharge and Water Tree Detections

（部分放電と水トリーの検出による電力ケーブルの状態モニタリング手法の開発）

Electric power transmission and distribution depends on a vast and expensive network of high and medium voltage cables for power delivery. To support the system operates properly with high reliability; thus, it is necessary to maintain the power cable in good condition. The reliability and availability of the power cable are determined by the conditions of its insulation system. Defects and degradations are known to be the major factors which give harm to the insulation power cable leading to failure. Defects are mainly created before an operation is started, and lead to the failure of the cable line in the early stage. Partial discharge (PD) measurement is useful to detect such defects and local breakdown. On the other hand, water tree is a degradation mode that takes place several tens of years after the operation has been started (aged). The cable may cause electric breakdown when a water tree grows and bridges the insulation, as it is significantly conductive. Diagnostic testing by means of water tree detection is often employed for preventive measurement.

In early stage (aged stage as well), PD measurement is very useful but conventional methods cannot afford to approach the discharge source although the cable is usually as long as several kilometers. In the wear-out stage, water tree is the most significant degradation mode. As the cable is practically long and water trees are not uniformly distributed along the length, the conventional diagnosing methods cannot afford to locate the degradation. Based on these backgrounds, two components of the studies were performed. First, we proposed a PD detection method that can easily approach the origin of the discharge by newly proposed capacitive coupling electrode. As the PD takes place spontaneously under commercial voltage, this detection is classified as a passive diagnosis. Second, water tree detection method that can locate the degradation by considering charge behavior accompanied by water tree. As the behavior takes place by applying several different waveforms of high voltage, this detection is classified as an active diagnosis.

For a newly developed PD detection method, we assumed that the outer shield is not a perfect conductor, the change in potential due to the current discharge and shield resistance would be seen as PD signal propagating through the cable. This will be more significant because of skin effect when higher frequency component is targeted. The change in potential along the shield electrode can be detected by the capacitive coupling between the foil electrode and shield electrode itself. In order to retain a ground potential, another identical cable was used as referent cable. In practice, a pair of cables in three phases can be taken as the object and reference. Basic experiment and numerical analysis were carried out by using a coaxial cable (RG58A/U). In this study, a mimic PD with the width of 20 ns was applied to the target cable line with 50 Ω characteristic impedance. The intensity of the calibration can be modified by adjusting the charging voltage. The change in potential along the cable line was

detected using a foil electrode made from aluminum. From the input of the mimic PD pulse signal, the detection point voltage signal appeared about 250 ns later.

A numerical simulation was performed in the same manner to measurement. As the pulse propagates, a displacement current is generated in the electric shielding layer, and the distribution of the voltage source appears. The detection signal is obtained by integrating the signals given to the output points by the respective voltage sources. This equivalent circuit is regarded as a lossless line, and the reflection of the signal is not considered. The experimental result and simulation result were compared, and it shows similar characteristics. In order to compare the sensitivity of this method, the same experiment was conducted on a mimic insulation joint. The detection intensity of the proposed method is almost 30 times lower than the conventional PD detection at the insulation joint, but the same intensity can be detected if an amplifier is installed during actual measurement on-site. Precise maintenance is needed as the cable gets old with time. Therefore, constant monitoring of PD is necessary. We decided to design and prototype an inexpensive PD monitoring instrument to monitor PD along the cable lines at all time, and the performance was satisfactory.

For the new water tree detection method, several different waveforms of high voltage were employed. A principle of this method is similar to the conventional residual charge method. In this method, the bias voltage is used for charge accumulation and depolarizing pulse voltage is used to release charge instead of AC voltage. If a pulse voltage is applied instead of the AC voltage in the residual charge method(conventional method), (1) a water-tree can be located based on the delay time of the residual charge signal from the pulse, and (2) By repeatedly applying the pulse and by averaging responses, the SN ratio can be improved. We named the method which measures the residual charge including information of the location by applying the pulse as "charge radar method" and we discussed the feasibility of this method.

In the active diagnosis measurement, a water-tree degraded cable with 5 m in length was inserted the 400-m-long communication coaxial cable in order to imitate a real cable line. Changing the location of the degraded section, we measured residual charge signals using the charge radar. Residual charge signals are observed at locations of degraded sections as time delay in every subtracted waveform. By integrating each residual charge signal, a few percents of the amount which is measured by the conventional method is calculated. Based on the proposed method, the degraded water-tree XLPE cable is detected.

The responses to high voltage pulse voltages were investigated in order to clarify the charge behavior with which the signal of newly proposed charge radar method is detected. The assessment of charge behavior under pulse voltages was studied by using a thin XLPE film sample contained water tree. Space charge measurement is performed by using Pulsed Electroacoustic method (PEA). A numerical simulation was also performed. Assuming the trapping and de-trapping process, the differences in pulse response were explained depending on the degree of water tree degradation. It was suggested that the degradation signal is based on the difference in a transient current through the water trees depending on the polarity of the bias pulse voltage applied prior to the pulse voltage.

Table of Contents

List of Figures

List of Tables

Chapter 1: Introduction

1.1 General Aspects

Electricity has become part of modern life and one cannot think of a world without it. It involves in almost every aspect of our day to day activities. It is used for working the home appliances such as lighting fans, television, air conditioner, washing machine, aroma lamp, etc. All of these provide comfort for human. In the industrial sector, including clothing factory foods factory, vehicle factory, etc. more machines are employed to help the human work. These machines are run with the help of electricity. These help to increase the production capacity as well as saving time and money.

Currently, transportation, communication, entertainment, and other equipment are worked by electricity. The conventional transportations such as electric train, cars, and some others have been and are being modernized by utilizing electricity. These modern means of transportations help to reduce the usage of fuel consumption, which is expected to run out shortly. Also, modern equipment such as computer, telephone, radio and more are operated by electricity.

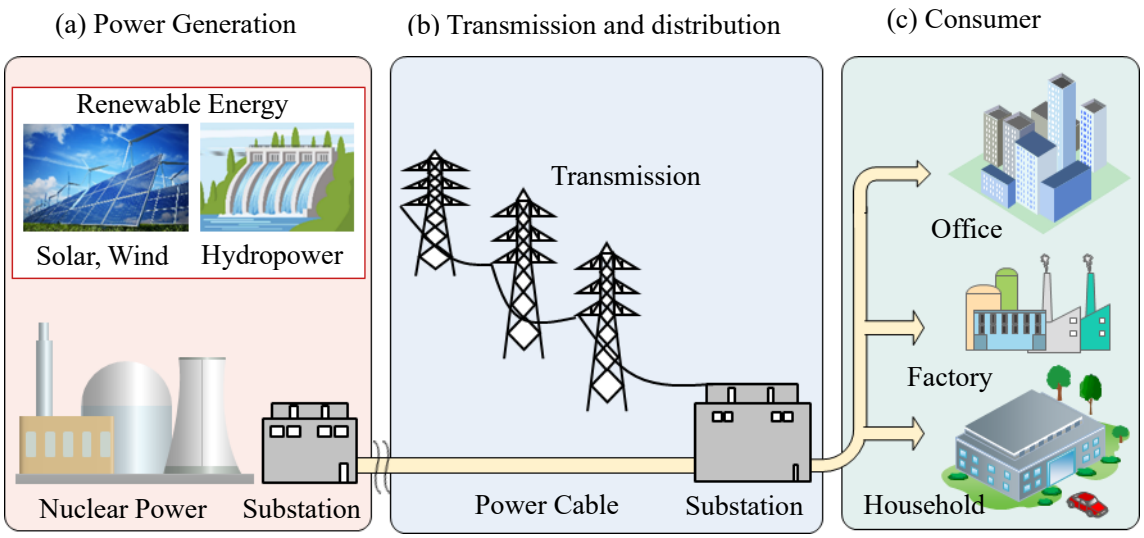

Fig. 1.1 Illustration of an electric power system (a) power generation (b) power transmission and distribution (c) customer.

As the demands for electricity keep increasing steadily in anywhere in the world, the need for more sources of electrical energy is required. Electricity generated by thermal, nuclear, hydropower, and other types of power plants is transmitted through overhead transmission and underground cables to

the urban area where the demand for electricity is very high. Fig. 1.1 illustrates the components of the electric power system: (a) power generation, (b) transmission and distribution, and (c) consumers.

During the intervening of 100 years, the major sources of the electricity generation are coal, nuclear, hydroelectric power plant. According to the recent review on sources of electricity generation made by the BP in June 2018 [1] shows that 38.1 % of electricity generation comes from the coal power plant, 23.2 % from oil, 10.3 % from nuclear, 3.5 % from gas and others 24.3 % come from the renewable energy such biomass, geothermal, solar, wind, and hydroelectric power plant (see Fig. 1.2). Japan, in particular, shows a lots interest in using renewable energy after the disastrous nuclear reactor accident leading which still give an effect until these days. A data collected between the year 2010 to 2015 made by Japan. For Sustainability (JFS) [2] shows that the percentage of electricity generated from the nuclear power plant in Japan has decreased significantly, and this lost capacity in electricity generation is replaced by the renewable energy such as hydroelectric power plant, solar power etc. Likewise, the world also shows an interest in renewable energy due to the concern in global warming. The world's largest hydropower electric power station was built in Three Gorges Dam, China, with the capacity of 22,500 MW and the second highest is located in Brazil/Paraguay with the capacity of 14,000 MW [3]. The world largest solar park is being installed in Karnataka, India, with the expected capacity of 2,000 MW [4].

For transmitting the vast amount of electric energy, the high voltage transmission system is necessary. In 1989, the 1200 kV AC transmission line was commercially operated on the line connecting Russia and Kazakhstan [5]. Unfortunately, the line was taken out of operation after the collapse of the Soviet Union. China is now operating the highest transmission voltage at 1000 kV [6][7].

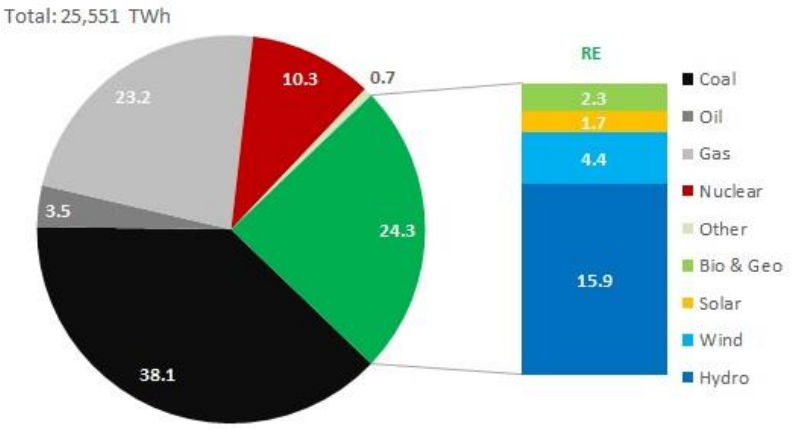

Fig. 1.2 BP, Statistical Review of World Energy 2018 [1].

1.2 Cable Maintenance Issues

Maintenance for power equipment is a significant issue in both economically developed and developing countries. In an economically developed country, a vast amount of equipment is being aged and facing the end of the lifetime (see Fig. 1.3). For economical reason, it is not advantageous to replace all the equipment at the same time. Therefore, power companies are looking for an excellent diagnosing technique to classify the degree of degradation in order to determine the priority of replacement. The diagnosis should be as precise as possible to avoid both unexpected failure and unnecessary replacement. In addition, the diagnosis has a price; it should be performed with a much lower cost than the maintenance cost reduction brought by avoidance of the unexpected failure and unnecessary replacement. In a rapidly developing country, a large amount of power equipment is being newly installed with low costs. In order to retain the reliability of such systems, reduction of initial failure (see Fig. 1.3) due to poor quality control and installation is strongly recommended. Diagnosing technique is thus highly appreciated in this point of view as well.

Among all types of power equipment, the power cable is one of the most important to be diagnosed because it spreads along a long distance. Once the failure happens, it takes a long time to locate and replace. Therefore, diagnosing techniques that can be performed with high precision, low cost, and short time is highly required. Especially, the technique that can approach or locate the defect and/or degradation must be very advantageous for the maintenance of cables.

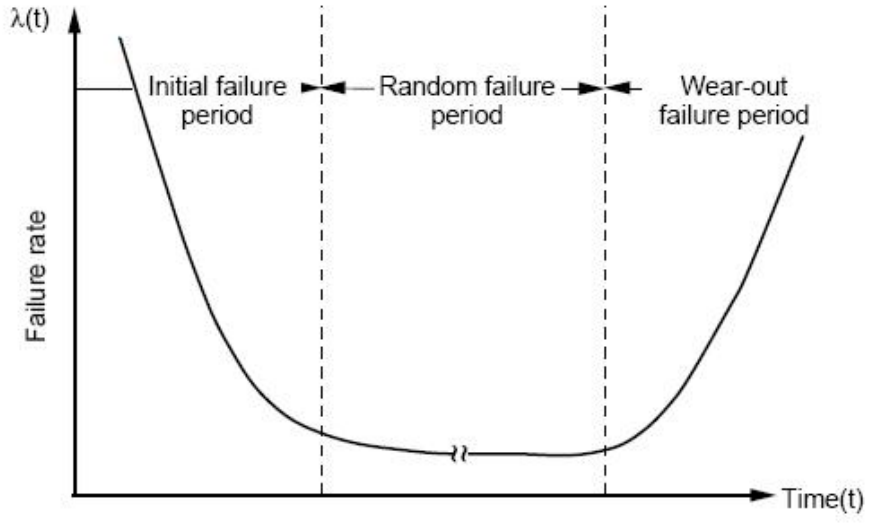

Fig. 1.3 Failure rate of power equipment over time (classical bathtub curve) [8].

Power cable is designed to be able to perform and function for a variety of different system operating conditions including temperature changes, electrical and mechanical stress, wet environment, and others. Although the power cable is fulfilling all the manufacturing test before its installation and used, it may not maintain the same operating characteristics during the many expected years of services. There may be built-in manufacturing imperfections and/or workmanship errors that were not detected during the commissioning test. Furthermore, as in any system, the insulation will experience aging, and eventually, the degradation that could decrease the insulation performance of insulation system. All these could cause premature and unexpected failures; thus, affecting the reliability and maintenance costs. These defects and degradation need to be detected in order to avoid as much as possible unexpected cable failures and the associated customer outages.

1.3 Motivation and Research Objective

This research will be focused on the development of condition monitoring method for newly installed and aged power cables. For newly installed cables, the quality control by means of partial discharge measurement is commonly used. However, the conventional partial discharge detection method cannot afford to approach the discharge location as the cable is practically long, and the partial discharge signal is strongly attenuated before being captured. For aged cables, water is one of the most significant degradation modes that take place several tens of years after the operational has been started. Thus, diagnosing measurement by means of water tree detection is useful for aged cable. As the cable spread in long-distance and the water trees are not uniformly distributed along the length, the conventional diagnosing methods cannot afford to locate the degradation part precisely. Based on these backgrounds, the following components of studies will be performed:

(1) We aim to develop a partial discharge detection method that can easily approach the origin of the discharge by newly proposed capacitive coupling electrode between the foil electrode and the cable shield electrode itself. As the partial discharge takes place spontaneously under commercial voltage, this detection will be classified as a passive diagnosis.

    After, the improvement of sensitivity and its validation of the new partial discharge detection method will be analyzed. We propose to evaluate our newly developed method based on the existing partial discharge detection method under differential installation condition conditions. Also, we propose to fabricate a simple partial discharge monitoring device and also the sensitivity evaluation of this monitoring device.

(2) We also target to fabricate a measurement method that can locate the degradation by considering charge behavior accompanied by water tree degradation. As the behavior takes place by applying several different waveforms of high voltage, this detection will be classified as an active diagnosis.

The mechanism of the residual charge related to water-tree of an XLPE film sample contained water tree will be investigated by using Pulsed ElectroAcoustic (PEA) method. Also, the numerical simulation will be demonstrated using multi-layers dielectric model. Assuming the trapping and de-trapping process, the differences in pulse response will be explained depending on the degree of water tree degradation.

(3) Lastly, we aim to discuss the improvements and extended applications to cable maintenance technique, namely the application of partial discharge measurement technique and also the diagnosis method for water tree aging XLPE cable.

1.4 Contribution of This Work

In industrialized countries, maintenance for power cables installed long time ago is becoming a significant problem to sustain the infrastructure. In developing countries, on the other hand, a vast of cable networks are being installed at a low cost due to their rapid economic development. Such cables may include initial defects and may be aged very rapidly. In both types of countries, therefore, maintenance technology is very essential. The proposed methods are highly specified to approach the origin of the defects or degradation. As the power cable is usually very long, these methods are believed to significantly improve the reliability of diagnosis.

1.5 Scope and Limitation of the study

When the partial discharge occurs in the power cable, it will produce current pulse propagated through the cable line. In practice, the partial discharge pulse is not periodically produced making it difficult for frequency measurement. For water tree detection method, high voltage pulse voltages will be employed. To produce such a high voltage equipment for frequency measurement is difficult and expensive. Based on this background, this study is limited to the time domain measurement for both partial discharge and water tree detection methods.

1.6 Summary

This study gives the failure causes and their diagnostic measurement for power cable, especially for crosslinked polyethylene (XLPE) cables. The aims of this research to develop the new diagnostic methods for condition monitoring method for power cable by means of partial discharge and water tree detection. Also, the critical assessment related to the detection sensitivity and the release mechanism of the residual charge is explained. This thesis is organized into 5 chapters. A brief description of each chapter is as follow:

Chapter 1 outlines the general introduction of this study. This chapter gives the significances of the maintenance for the power system, especially for the power cables. Also, the motivation and research objective of this study, as well as the contribution of this research work are provided in this chapter. The summary of each chapter is outlined in the last part of this chapter.

Chapter 2 provides the details on the current issues related to the failure causes and their diagnosis methods. The failure causes, including defects and degradations are outlined in this chapter. After, this chapter gives the literature review on the existing diagnosis methods that are commonly used for the insulation assessment of the power cables. Finally, the limitation and disadvantages of the existing diagnostic methods will be covered in this chapter.

Chapter 3 provides the details of the newly developed diagnostic method for the partial discharge detection of a long-distance cable by using a capacitive coupling method. The theoretical background, such as the generation, propagation, and detection of the partial discharge signal is provided in this chapter. After, the experiments of a communication and full-sized 6.6 kV XLPE cables are performed using mimic partial discharge. Also, the numerical simulations of partial discharge pulse propagation through the cable are performed in the same manner to the actual measurement systems by considering the skin effect of the cables shield resistance. After the detection sensitivity of the proposed method is evaluated using partial discharge measurement under differential installation conditions. Finally, the detail of a simple partial discharge monitoring device is given.

Chapter 4 gives the details of the proposed diagnostic method for water tree detection of degraded XLPE cables using bias and pulse voltages. The measurement principle and procedure of the proposed method are described in this chapter. After, the experiment using communication containing water tree degradation is performed. This chapter also provides an assessment on charge behavior of a thin XLPE film sample that contains water tree by using Pulsed ElectroAcoustic (PEA) method. Also, a numerical simulation is demonstrated using multi-layers dielectric model. Finally, a conclusion on the release mechanism of the residual charge is provided.

Chapter 5 discusses the improvement, and extended applications to cable maintenance techniques, namely the application of the partial discharge measurement technique and also the diagnostic method for water tree aged XLPE cables are discussed. Finally, the conclusion of this research work, including the evaluation of the proposed diagnostic methods and the proposed future works are provided.

References

[1] BP, '*Statistical Review of World Energy*', Jun 2018.

[2] Japan for Sustainability, "Current Status of Renewable Energy in Japan," *JFS Newsletter* No.176, 2017.
[Online]. Available: https://www.japanfs.org/en/news/archives/news_id035824.html.
[Accessed: Apr. 27, 2019].

[3] Water.usgs.gov, 'Three Gorges Dam: The world's largest hydroelectric plant', Dec, 2016 [Online]. Available: https://www.usgs.gov/special-topic/water-science-school/science/three-gorges-dam-worlds-largest-hydroelectric-plant?qt-science_center_objects=0#qt-science_center_objects.
[Accessed: Apr. 27, 2019].

[4] Economictimes.indiatimes.com, World's largest solar park launched in Karnataka', Mar, 2018 [Online].Available: https://m.economictimes.com/industry/energy/power/worlds-largest-solar-park-launched-in-karnataka/articleshow/63130074.cms [Accessed: Apr. 27, 2019].

[5] W. A. Mittelstadt, 'Round table on UHV technology in the USSR', *IEEE Power Engineering Review*, Vol. 11, No. 2, pp.9-14, Feb 1991.

[6] F. Kiessling, P. Nefzger, J. F. Nolasco, U. Kaintzyk, 'Overhead Power Lines Planning Design Construction,', *Springer Verlag*, 2003.

[7] H.T. Kennedy, China, India, and SE Asia to spend billions constructing, upgrading transmission systems, *Power Engineering International*, Jul 2009.

[8] G. A. Klutke, P. C. Kiessler, M. A. Wortman, "A critical look at the bathtub curve", *IEEE Trans. Rel.*, Vol. 52, No. 1, pp. 125-129, Mar 2003.

Chapter 2: Literature Review

2.1 Introduction

Power system depends on a vast and expensive power cable networks. Some of these cable networks are relatively new and are in the early year of their in-service life. And, some population of this cable network were installed long time ago and are approaching or even past their designed lifetime. For the newly installed cable networks, the failure may occur due to the presence of extrinsic defects such as contaminants, protrusions, and voids. These defects may create during cable manufacturing and poor cable installation technology. The existences of these defects may increase the local electrical stress, which in turn may lead to the breakdown due to the partial discharge. In contrast, some of the cable population that were installed several tens of years ago are rather old enough to show possible degradations. The degradation may take place when the cables are installed in the wet environment without water impervious outer sheath. Also, their insulation systems and their accessories are subjected to different kind of stresses such as electrical, thermal, and chemical during their service life, which may also result in degradation. These may decrease the insulation performances and eventually lead to the insulation breakdown as well.

Preventive measurements are often carried for reliability reasons. A lot of research activities and publications are directed toward the understanding of these defects and degradations. Also, the establishment of the remaining life estimation techniques is given. These commissioning and diagnostic testing can help the system from expected failures and also unnecessary replacement.

This chapter gives a literature survey related to the power cable including the structures, insulation material, and also its electrical properties. After, the details of the failure causes, which harm and reduce the dielectric performance of the insulation power cable will be described in this chapter. At the end of this chapter, the existing diagnostic methods and also the critical assessment of their performances will be also covered in this chapter.

2.2 Power Cable and Its Accessories

The definition described in [1] refers to a long current-carrying device that carries their insulation and presents an earthed on the outer surface. In this context, an overhead line, for example, are not considered as cables. Power cables are commonly used for the underground or underwater (submarine) transmission and distribution of electrical power from the power station to the urban area where the demand is high. For the underground transmission and distribution, cables are usually installed using the underground tunnel or directly buried above the ground surface, while the submarine cable lines are installed under seawater. As the distance between the electrical source to the island is practically long, DC transmission is usually adopted.

Power cables are also being used as an overhead distribution network to supplement the underground network, or, in some case, they can form the whole backbone. The overhead covered conductors allow smaller phase clearance between the conductors on medium voltage lines. For example, objects such as tree branches may touch the lines without tripping or customer outage. In the following sections, we will outline the structures, insulation materials, and the accessories of power cables.

2.2.1 Structures

Basically, power cables have a coaxial structure and spread in a long distance. Power cables used for the distribution and transmission system mainly consist of conductors stranded from high conductivity metals, such as copper or aluminum that are insulated with fluid impregnated Kraft paper tapes or polymer-based materials that are extruded around central conductors.

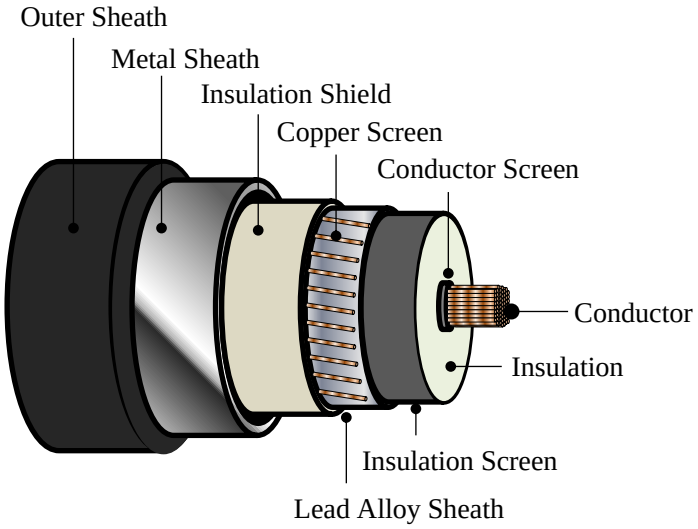

Fig. 2.1 A cut-away section of a polymer insulated power cables.

They are typically designed with following significant components such as conductor, conductor screen, insulation, insulation screen, copper screen, lead alloy sheath, metal sheath, outer sheath (Fig. 2.1). These layers have different functions and purposes [2]. The interface between the metal conductor and the polymeric insulation may include protrusion and voids; feature that would lead to the electric field concentration and premature failure. To overcome this, a conductor screen or otherwise known as polymer semicon, a conductive polymeric composite, is placed at both interfaces. The inner semicon, the insulation, and the outer semicon are coextruded to ensure the interfaces are smooth and contaminated free. Surrounding this cable are layers to protect the cable during installation/operation and carry the loss/fault currents. These layers also serve to keep out water that may lead to water trees.

2.2.2 XLPE Insulation

2.2.2.1 Molecular Structure

Over the past years, the prominent products developed for power cables were paper insulations filled with oil, or mass impregnated paper [3]. The insulation for these types cable is made of the paper oil-paper, which consists of thin paper strips impregnated with dielectric oil lapped around the inner conductor. This particular type of cable is still manufactured today due to the ability for quick voltage reversals (in DC application) and high reliability. These properties make them suitable for the high voltage DC (HVDC) application. At the present time, polymeric insulation; especially, crosslinked polyethylene (XLPE) has become the most prominent product developed for insulation power cables throughout the world. All new installations and replacement of old cables are performed using XLPE cables. Taking Japan as an example, over 90 % of all cables installed by 1991 were XLPE insulated cables [4].

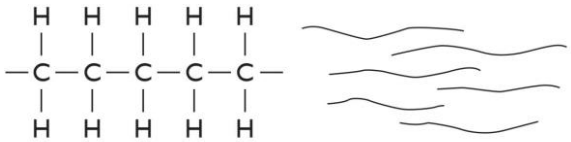

(a) Molecular structure of polyethylene

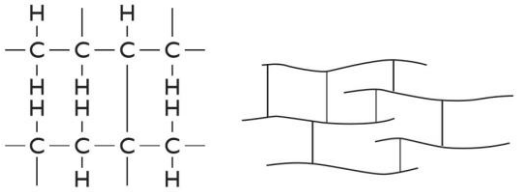

(b) Molecular structure of XLPE

Fig. 2.2 Schematic representation of the molecular structure of (a) polyethylene (b) XLPE [6].

XLPE is a thermoset material produced by the compounding of low-density polyethylene (LDPE) with a cross-linking agent such as dicumyl peroxide. (Fig. 2.2). This particular type of insulation was developed and introduced by the General Electric Research Laboratory which located in Niskayuna, New York in 1963 [5]. During the cable manufacturing process, polyethylene mixed with activation chemical agent dicmyl peroxide is pressed onto the conductor forming the inner conductor screen, and the primary insulation and outer semiconductive layers are extruded at the same time. Under the application of high temperature and high pressure, the long chain of polyethylene molecules "crosslinked" is linked with one another which in turn cause the material to change from a thermoplastic to an elastic material, but with better mechanical properties, particularly at high temperatures.

2.2.2.2 Electrical Properties

In its thermoplastic state, PE is a semicrystalline polymer that has a good electrical property (low dielectric constant, low dielectric loss, and high breakdown strength) together with other desirable properties such as mechanical toughness and flexibility, good resistance to chemicals, easy processing, and low cost (Fig. 2.3). Despite having a good electrical property, it has a drawback of its low melting temperature. This restricts the maximum operating temperature to 75°C. Consequently, it cannot match the temperature rating of paper-oil insulated cables [3][4]. To improve this property, PE is crosslinked so that the maximum operating temperature can be improved.

Crosslinking increases the maximum operating temperature to 90°C (see Table 2.1), the emergency temperature to 130 °C, and short-circuit maximum temperature to 250 °C. Crosslinked also increases impact strength, dimensional stability, tensile strength, thermal properties, chemical resistance, and it improves electrical properties (see Table 2.1). XLPE has excellent dielectric properties, making it useful for an extensive range of voltage applications from 600 V to 500 kV.

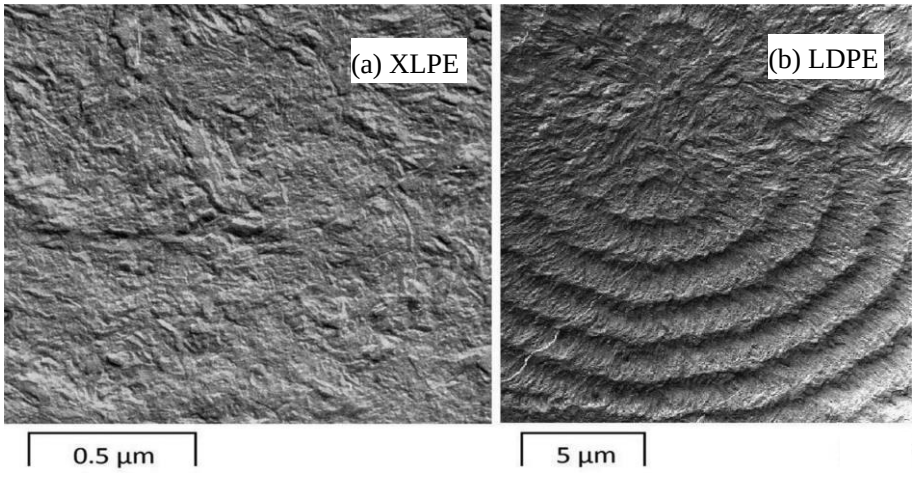

Fig. 2.3 Photograph of insulation by microscope of (a) XLPE and (b) LDPE [7].

Table 2.1 Comparison of typical properties of insulation materials [3].

Insulation materials	Dielectric constant	Tangent delta
Kraft paper	3.6	0.0030
XLPE	2.3	0.0010
WTR-XLPEs	2.4	0.0004
EPR	3.2	0.0080
PPLP (at 90°C)	2.7	0.0008

2.2.3 Cable Accessories

Cable accessories, including joints and termination are as important as the cable. These accessories are used to connect the cables together and into other electrical equipment. The research and development (R&D) of the cable accessories have been well established in a relatively short period of time thanks to the recent progress in technology development that provides components to make the task of joints and terminations of cable much easier safer, and faster.

Basically, there are two different types of accessories, joints, and terminations. Joints (splices) are used to connect the cables together. The main purpose of a joint is to preserve the cable structure at a point where cables are connected to each other. Terminations are needed to connect cables into other electrical equipment. The primary purpose of termination is to prevent harmful electric field concentrations at the end of a cable. In this section, the details of joints and terminations are discussed.

2.2.3.1 Cable Joints

The primary function of cable joints is to provide electrical and mechanical connections between power cable sections. As the processes of jointing usually take place in the adverse environment, the defects may be created leading to the failure. Thus, this task needs to be done with great care to ensure the reliable operation of a joint during its lifetime. Joints are usually made from materials of the same kind as cables. Fig. 2.4 shows a typical single-phase joint and its main parts. Generally, joint composes of connector that connects the conductors together and carries current, a conductive electrode layer on top of the conductor that forms a smooth interface between the insulation and the connector, insulation layer, a semiconductive insulation screen that is a connected into the insulation screens of the cables and necessary shielding and jacketing layers.

Fig. 2.4 Single-phase of premolded joint [8].

2.2.3.2 Cable Terminations

Cable terminations are required when connecting the insulation shielded power cables to uninsulated conductors such as a busbar or uninsulated overhead lines (Fig. 2.5). When a shielded power cable is cut or terminated, there is a very high concentration of electric field at this point which is considered to be one of the most problematic points. Thus, terminations must contain a method of controlling this high stress (stress-cone or stress-grading materials), an outer non-tracking surface, and means of providing an environmental seal to prevent moisture ingress [4].

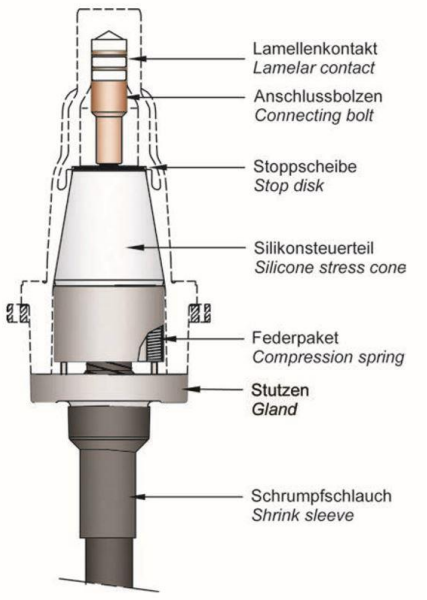

Fig. 2.5 shows the typical structure of cable for GIS termination (stress cone) [9].

2.3 Causes of Failures and Their Mechanisms

Although XLPE insulation has proven to be the most reliable developed for power cable insulation, failures may still occur due to many reasons (see Fig. 2.6). These failures are mainly caused the third-party damage, ageing, quality, installation, and unknown reasons. Some of these failure causes are instantly disrupted the operation of power and some others progressive reduce the dielectric performance of the insulation during its in-service life.

A review of recent research towards the life cycle management of power cable made by Chengke Zhou et al. of Glasgow Caledonian University, UK, shows the various causes, which lead to the failure of power cable [10]. Fig. 2.6 shows the failure data between 2009 and 2011, and failure data collected from different provinces in 2013, China. These data indicate the causes related to MV, rated at 10 and 20 kV distribution cables (Fig. 2.6a) and HV, rated at 35, 110 and 220 kV transmission cables (Fig. 2.6b) in China. The third-party damage is known to be the major cause which leads to cable failure (58.21%). This sort of failure may cause by human activity such as construction, and natural disaster. After, the poor installation technology also accounts for the failure of the power cable. Cable accessories, including joints and terminations, need to be installed in the field and connected to the body of the cable. Poor installation usually results in early failures in cable accessories.

Poor manufacture of cable body or accessories has also been found to be a reason for failure, due to deficiencies in pre-qualification tests and type tests in previous years. Ageing factors, i.e., thermal, electrical, mechanical and environmental stresses, can act singly or synergistically on cable insulation defects. The applied stresses and factors of influence, such as partial discharge and water trees, which affect insulation ageing can be summarized (Table 2.2).

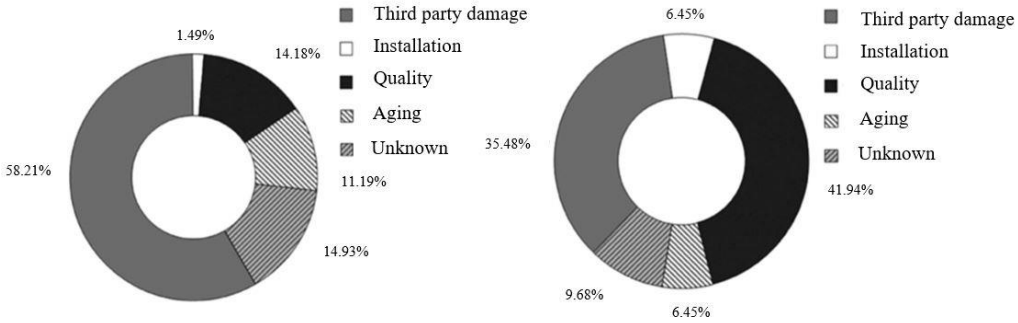

(a) (b)

Fig. 2.6 Failure data and a breakdown of failure causes (a) composition of MV cable failures, (b) composition of HV cable failures [10].

Table 2.2 Summary of aging mechanisms in cables [10].

Ageing Factor		Ageing Mechanism
Thermal	High temperature Temperature cycling	Chemical reaction Thermal expansion Diffusion Insulation melting Anneal locked-in mechanical stresses
	Low temperature	Cracking Thermal contraction
Electrical	Voltage, AC, DC, Impulse	Partial Discharges Electrical trees Water trees Charge injection Intrinsic breakdown Dielectric losses and capacitance
	Current	Overheating
Mechanical	Cyclic bending, vibration, fatigue, tensile, compressive, shear stresses	Yielding of materials Cracking Rupture
Environmental	Water, humidity Contamination Liquids, gases	Electrical tracking Water treeing Corrosion Dielectric losses and capacitance
	Radiation	Chemical reaction rate increase

2.3.1 Partial Discharge Degradation

Partial discharge (PDs) is known for many to be one of the major problems which substantially reduces the insulation lifetime of most high voltage plant if left undiscovered/unchecked [11][12][13]. Partial discharge may result from the discharge in the cavities developed inside the insulation, tracking discharge along with the interface, or discharge from the degradation mode such as electrical tree or water tree growth (Fig. 2.7).

Extrinsic defects including amber, foreign substance may be created during the process of cable manufacturing [14][15]. The presences of these defects may increase the local electrical stress, which in turn may lead to local electrical breakdown. It leads to the partial discharge in the cavities developed in the insulation that has been created by the local breakdown. Voids are a local cavity that may be created in the cable accessories including joints and terminations due to adverse installation conditions and/or poor workmanship [16][17][18]. This may also increase the local electrical stress in the insulation which in turn may lead to the local breakdown as well. These defects are mainly created before the operation is started, and lead to a failure of the cable line in the early stage. They are called as initial risks. After the cable has been used for long time delamination of the insulation may take place, which in turn may increase the electrical electric field and may lead to the tracking discharge along the surface [19]. Besides, the discharge may result from the degradation mode such as an electrical tree or water tree growth which in turn may apply stresses and factors influences insulation degradation and eventually lead to the partial discharge as well [20][21].

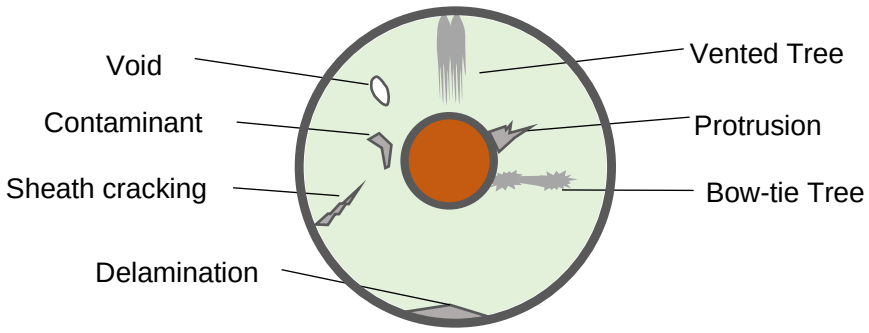

Fig. 2.7 Typical causes of cable failure.

2.3.1.1 Breakdown Mechanism

As previously mentioned, the presence of extrinsic defects including void, contaminants, and protrusions developed inside the insulation during the cable manufacturing and jointing. These microcavities may increase the local electrical field within the solid insulation material (see Fig. 2.8). Microcavity, a local gas-filled void in solid insulation material, has relatively lower electrical

permittivity and breakdown strength compared to the rest of solid insulation. This leads to local electrical field enhancement that may exceed the intrinsic field strength resulting in the ignition of self-sustaining electron avalanches [22]. Consequently, partial discharges may initiate in these microcavities at higher voltage stresses. The presence of these small partial discharges together with the combination of the chemical, mechanical thermal and radiative process may degrade the insulation material and eventually result in insulation failure.

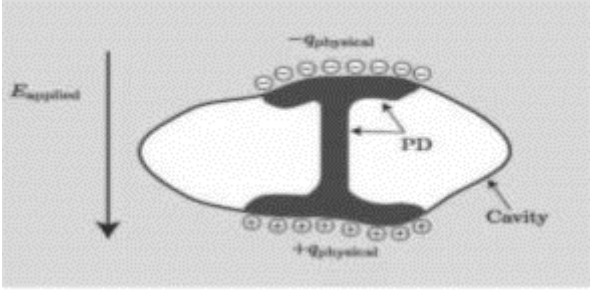

Fig. 2.8 Schematic diagram of partial discharge inside a cavity [22].

2.3.1.2 Classification of Partial Discharge Sources

Basically, partial discharge can be distinguished into three types; internal discharge, surface discharge, and corona discharge (see Fig. 2.9) [23]. The details of each type are as follow:

- Internal discharge: Internal discharges can occur in cavities that are present in solid insulation. They are also formed by the electrical treeing process that wears out a cavity in the insulation. There can be made a distinction between cavities that are electrode bounded or totally enclosed by insulation material.
- Surface discharge: Surface discharges are streamer discharges that could initiate at a high tangential field strength along with interface. When partial discharges are detected near their inception voltage, it shows no difference between surface and internal partial discharge. In case the voltage applied is raised, the discharge occurs along a longer surface. Thereby the surface discharge increases in length and magnitude. In this way, surface discharge is easy to distinguish from internal discharges.
- Corona discharge: Corona occurs around sharp points in a high electric field. During partial discharge measurement in cables, sharp edges at the end terminations can cause corona and could be covered with metallic round caps to bring the surrounding of the sharp point at equal potential. Corona can mask the detection of other discharges during partial discharge measurement. There are two types of corona: positive and negative corona.

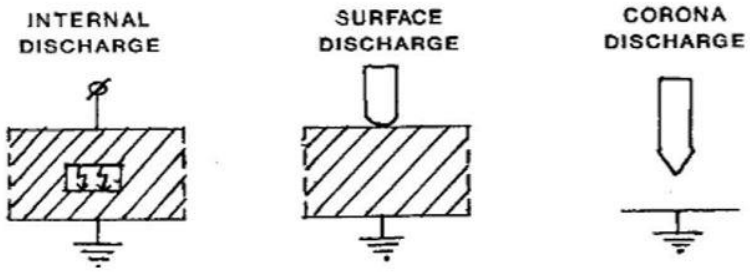

Fig. 2.9 Internal discharges in solid dielectrics [23].

2.3.2 Water Trees Degradation

Water tree degradation is the degradation phenomena creating structure in polymer insulation under the influence of moisture and electrical field [24][25]. Water trees have a shape of a tree and will evolve in a place where water and electrical filed concentration exist. Water tree degradation influences the dielectric performance of XLPE cables such as its breakdown strength which in turn lead to the initial failure or higher rates of ageing [26][27]. The discovery of water tree degradation of polyethylene was first reported in 1969 by Takao Miyashita by combining action of water and electrical stress [28]. In the examination, tree-like structures were seen to have grown through the whole insulation. It was assumed that they continued to grow and failure occurred when the whole insulation was breached.

2.3.2.1 Growth of Water Trees

Water trees may be created in the insulation cable in the form of water vapour by the ionic contaminants, especially at the semiconducting screen of the cable (see Fig. 2.10). The growth of water treeing can be explained using a combination of electrical, chemical, and mechanical processes combined or only 1 or 2 of these methods [29][30][31]. Growth of the water trees depends on the presence of water content, intensity, and frequency of the electric field, the insulation material, temperature, and mechanical stresses.

Typically, water trees are found to initiate and growth in the insulation exposed to an alternating electric field and humidity. The presence of defects, including contaminants and protrusions and voids in the insulation will increase the risk of water tree initiation. Water trees can grow in the range of 0.1 to 1 mm in size and usually “rooted” at an interface between the insulation and another substance. Water can penetrate the insulation from the outside environment of the cable if water blocking barriers are not used. Water can also enter cable insulation from termination or joint faults.

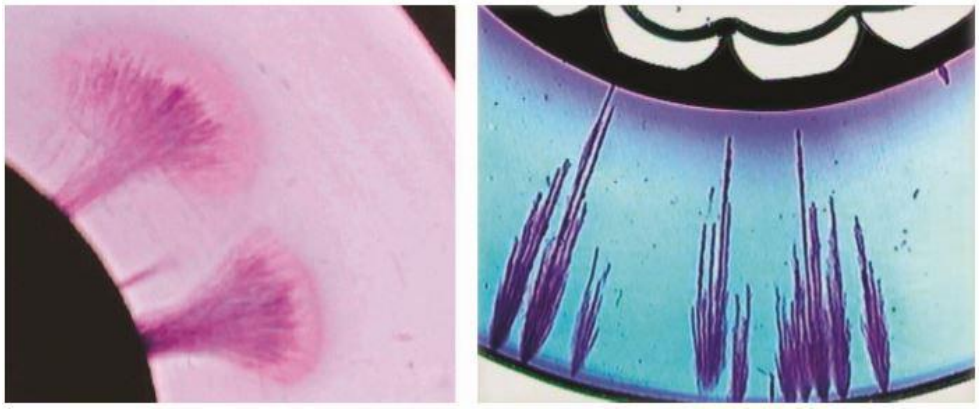

Fig. 2.10 Water trees growing from the outer (right) and inner (left) semi-conductive screens [4].

2.3.2.2 Classification of Water Trees

Water trees generally grow into different shape and size. However, the most recognizable shapes are known to be vented and bow-ties trees (see Fig. 2.11). Vented trees are generally created by deformations at the edge of the insulation while bow-tie trees are created by contaminants inside the insulation. Bow-ties trees initiate from the defects including contaminants and voids within the bulk insulation and tend to grow in two directions. Bow-ties trees typically grow and reach a limiting range (some tens of μm) which turn does not give a significant effect on the degradation at the low electric field stress [32][33].

On the other hand, vented trees are initiated at the interface between the semi-conductive screens and insulation and grow in the same direction as the applied electric field (Fig. 2.11). Vented water trees typically need a longer initiation time than bow tie trees. Bow tie water trees saturate after a certain length, but vented water trees continuously grow and may eventually penetrate the entire insulation thickness. Thus, vented water trees are considered to cause more severe degradation than bow tie water trees. Water trees produce local stress enhancement that may be the initiation phase for an electrical tree. Alternatively, significant oxidation may occur in trees at high temperatures, leading to increased absorption, higher conductivity, and eventually thermal runaway.

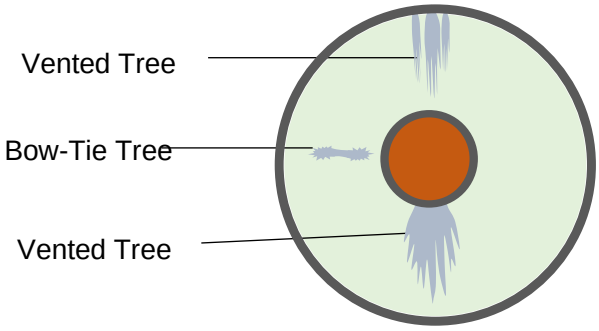

Fig. 2.11 Typical water tree occurred in the insulation of power cable.

2.3.3 Electrical Trees Degradation

An electrical treeing is a network of fine conductive channels that propagates relatively quick through the insulation leading to the failure (see Fig. 2.12) [34][35]. Electrical trees can initiate from the eroded surface of void, or water treeing or initiation can take place in the microcavities of the polymer if the electric field enhancement is large enough. With the time passed by the microcavities are connected to one another and forming a treelike structure. Once the electrical tree is initiated, it would grow to split and lead to insulation deterioration which in turn may result in insulation breakdown.

Fig. 2.12 Typical patterns of electrical trees [36].

2.3.3.1 Growth of Electrical Tree

Fig. 2.13 shows an example of the generation mechanism of the electrical tree. As stated earlier that the electrical trees can initiate from the eroded surface of void or water treeing or initiation can take place in the microcavities. These week points would enhance the local electrical field and tree

may be initiated. The area degraded by the tree initiation is further eroded by electron bombardment, creating the first tube. As the tree increases in size, the electric field is moderated. This is due to the graphite and semiconducting decomposition products present on the tree walls. As the tree propagates, the field at its tip will increase. At a certain moment, the growth speed will begin to increase, to create a runaway of treeing just before the breakdown is triggered in the material. The breakdown is triggered due to the weakening in the polymer, which at last will allow for a full streamer to develop through the material.

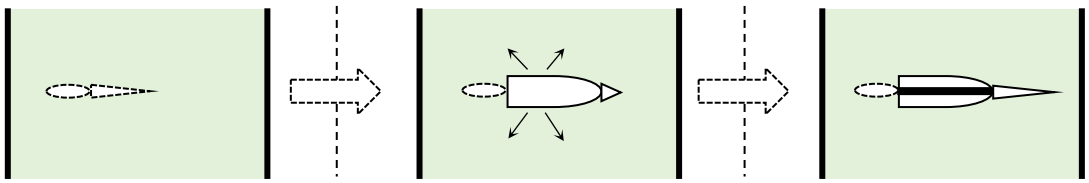

Fig. 2.13 Mechanism of electric tree inception and propagation.

2.3.3.2 Types of Electrical Tree

Electrical trees can grow into different shapes and sizes depending on the conductivity of the treed zone and local electrical field near to the defect site. Fig. 2.14 shows the optical photographs of different type of electrical trees formed in the XLPE cable specimen under the AC voltages [37]. It is observed that bush type of tree (a), a treelike (b) a fibrillar type tree (c) and an intrinsic type tree structures (d) are formed at the tip of the needle electrode, which is connected to high voltages. Fig. 2.14 (e) shows a typical breakdown path formed in the insulation structure due to the propagation of electrical tree and terminating to the ground electrode. Electrical tree generally is in the range of several of tens of micrometers in diameter, while the filament only is a couple of micrometers.

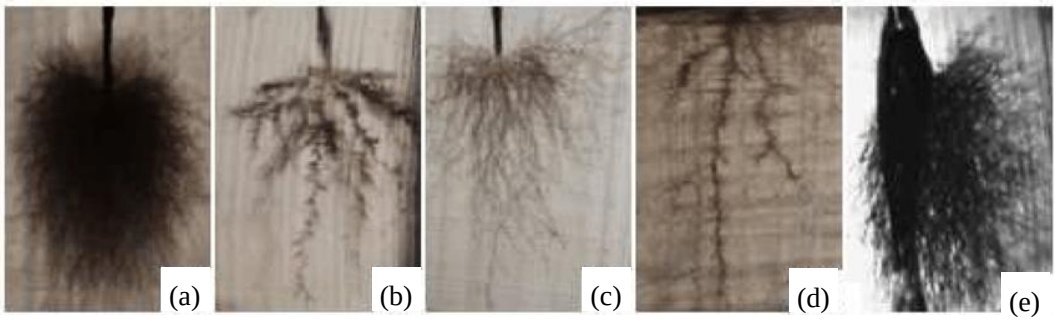

Fig. 2.14 Electrical tree in XLPE cable insulation under AC voltage (a) bush type tree (b) tree-like-tree (c) fibrillar type tree (d) intrinsic type tree (e) tree followed with breakdown insulation [37].

2.3.4 Chemical and Thermal Degradation

Chemical and thermal degradation also contribute to the failure of power cable as well [38] (see Fig. 2.15). Chemical degradation may progressively change the mechanical properties of the polymer insulation causing the long-term polymer chain to break up. This progress is known to be "depolymerization". The structure of the polymeric insulation will become brittle if these mechanisms are in play. Chemical degradation occurs due to many reasons. Partial discharges are one of the significant factors which lead to this type of degradation. During the ionization, partial discharges may produce some harmful gases and acids in the cavity of the insulation leading to the change in polymer structures. Sunlight contains UV-radiation, which is also harmful for polymeric insulation as well.

Thermal degradation takes place when the insulation temperature exceeded its limitation [39]. For example; during normal operation cable XLPE insulation temperatures should be below 90 ºC and during fault conditions cables can be used at temperatures of up to 120 ºC. However, in some abnormal operational condition such as overloading cables can be used at temperature up to 120 ºC. At temperatures between 150 to 225 ºC, free radicals may attach to the backbone of the other polymer chains causing crosslinking. Crosslinking will decrease mechanical strength, density, and crystallinity. At temperatures higher than 225 ºC, the formation of trans-vinyl groups is observed. Formation of trans-vinyl groups indicates radical rearrangements. At very high temperatures above 350 ºC, polyethylene degradation takes place through de-polymerization and incomplete thermal cracking forming coke.

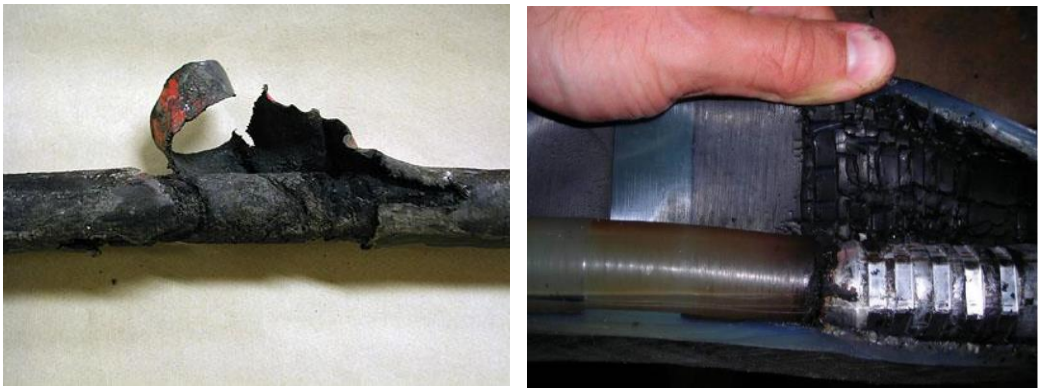

Fig. 2.15 Possible insulation failure due to the thermal and chemical degradation at the main body (left) and joint (right) of power cable [40].

2.4 Model for Insulation Ageing

During their service life, the insulation of power cables and their accessories are suffered from the electrical, mechanical, chemical and also thermal stress causing the deterioration, and therefore leading to unexpected failure. Thus, the information about the residual lifetime of the insulation is essential for power utility company to take a countermeasure such as diagnosing measurement or replacement. The residual lifetime of the electrical insulation can be estimated based on the models for insulation ageing which was reviewed by P. Cygan et a [41].

2.4.1 Life Model for Electrical Stress

Electrical stress is considered to be one of the main factors which causes the deterioration and lifetime shortening of the electrical insulation. Over the past years, numerous of research have been directed toward the endurance lifetime to electrical insulation under the electrical stress only. Two major models relating the test stress with the time to failure are universally accepted; the inverse power model and the exponential model. According to the IEEE standard 930 [42], the details of each method can be described as follow:

2.4.1.1 Inverse Power Law

Inverse power law model has been widely adopted as a tool for estimating the remaining lifetime of electrical insulation by studying the relationship between applied voltage and time. In this method, several levels of electrical stress which are lower than the breakdown strength is applied using a stepwise method until breakdown occurs. Apart from the variable, empirical constants are employed in this model and are needed to be extrapolated from the experimental model.

Assuming that the relationship between the voltage and the lifetime can be approximated by a straight line (*V- L* characteristic), the relationship between breakdown strength and time is expressed as following relationship.

$$L = kV^{-n} \tag{2.1}$$

$$\log L = \log k - n \log V \tag{2.2}$$

where L is the time to failure (usually it is a Weibull scale parameter, the mean or some percentile), V the applied voltage, and k, n are constants to be determined. To test the validity of the validity of applying this model, data are plotted on log-log paper and checked to see if a straight line results. Fig. 2.16 shows the typical inverse power law.

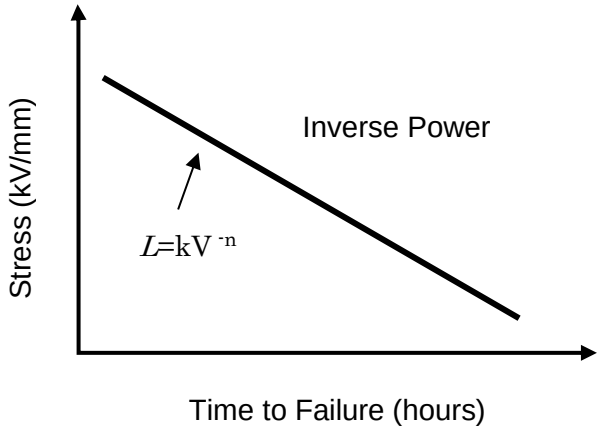

Fig. 2.16 Inverse power law.

2.4.1.2 Inverse Power Law

Likewise, the exponential model is one of the most frequently used for estimating the residual lifetime of electrical insulation. In this model, the time to failure is estimated based on an exponential function of the test stress as shown in Fig. 2.17. It is described under the following relationship.

$$L = c\exp\left(-kV\right) \tag{2.3}$$

$$\log L = \log c - kV \tag{2.4}$$

where L is the time to failure, V the applied voltage, and c, k are the empirical constants, which need to be extrapolated from the experiment model.

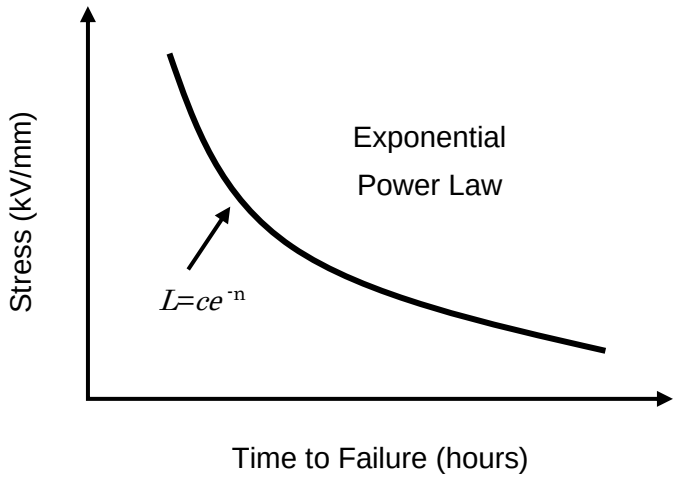

Fig. 2.17 Exponential model law.

2.4.2 Multistress Ageing Models

Multistress models are gaining a lot of interest over the past recent years as means for estimating the residual life of electrical insulation. These new models have an ability to estimate the remaining lifetime of an electrical insulation under electrical and thermal stress simultaneously. A graphic example of the multistress models is presented in Fig. 2.18.

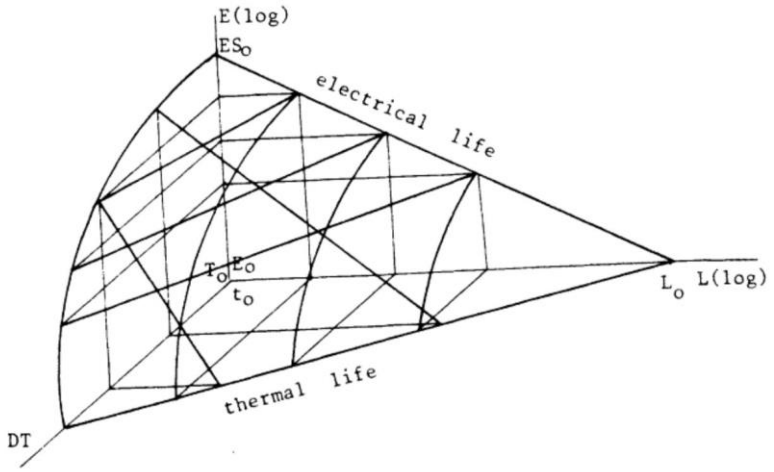

Fig. 2.18 Life surface for combined stresses using Simoni's model [43].

2.5 Diagnostic Methods and Their Applications

The diagnostic measurements are often employed as a tool for the insulation assessment of high voltage equipment, especially for the power cables [44]. Basically, the diagnostic measurements are divided into main categories; destructive and non-destructive methods, which can either be performed online or offline depending on their applications. All the diagnostic measurements should be performed using a non-destructive method because these methods do not damage or harm to the insulation. On the other hand, some of these destructive methods are still used to determine the strength, deterioration process, etc. of the insulation systems.

Various methods have been proposed and developed for the insulation assessment of power cable. Among these methods, the condition monitoring method for power cables by means of partial discharge and water tree detection are often employed. The details of each method are as follow:

2.5.1 Partial Discharge Detection

Partial discharge measurement is becoming a commissioning and diagnostic testing for power cables [45]. Partial discharge measurements are often carried out by most of the power companies as the type of tests and routine test (factory acceptance test, FAT) for high voltage equipment, especially for power cables. Over the past years, numerous researches and publications have been directed towards the generation mechanism of partial discharges and their detections.

When the partial discharge occurs, the partial discharge pulse current and voltage flows away from the partial discharge site towards the cable joints and terminations which can be detected in various ways. Any sensor (also called a partial discharge coupling device) sensitive to high frequencies can detect the partial discharge pulse current and voltage. The following sections give the details of the key features of modern partial discharge measurement systems and review some of the technology advancements in the past years. Also, the discussion of the existing partial discharge detection method, including their advantages and disadvantages.

2.5.1.1 Partial Discharge Detection Principle

Fig. 2.19 shows the typical off-line partial discharge test arrangement [46][47]. In an off-line partial discharge test, the most common means of sensing the partial discharge current is set to use a high voltage capacitor connected to the high voltage terminal of the testing object. The value of this high voltage capacitor ranks from 80 to 1000 pF. The capacitor is a very high impedance to the high AC voltage while being a very low impedance to the high-frequency partial discharge pulse currents. The output of the high voltage capacitor drives a resistive, or inductive-capacitive load called a ‘detector’.

Partial discharge detection normally consists of converting the partial discharge pulse current from the sensor to a high voltage signal, since the most measurement is sensitive to voltage rather than

current. Resistor or more elaborate detection impedance is often employed for this purpose. A resistor yields a wide band of the detection system with output typically measured in mV or μV. The detail of this detection method is described in IEC 60270 and ASTM 1868 standard.

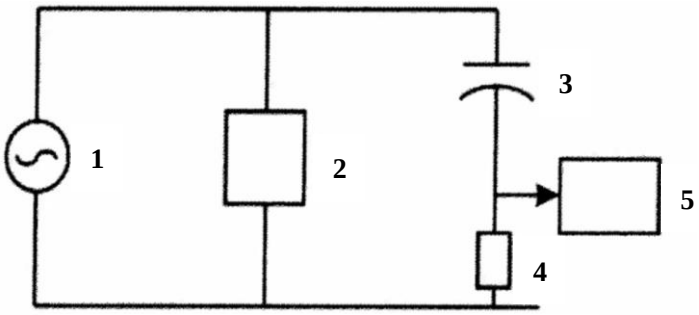

1. HV Supply
2. Test Object
3. PD Coupling Capacitor (sensor)
4. Detection Impedance
5. Recording instrument

Fig. 2.19 A Schematic diagram of a typical off-line partial discharge test arrangement [46].

2.5.1.2 Partial Discharge Detection at Cable Terminal

A long-distance cable line is mainly composed of the main body of the cable, terminals, insulating joints and normal joints. The partial discharge measurement is often performed at the terminal, as the access is relatively easy (Fig. 2.20). Basically, partial discharges occur in the cable lines can be sensed from the following physical attributes of discharge [48]:

- Impulse current
- Acoustic noise
- Electromagnetic radiation

To measure the partial discharge pulse current, high-frequency current transformer (HFCTs) are often employed [49]. HFCTs typically measure the high-frequency current that may flow in the ground lead from a test object. They may also measure the partial discharge pulse currents from the test object to the HV supply. HFCTs are often wound on split ferrite cores that can respond to frequencies excess of 30 MHz. For HFCTs applied to the HV leads, a large electrical clearance is needed; thus air-core HFCT (usually a Rogowski coil) are used.

Partial discharges also generate acoustic emission wave caused by collisions between molecules at the discharge site which can be detected acoustically [50]. Compared with the electrical measurement of partial discharge, acoustic measurement has advantages in noise reduction and the no need to shut down the power line. The acoustic pulse created by each discharge is concentrated in the 40 kHz (ultrasonic) range. By using directional ultrasonic microphones, the location of partial discharge occurred in the cable line can be located.

If partial discharge occurred in cable or cable termination, it will excite an ultra-high frequency electromagnetic signal (UHF EM) to the surrounding environments [50]. The frequency range of UHF signal can reach as high as 1.5GHz. In order to capture these very high frequency signals, UHF sensors are often employed. Antenna sensors (bow-tie antenna and planar equiangular spiral antenna) cover a wide range of bandwidth from 300 MHz to 1.5 GHz. The cable terminations are almost shielded by the metallic sheath. But there still exist some ways without complete shielding for the UHF signals to transmit outwards. The UHF EM wave attenuates heavily in the air, and it is not sensitive enough for detecting the signals far from the partial discharge source.

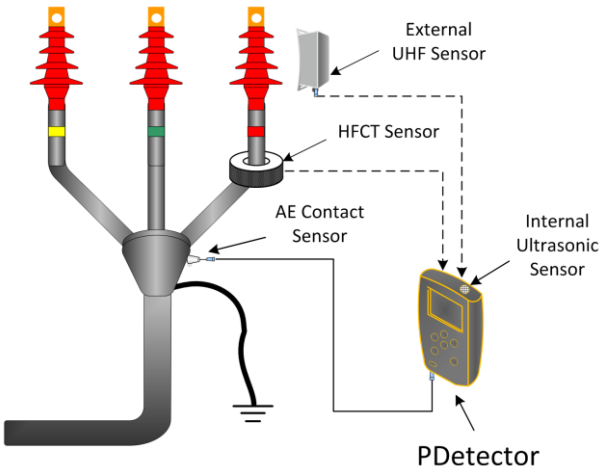

Fig. 2.20 A Schematic diagram of a partial discharge measurement at the cable terminal [50].

2.5.1.3 Partial Discharge Detection at the Insulation Joint

G. Katsuta et al. proposed a method to detect partial discharge at the insulation joint of a long-distance cable line using capacitive coupling between the shield electrode formed between the shield electrode and an additional foil electrode [51]. The measurement principle of this method is shown in Fig. 2.21(a). As shown in Fig. 2.21(b), two electrodes have to be placed across the insulation joint where the metallic shield is electrically discontinued. When a partial discharge signal reaches to such joint, it will eventually bound back towards the discharge site. Consequently, the partial discharge signal can be detected by means of a potential difference between point A and B. It has been reported that this method is very effective as the detection sensitivity is as high as 1 pC when it was performed in the cable tunnel.

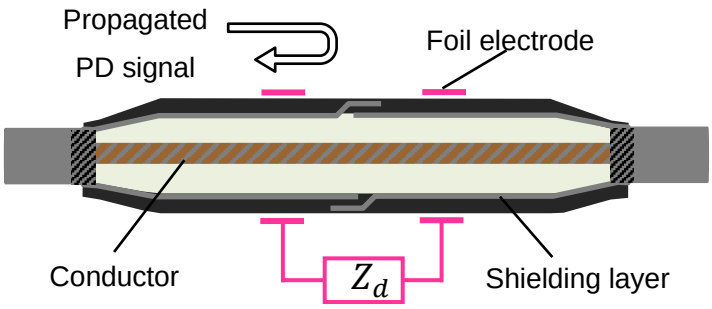

(a) Detection circuit

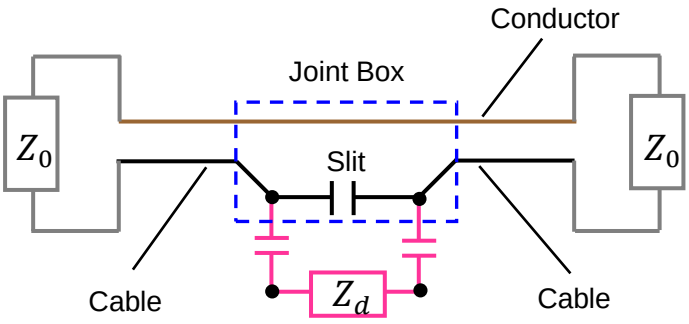

(b) Equivalent circuit

Fig. 2.21 A Schematic diagram of the partial discharge detection at the insulation joint (a) detection circuit (b) equivalent circuit [51].

2.5.1.4 Discussion

Recently, capacitive coupling method has been widely applied for the detection of partial discharge in most of the high voltage equipment [51][52]. For power cable, in particular, capacitive coupling method is used to detect partial discharge at the insulation joint, where the metallic shield layer is electrically discontinued (Fig. 2.21). It is reported that, in the case of the measurement across the insulation joint, the sensitivity using capacitive coupled electrodes was as high as 1 pC [51] when it is performed in the tunnel.

On the other hand, a normal joint that occupies as much as one-third of joints that compose the cross-bonding has no such discontinuity in terms of the metallic shield layer (Fig. 2.22). Furthermore, there might be a request to do the partial discharge measurement at a certain point along the main body of the cable. In addition, such insulation joint can be found with the interval of several hundreds of meters which reduce the detection sensitivity as the pulse, being propagated through such a long distance, may be strongly attenuated when it is captured at the joint.

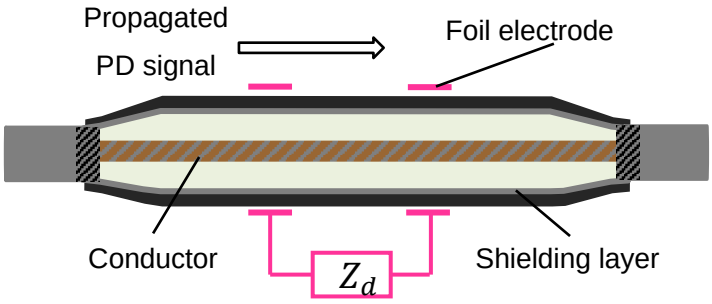

(a) Detection circuit

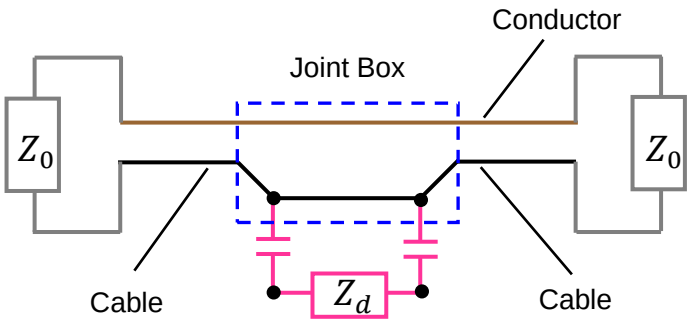

(a) Equivalent circuit

Fig. 2.22 propagation of partial discharge pulse at the normal joint.

2.5.2 Water Tree Detection

Over the past decades or so, numerous research and studies have made to study on the detection of water tree degradation in the aged XLPE cables that were installed in the early stage without water barrier. Several methods have been proposed and developed for water trees detection for both low-class cables and medium-class cables.

For higher class cable (for example, 22 kV to 77 kV), in contrast, non-bridging water trees are usually found [53]. This type of water tree requires more sophisticated and more sensitive techniques as the cables have higher rated voltage, and also greater insulation thickness. In this particular case, loss current method and residual charge are normally employed. Takahashi et. al have proposed to detect water tree degradation in both LV-class and also MV-class cables. Following are the details of the measurement principle of each method and their applications:

2.5.2.1 DC Leakage Current Methods

DC leakage current measurements have been carried out regularly to diagnose the insulation of XLPE cables [54]. In this method, the degree of deterioration of the cable insulation is determined by DC leakage current value as shown in Table 2.3. The principle of this method is based on the application of a DC voltage together with the measurement of the leakage current over a period of time (Fig. 2.23). The test voltage is increased stepwise; each step usually takes 30 seconds. The duration of the test is about 7 to 10 minutes. The maximum step voltage is typically about twice the peak value of the cable operating voltage. Following the voltage application, the cable must then be grounded for a period of at least four times the duration of the test before retesting or being returned to service. The DC currents are typically much less than one microamp so that careful measurement techniques must be used to avoid errors due to stray currents. Any currents due to a local corrosion cell are considered to be too small to affect the DC leakage current.

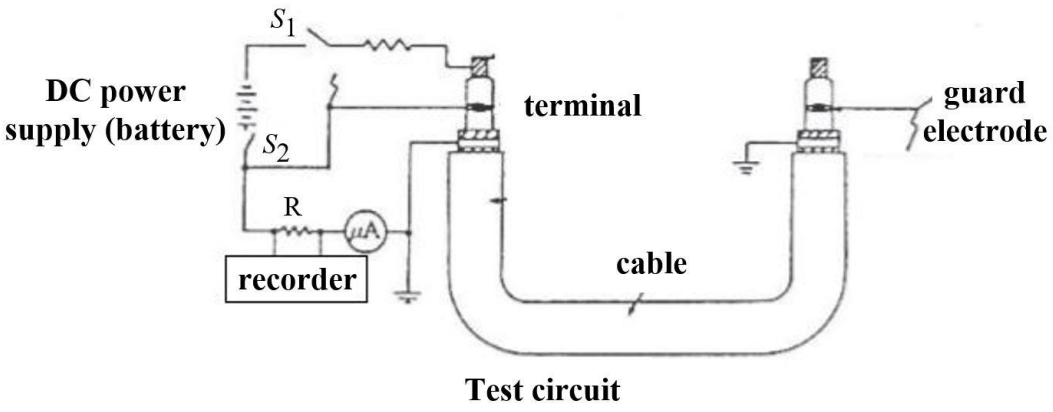

Fig. 2.23 A Schematic diagram of the measurement principle of DC leakage current method [54].

Table 2.3 Judging standard for DC leakage current [54].

	Good		Caution or Defect	
Leakage current value	≤ 0.1 μA	0.1−1 μA		> 0.1 μA
	−	Normal	$PI(=I_1/I_{10})$ <1 Existence of kick	

2.5.2.2 Tanδ Method

Dissipation factor known as tanδ is one of the most commonly used for water trees degradation in XLPE cables. The measurement principle of this method is verified in [55]. The dissipation factor is measured by applying AC voltage and measuring the phase difference between the voltage waveform and the resulting current waveform. Under an AC applied voltage, most of the current flowing in the insulation is capacitive current leading the voltage at a phase of 90 degrees, as shown in Fig. 2.24. However, a small amount of current has the same phase as the voltage which is later called loss current as it related to the power loss in the insulation. The dissipation factor is the ratio of the loss current to the charging current. In the case of underground cables, this test measures the bulk losses rather than the losses resulting from a specific defect. The dissipation factor can be applied to all cable types; however, test results must be considered with respect to the specific cable insulation material and accessory type.

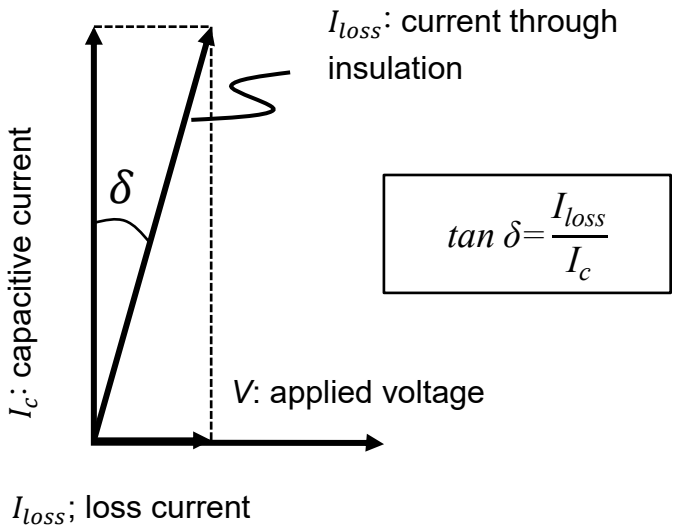

Fig. 2.24 A Schematic diagram of the measurement principle of DC leakage current method [55].

2.5.2.3 AC Superposition Method

An alternative to the DC leakage current, AC superposition method is usually employed for a hot-line of XLPE cable to avoid the power disruption. This method was proposed and developed by Takao Kumazawa et al. in 1997 [56]. The measurement system of this method is shown in Fig. 2.25. The voltages of various frequencies were applied to onto the cover layer of the hot-line cables. After, the relationship between the water tree deterioration and the detected signal is investigated. In this analyses, two major components are investigated; the relationship between the AC superposition voltage measurement current, and the relationship between AC superposition frequency and measurement current. This method has advantages over the conventional method such as DC leakage current and DC superposition as there is no interrupt of the electric service for the diagnostic measurement.

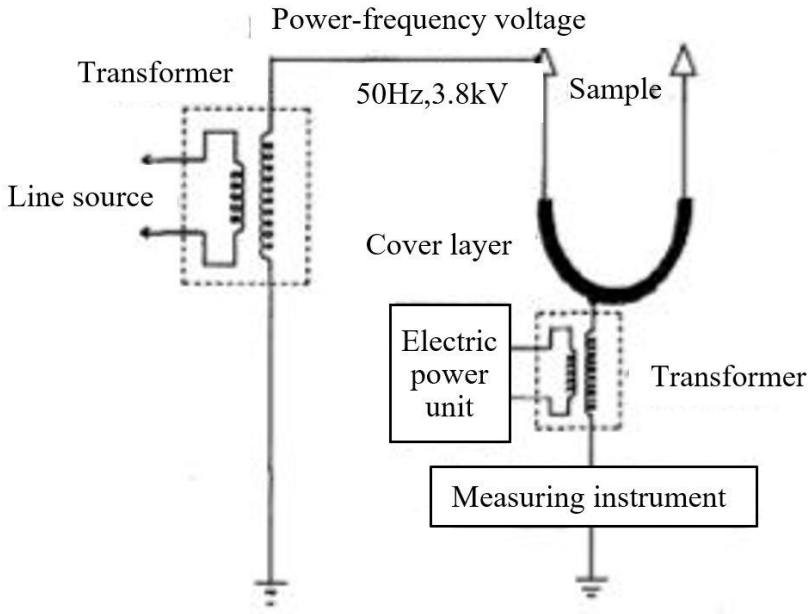

Fig. 2.25 A Schematic diagram of measurement of AC superposition method [56].

2.5.2.4 AC Loss Current Method

Fig. 2.26 illustrates measurement system of a loss current method [57][58]. A no-loss standard capacitor is connected to in parallel with the sample, and a bridge circuit maintains the current balance in both components. The loss current is obtained by subtracting the current capacitive from the current flowing in the sample. Loss current waveforms are obtained as discrete numerical data using a digital oscilloscope, and FFT analysis is used to separate the fundamental and harmonic components (Fig. 2.27).

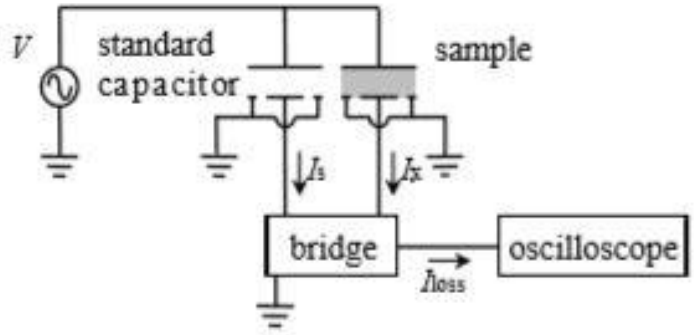

Fig. 2.26 A Schematic diagram of the measurement principle of AC loss current method [57].

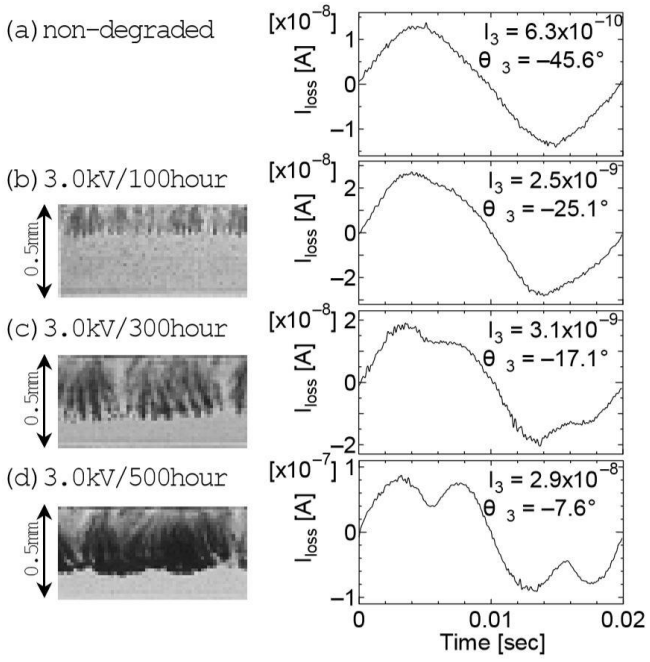

Fig. 2.27 AC loss current waveform of water tree aged XLPE [53].

2.5.2.5 Residual Charge Method

The residual charge method has been widely used to measure water tree aging for 22~66 kV XLPE cable [59]. Fig. 2.28 shows the measurement principle of the residual charge method. In this method, the charge is injected and trapped in the cable insulation with water tree and vicinity by the application of DC voltage. After that the specimen is short-circuited. In this state, most of the shallow charge is removed while the others remain trapped as shown in Fig. 2.28. Finally, the trapped charge can be discharged by the AC voltage application, and then the charge can be detected as the transient DC current.

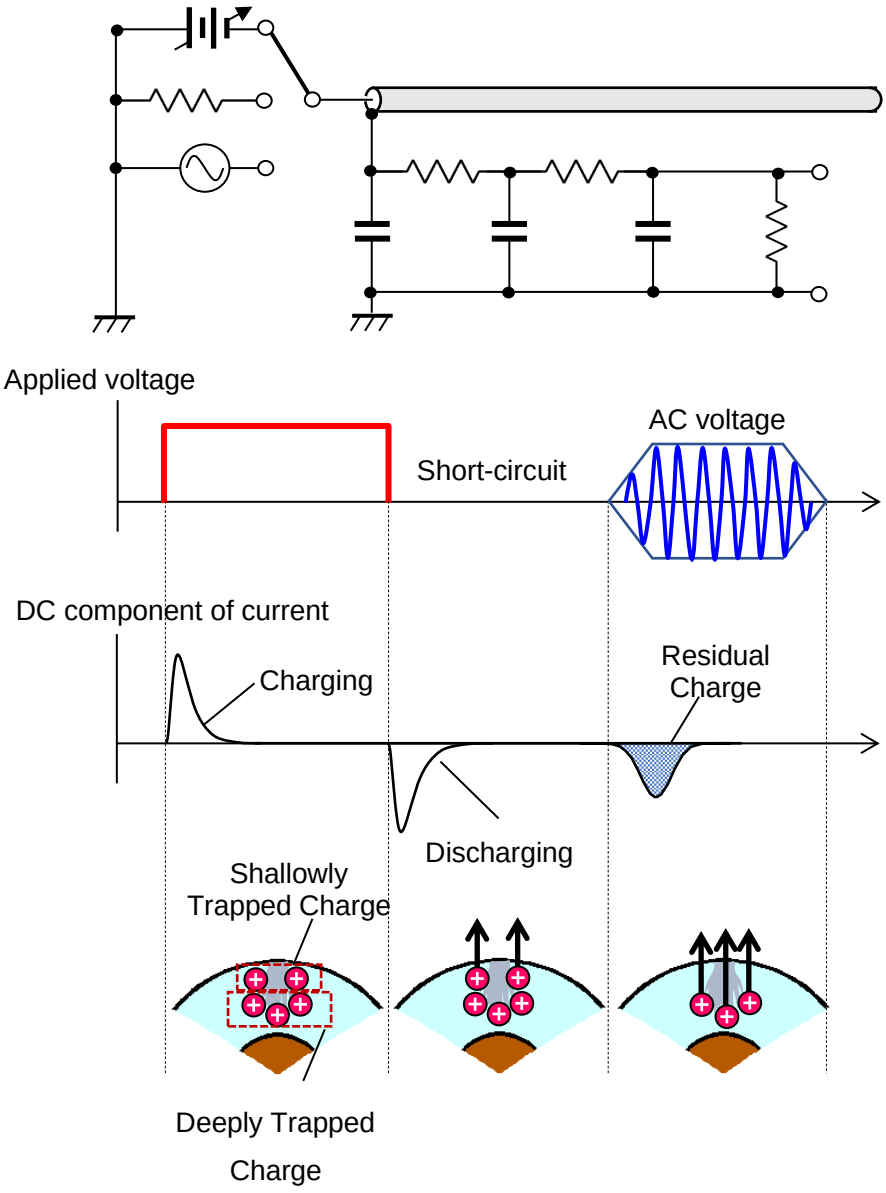

Fig. 2.28 Charge mechanism of under DC, short-circuiting and AC voltage application.

2.5.2.6 Pulse Voltage Methods

Gaining some enlightenment for residual charge method, Kurihara et al. developed the residual charge method by using pulse voltage applications [60]. The measurement principle of this method is similar to the conventional residual charge method (Fig. 2.29). In this method, the pulse voltages are used for rapid charge accumulation and also the release of the residual charge instead of DC and AC voltages. The authors claim that the improvement of the detection sensitivity for signal related to water trees can be realized because of the averaging effect of signals by repeated application of pulse voltages in a shorter time than that of the conventional method.

This method has provided a significant improvement compared to the conventional residual charge method in term of lightweight equipment. Furthermore, the method can be applied to the XLPE cables connected to GISs when the pulse-width is smaller than the half period of an AC voltage with power frequency.

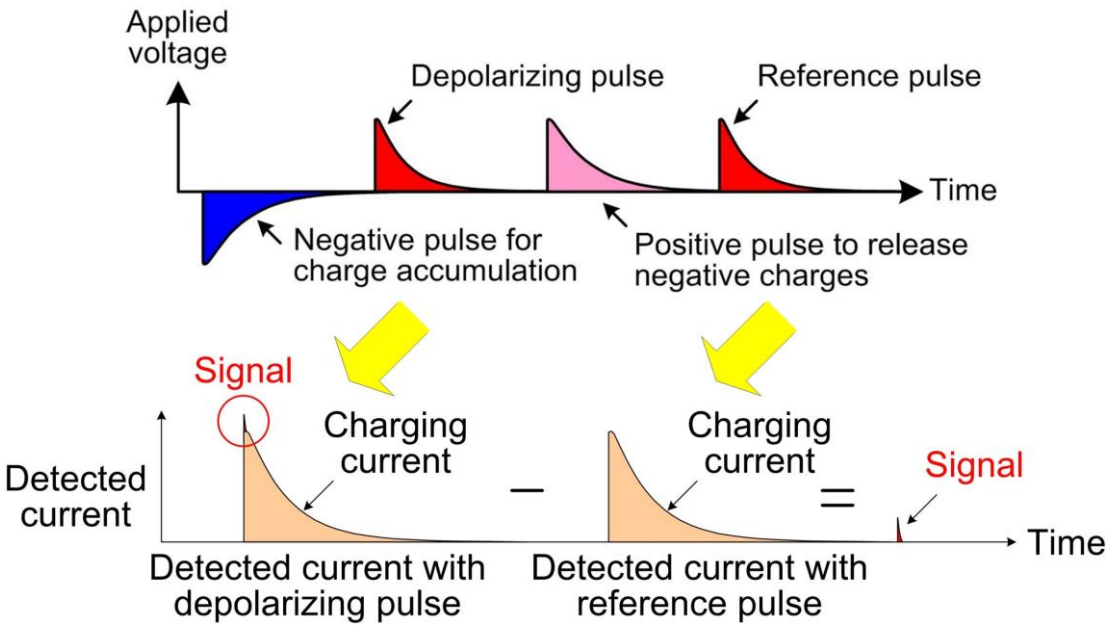

Fig. 2.29 Applying sequences of residual charge detection with pulse voltage and their transition of current responses [60].

2.5.2.7 Discussion

Among the diagnostic all the diagnostic methods for detecting water tree degradation, the residual charge is often used. Although this method has proven to be the most prominent diagnostic method for water tree aging XLPE cable, there are some drawbacks. A result obtained from the residual charge method can only show the degree of the degradation, it is difficult to identify the degradation points in the cable. In some case, the degradation is not uniformly distributed making it difficult to determine the exact location of the degradation point. (Fig. 2.30). Also, this method is not applicable to XLPE cables connected to gas-insulated switchgears (GISs) because charge accumulation may occur on insulation spacers in GIS by a DC voltage. Furthermore, the measurement system becomes large and heavy because a transformer is required to apply the AC voltage to release the charges.

These drawbacks can be avoided by using the recent diagnostic method using pulse voltage which was developed by Kurihara et al where the pulse voltage is used instead of AC voltage in the conventional residual charge method. Although, the signal related to water trees can be released, the location of the degradation is not precisely located as the signal acquired from measurement is not so clear because it includes the miss matching and reflection signal. For economical reason, it will be very advantageous if the location of the degradation is precisely located. In this case, a shaper pulse voltage should be employed so that the spatial resolution of the degradation can be realized.

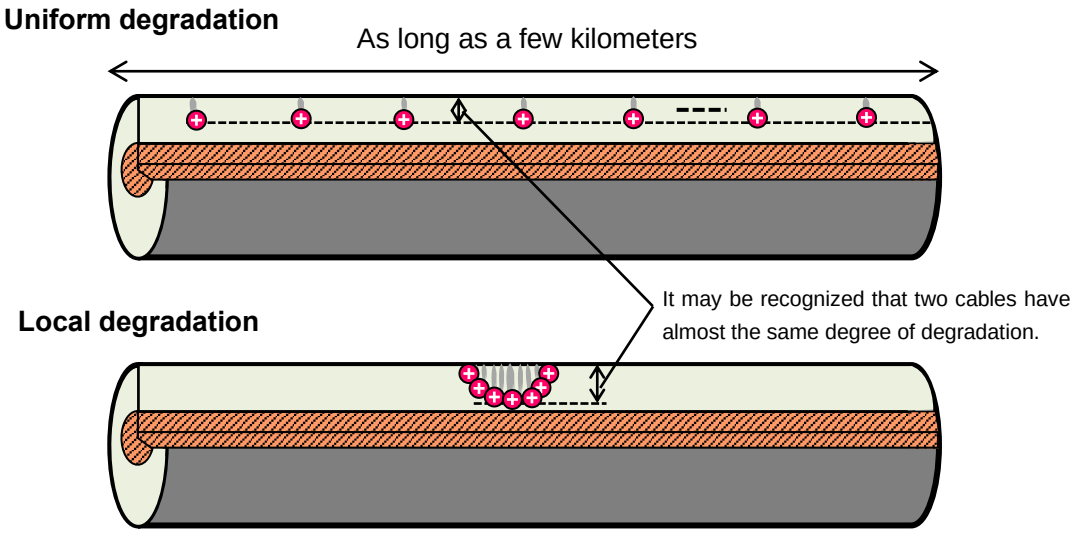

Fig. 2.30 Uniform and location distribution of water tree in insulation.

2.6 Conclusions

Power cable plays an essential role in the transmission and distribution of electrical power. The availability and reliability of the power cable depending on the conditions of the insulation system and its accessories. Defects and degradations are known to be the major problems which substantially reduce the dielectric performances of insulation power cable. Defects are mainly created during the cable manufacturing and poor workmanship during cable installation. Degradations, on the other hand, are developed in the insulation of power cable due to electrical stress, mechanical stress, thermal stress, and chemical stress. Over the passing time, these defects and degradations may lead to the electric field enhancement and eventually lead to the cable breakdown. To prevent these problems, manufacturing and diagnostic testing are often employed. These routine tests can prevent cables from unexpected failure and unnecessary replacement.

Following are the summary of the diagnostic testing for the power cable:

(1) Partial discharge (PD) measurement is widely used for the commissioning and diagnostic testing for most of the high voltage equipment, especially for the power cable. Partial discharge occurred in cable can be detected electrically, and acoustically. Also, partial discharge can be sensed by an electromagnetic signal emitted from the discharge site.

The specific methods are as follow:

(a) Detection impedance method: A coupling capacitor is placed in parallel to the test object (sample) and the detection impedance can be placed in series either with the coupling capacitor or the test object. When discharges occur in the test object, the voltage across the test object experiences a sudden voltage drop corresponding to the apparent charge. The coupling capacitor will deliver current into the test object to counteract the voltage difference between them due to the discharge of a low impedance circuit for high-frequency signals. The voltage drop during discharge will result in a small transient current, and the measuring impedance will result in a detectable voltage due to this current.

(b) High-frequency current transformer (HFCT) method: An HFCT are often wound on slit ferrite core or open core (usually Rogowski core) that can respond to high-frequencies in excess of 30 MHz. A HFCT is coupled to the ground wire of the high voltage equipment so that the partial discharge current pulse can be measured.

(c) Acoustic measurement method: If discharges are occurring on the surface of an insulation system, then a rapid flow of electrons and ions create a gas pressure wave which can be detected acoustically. To detect this acoustic wave, an acoustic emission (AE) sensors place on the surface of the insulation. The location of partial discharge occurred in the cable line can be located by using Time Difference of Arrival (TDoA) techniques.

(d) If partial discharge occurred in cable or cable termination, it would excite an ultra-high frequency electromagnetic signal (UHF EM) to the surrounding environments. The frequency range of UHF signal can reach as high as 1.5GHz. To capture these very high-frequency signals, UHF sensors are often employed. Antenna sensors (bow-tie antenna and planar equiangular spiral antenna) cover a wide range of bandwidth from 300 MHz to 1.5 GHz. The cable terminations are almost shielded by a metallic sheath. But there still exist some ways without complete shielding for the UHF signals to transmit outwards. The UHF EM wave attenuates heavily in the air, and it is not sensitive enough for detecting the signals far from the partial discharge source.

(2) Condition monitoring by means of water tree detection has been used as a preventive measurement for the power cables that were installed without a water barrier. Various methods have been proposed and developed for water trees detection for both low class cables and medium class cables. For higher-class cable (for example 22 kV to 77 kV), in contrast, non-bridging water trees are usually found. This type of water tree requires more sophisticated and more sensitive techniques as the cables have higher rated voltage, and also greater insulation thickness. In this particular case, loss current method and residual charge are normally employed. Takahashi et al have proposed to detect water tree degradation in both LV-class and also MV-class cables.

Following are the details of the measurement principle of each method and their applications:

(a) DC leakage current method: The principle of this method is based on the application of a DC voltage together with the measurement of the leakage current over a period of time. Following the voltage application, the cable must then be grounded for a period of at least four times the duration of the test before retesting or being returned to service. This leakage current from the deterioration part of insulation is used to determine the deterioration index. The DC currents are typically much less than one microamp so that careful measurement techniques must be used to avoid errors due to stray currents.

(b) tan δ (dissipation factor) method: The dissipation factor is measured by applying AC voltage and measuring the phase difference between the voltage waveform and the resulting current waveform. Under an AC applied voltage, most of the current flowing in the insulation is capacitive current leading the voltage at a phase of 90 degrees. However, a small amount of current has the same phase as the voltage which is later called loss current as it related to the power loss in the insulation. The dissipation factor is the ratio of the loss current to the charging current.

(c) AC superposition method: The voltages of various frequencies are applied to onto the cover layer of the hot-line cables. After, the relationship between the water tree deterioration and the detected signal is investigated. In this analyses, two major components are investigated; the relationship between the AC superposition voltage measurement current, and the

relationship between AC superposition frequency and measurement current. This method has advantages over the conventional methods such as DC leakage current and DC superposition as there is no interrupt of the electric service for the diagnostic measurement.

(d) Loss current method: The loss current method is one of on-line diagnostic methods for performing tree degradation diagnosis using high-frequency components included in the loss current component of the current flowing through the power cable. The third harmonic is used as an index because the third harmonic component increases with the water.

(e) Residual charge method: In this method, the charge is injected and trapped in the cable insulation with water tree and vicinity by the application of DC voltage. After, the specimen is short-circuited. In this state, most of the shallow charge is removed while the others remain trapped. Finally, the trapped charge can be discharged by the AC voltage application, and then the charge can be detected as the transient DC current.

(f) Pulse voltages method: The measurement principle of this method is similar to the conventional residual charge method. In this method, the pulse voltages are used for rapid charge accumulation and also the release of the residual charge instead of DC and AC voltages. This method has provided a major improvement compared to the conventional residual charge method in term of lightweight equipment.

References

[1] A. Haddad and D. Warne, Advances in High Voltage Engineering. London, UK: *Institution of Electrical Engineering*, London, 2004, Ch. 10, pp. 477-507.

[2] Vahdat Vahedy, "Polymer Insulated High Voltage Cables", *IEEE Electr. Insul. Mag*, Vol. 22, No. 3, pp. 13-18, May./Jun 2006.

[3] H. Orton, "History of underground power cables," *IEEE Electr. Insul. Mag*, Vol. 29, No. 4, pp. 52-57, Jul 2013.

[4] H. Orton, "Power cable technology review", *High Voltage Engineering*, Vol. 41, No. 4, pp. 1057-1067, Apr 2015.

[5] F. Precopio, "The invention of chemically crosslinked polyethylene", *IEEE Electr. Insul. Mag*, Vol. 15, No. 1, pp. 23-25, Jan./Feb 1999.

[6] Open Electrical, “Thermoplastic and Thermosetting compounds,”, May 15, 2017. [Online]. Available:https://wiki.openelectrical.org/index.php?title=Thermoplastic_%26_Thermosetting_compounds [Accessed: Apr. 28, 2019].

[7] T. Andritsch, A. Vaughan, G. C. Stevens, "Novel insulation materials for high voltage cable systems", *IEEE Electr. Insul. Mag*., Vol. 33, No. 4, pp. 27-33, Jul./Aug. 2017.

[8] SSCC Showa Holdings, “Cable Joint,”. [Online]. Available: http://www.swcc.co.jp/eng/products/siconex/cable_joint.html [Accessed: June. 26, 2019].

[9] BRUGG, High Voltage Cable Accessories, Product catalog. [E-book] Available: https://bruggcables.com/en/.

[10] C. Zhou, H. Yi, X. Dong, "Review of recent research towards power cable life cycle management", *High Volt.*, Vol. 2, No. 3, pp. 179-187, Sep 2017.

[11] M. G. Danikas: "Small Partial Discharges and their Role in Insulation Deterioration", *IEEE Trans. Dielectr. Electr. Insul*, Vol. 4, No. 6, pp. 863-867, Dec 1997.

[12] T. Okamoto; M. Kanegami; N. Hozumi; M. Ikeda: "Partial Discharge Endurance Life of Polymer Insulating Materials at High Temperature", Electrical Engineering Japan, Vol. 126, No. 1, pp. 15-22, Jan 1999.

[13] E. Sili, J.P. Cambronne, N. Naudé and R. Khazaka: "Polyimide Lifetime under Partial Discharge Aging: Effects of Temperature, Pressure and Humidity", IEEE Trans. Dielectr. Electr. Insul, Vol. 20, No. 2, pp.435-442, Apr 2013.

[14] S. Gutiérrez, I. Sancho, L. Fontán and J. De Nó: "Effect of protrusions in HVDC cables", *IEEE Trans. Dielectr. Electr. Insul*, Vol. 19, No. 5, pp.1774-1781, Oct 2012.

[15] S.A. Boggs: "Partial Discharge-Part III: Cavity-Induced Partial Discharge in Solid Dielectrics", *IEEE Trans. Electr. Insul*, Vol. 6, No. 6, pp.11-20, Nov./Dec 1990.

[16] C. Mayoux, C. Laurent: "Contribution of Partial Discharges to Electrical Breakdown of Solid Insulating Materials", *IEEE Trans. Dielectr. Electr. Insul*, Vol. 2, No. 4, pp.641-652, Aug 1995.

[17] R. Patch, M. Hoof: "Physical Modeling of Partial Discharge patterns", *International Conference*

on Conduction and Breakdown in Solid Dielectrics, Sweden, pp. 114-118, Jun 22-25 1991.

[18] H. Ohno, G. Katsuta, R.Sakaguchi, Y.Ebinuma, N. Sakai, A.Nagaoka: "Influence of defects on insulating properties of XLPE cable", *Proceedings of the 3rd International Conference on Properties and Applications of Dielectric Materials*, Vol. 1, pp.485-489, Jul 1991.

[19] Y. Iwashita, T. Kurihara, T. Takahashi, and T. Okamoto: "Partial Discharge Characteristics of Oil Impregnated Insulation System with an Oil Gap under Continuous AC Voltage Application", *Conference Proceeding of ISEIM* 2014, pp.212-215, Jun 2014.

[20] X. Chen, Y. Xu, et al: "Effect of Tree Channel Conductivity on Electrical Tree Shape and Breakdown in XLPE Cable Insulation Samples", *IEEE Trans. Dielectr. Electr. Insul*, Vol. 20, No. 2, pp.435-442, Apr 2013.

[21] D,M. Hepburn, I.J. Kemp, A.J. Shields, and J. Cooper: "Degradation of epoxy resin by partial discharge", *IEEE Proc. Sci, Meas. Technol*., Vol. 147, No.3, pp.97-104, May 2000.

[22] S.S. Shady and A.S. Mohammaed: 'A review of partial discharge detection diagnosis techniques in high voltage power cable'. 2018 *IEEE 12th International Conference on Compatibility, Power Electrionics and Power Engineering*, Doha, Qatar, pp.1-5, Apr 2018.

[23] C Sunil kumar, K S. Harisha, N. Gouthami, V. Harshitha, C. Madhu: 'Failures in underground power cables – return of experience'. *IJIREEICE International Journal of Innovative Research in Electrical, Electronics, Instrumentation and Control Engineering*, Vol. 4, Issue. 6, pp. 75-79, Oct 2016.

[24] M. T. Shaw and S. H. Shaw, "Water Treeing in Solid Dielectric," *IEEE Trans. Dielectr. Electr. Insul*, Vol. E1-19, No.5, pp. 419-452, Oct 1984.

[25] L.A. Dissado, and J.C. Fothergill, "Treeing degradation in Polymers," *Electrical degradation and breakdown*, G.C. Stevens, Eds. London, UK, pp. 75-113, Jun 1992.

[26] J. Martine-Vega, Dielectric Materials for Electrical Engineering, John Wiley, and Sons, Hoboken, USA, pp-189-207, Mar 2010.

[27] E. F. Steen, "Water Treeing: the behavior of water trees in extruded cable insulation," Ph.D. thesis, Delf University of Technology, Delf, 1st, Jun 1989.

[28] T. Miyashita: "Deterioration of water-immersed polyethylene-coated wire by treeing", *IEEE Trans. Dielectr. Electr. Insul*, Vol. 6, Issue. 3, pp.129-135, Sep 1971.

[29] C. N. Sanniyati, Y. Z. Arief, Z. Adzis, N.A. Muhamad, M.H. Ahmad, M.A.B. Sidik, and K.Y. Lau: "Water tree in polymeric cables−A review,", *Malaysian Journal of Fundamental and Applied Sciences*, Vol.12, No.1, pp. 12-21, 2016.

[30] R. Patsch, and J. Jung, "Water Trees in Cables: generation and detection," *IEEE Proc-Sci, Meas. Tecnhol*. Vol.146, No.5, pp. 253-259, Sep 1999.

[31] R. Ross, "Inception and propagation mechanism of water treeing," *IEEE Trans. Dielectr. Electr. Insul*, Vol. 5, No.5, pp. 660-680, Oct 1980.

[32] Y. Ikeda, and T. Tanaka, "Possibility of Deterioration Diagnosis of XLPE Cable with Water Trees by Residual Electric Charge," *IEEJ Transaction on Power and Energy*, Vol.107, No.9,

pp.465-465, Sep 1987 (in Japanese).

[33] S.L. Nunes and M.T. Shaw, “Water treeing in Polyethylene−A review of mechanisms,” *IEEE Trans. Dielectr. Electr. Insul*, Vol. E1-15, No.6, pp. 437-450, Dec 1980.

[34] L.A. Dissado: “Understanding electrical trees in solids: From experiment to theory,” *IEEE Trans. Dielectr. Electr. Insul*, Vol. 9, No.4, pp. 483-497, Aug 2002.

[35] M. G. Danikas, T. Tanaka, "Nanocomposites−A Review of Electrical Treeing and Breakdown", *IEEE Electr. Insul. Mag.*, Vol. 25, No. 4, pp. 19-24, Sep 2009.

[36] J. Fothergill, "The Coming of Age of HVDC Extruded Power Cables", *IEEE Electr. Insul. Conf.* (*EIC*), pp. 124-137, Jun 2014.

[37] R. Sarathi, A. Nandini and T. Tanaka, “Understanding Electrical treeing phenomena in XLPE cable insulation under Harmonic AC voltages adopting UHF technique”, *IEEE Trans. Dielectr. Electr. Insul*., Vol. 19, pp. 903-909, Jun 2012.

[38] A. Tzimas, S. Rowland, L. A. Dissado, F. Mingli, U.H. Nilsson, "Effect of Long-Time Electrical and Thermal Stresses upon the Endurance Capability of Cable Insulation Material", *IEEE Trans. Dielectr. Electr. Insul.*, Vol. 16, pp. 1436-1443, May 2009.

[39] A. Motori, F. Sandrolini, G. C. Montanari, "A Contribution to the Study of Aging of XLPE Insulated Cable Models", *IEEE Trans. Power Delivery*, Vol. 6, No. 1, pp. 34-42, Jan 1991.

[40] F. Steennis, P. Soepboer, J. Mosterd, P. Buys, P. Oosterlee, L. BOKMA, R. Meier, “The Effect of High Current Loads on Joints in MV Cable Systems,” *21st International Conference on Electricity Distribution*, Frankfurt, pp. 1-4, 6-9 Jun 2011.

[41] P. Cygan, J. R. Laghari, "Models for insulation aging under electrical and thermal multistress", *IEEE Trans. Elect. Insul.*, Vol. 25, No. 5, pp. 923-933, Oct 1990.

[42] IEEE Standard 930-1987, "Guide for the Statistical Analysis of Electrical Insulation Voltage Endurance Test Data", pp. 1-32, Aug, 1987.

[43] L. Simoni, “General Equation of the Decline in the Electric Strength for Combined Thermal and Elec- trical Stresses”, *IEEE Trans. Electr. Insul*., Vol. 19, pp. 45-52, Feb 1984.

[44] M. Ekberg, A. Gustafsson: "Recent Results in HV Measurement Techniques ", *IEEE Trans. Dielectr. Electr. Insul*, Vol. 2, No. 5, pp. 906-914, Oct 1995.

[45] G.C. Montanari: " Partial Discharge Detection in Medium Voltage and High Voltage Cables: Maximum Distance for Detection, Length of Cable, and Some Answers,", *IEEE Electr. Insul. Mag*., Vol. 32, No. 5, pp. 41-46, Sep./Oct 2016.

[46] G.C. Stone: "Partial discharge diagnostics and electrical equipment insulation condition assessment", *IEEE Trans. Dielectr. Electr. Insul*, Vol. 12, No. 5, pp.891-904, October (2005).

[47] R. Bartnikas: "Nature of Partial Discharges and Their Measurement ", *IEEE Trans. Dielectr. Electr. Insul*, Vol. 9, No. 5, pp. 763-808, Oct 2002.

[48] M. M. Yaacob, M. A. Alsaedi, J. R. Rashed, A. M. Dakhil, S. F. Atyah, "Review on partial discharge detection techniques related to high voltage power equipment using different sensors", *Photonic Sensors*, Vol. 4, No. 4, pp. 325-337, Dec 2014.

[49] C. Suwanari: "Investigation on Partial Discharge of Power Cable Termination Defects using High Frequency Current Transformer ", *ECTI Trans. Electrical. ENG., Electronics and Communication*, Vol. 12, No. 1, pp.16-23, Jan 2014.

[50] G. Chen, J. Tao, Y. Ma, H. FU, Y. Liu, Z. Zhou, C. Huang, C. Guo, "On-site Portable Partial Discharge Detection Applied to Power Cables Using HFCT and UHF methods", *WSEAS Transactions on Circuits and Systems*, Vol. 15, pp.83-90, 2016.

[51] G. Katsuta, A. Toya, et al: "Development of a new detection method of partial discharge for Extra-High voltage cross-linked polyethylene insulated cable lines", *IEEE Trans. Power Delivery*, Vol. 7, No. 3, pp. 1068-1079, Jul 1992.

[52] H. Yasukawa, T. Takahashi, K. Kajimura, and T. Tanaka: "Development of The New Partial Discharge Measuring Method and Device", *Proc. 2011 CIGRE A2/D1 Kyoto Colloquium*, PS1-O-25, Sep 2011.

[53] A. Toya, M. Nakade, Y. Okuyama, K. Uchida, H. Tanaka and K. Watanebe: "Trends in Degradation Diagnostic Technique for XLPE Cables in Japan", *21, rue d'Artois Paris, F-75008*, Jun 2004.

[54] C. Shinoda, T. Hashizume, T. Tani, Y. Takada, and T. Takada, “A consideration of Mechanism of DC Leakage Current Peak in XLPE Cables” *Proceeding of the 5th International Conference on Properties and Applications of Dielectric Materials*, pp. 402-405, May 1997.

[55] Y. Yagi, H. Tanaka, H. Kimura, "Study on Diagnostic Method for Water Treed XLPE Cable by Loss Current Measurement", *IEEE CEIDP*, Vol. 2, pp. 653-656, Oct 1998.

[56] H. Oonishi, F. Urano, T. Mochizuki, K. Soma, K. Kotani, K. Kamio, "Development of a New Method for Hot-Line XLPE Cables with Water Trees", *IEEE Trans. on Power Delivery*, Vol. 2, pp. 1-7, Jan 1987.

[57] Tanaka A, Toya A, Tujimoto T, Nakade M, Yagi Y, Adachi K, Tanaka H, “Actual Application of On-site Diagnostic Method for Water Treed XLPE Cable by Harmonics in AC Loss Current,” *JICABLE03*, C8.3.2, pp.706-pp.710, Jun 2003.

[58] T. Tsujimoto, M. Nakade, Y. Yagi, K. Adachi, H. Tanaka, Egasakicho, Tsurumi-ku, Yokohama, Kanagawa, Yawata-kaigandori, Ichihara, Chiba, Higashi-shinagawa, Shinagawa-ku, "Development of ON-SITE Diagnostic for XLPE Cable by Harmonics in AC Loss Current," *Proceedings of the 7th International Conference on Properties and Applications of Dielectric Materiais*, Nagoya, pp 73-76, Jun 2003.

[59] Y. Ikeda, and T. Tanaka, “Diagnosis Method for Water Tree Aging of XLPE cables-Development of Residual Charge Measuring Device,” CRIEPI, *Yokosuka Engineering Laboratory, Japan, Tech. Report W86008*, Jul 1986 (in Japanese).

[60] T. Kurihara, T. Okamoto, N. Hozumi et al., "Evaluation of relationship between residual charge signal and AC breakdown strength of water-tree degraded 22 to 77 kV classes XLPE cables removed from service using pulsed voltages", *IEEE Trans. Dielectr. Electr. Insul*, Vol. 24, pp. 656-665, Mar. 2017.

Chapter 3: Partial Discharge Detection Method for Power Cable

3.1 Introduction

Partial discharge (PD) is considered to be one of the major problems which substantially reduce the dielectric performance of insulation power cable [1][2]. The presences of partial discharge caused by the defects and degradations. Defects, such as the protrusion on the electrode, amber (localized change in the chemical property), and foreign substances may increase the local electrical field and can lead to the breakdown through a treeing process that is accompanied by partial discharge as a pre-breakdown phenomenon [3][4]. Voids may be created in the process of production, such as jointing and termination of cables, which can lead to partial discharge as well [5]. These defects are mainly created before a cables operational use and lead to the failure of the cable in the early stage. Partial discharge measurement is widely used to detect such defects and local breakdown. After the cable has been used for a long period of time, delamination of the insulation may take place, which leads to the final breakdown [6][7]. Partial discharge could be detected in such cases as well.

Partial discharge measurement is usually performed at the cable terminations as the access is relatively easy [8][9]. As the cable line is practically spread in a long distance making it difficult to detect the discharge signal. Arising from this problem, G. Katsuta et al. [10] proposed to detect partial discharge at the insulation where the metallic shield is electrically discontinued. The authors claimed that the sensitivity of this method was high as 1 pC when it was performed in the tunnel. On the other hand, normal joint that occupies as much as one-third of joints that compose the cross-bonding has no such discontinuity in terms of the metallic shield layer. Furthermore, there might be a request to perform partial discharge measurement at a certain point along the main body of the cable.

We propose that partial discharge measurement can be performed even in such conditions where no discontinuity along the shield electrode exists, although a significant reduction in sensitivity compared with the case of insulation joints may take place. This method is assuming that the screen shield is not a perfect shield conductor and that change in potential would be seen as partial discharge signal propagating through the cable. As this detection considered the skin effect of the screen shield, the change in potential may be more significant as the frequency goes higher.

3.2 Measurement Principle

When a partial discharge occurs in the power cable, it will produce an electrical signal propagating through the cable line. Although coaxial cable does not theoretically radiate any electromagnetic signal to outside, in practice, some signal can be detected because the outer shield is not a perfect shield [11][12]. This will be more significant because of the skin effect when the higher frequency is targeted. It may lead to the increase in the potential of the shield electrode, which may be able to be detected by mean of capacitive coupling between the shield electrode and additional foil electrode pasted onto the plastic jacket.

Fig. 3.1 illustrates the basic idea of the newly developed method for partial discharge detection in a long-distance cable by using a capacitive coupling method. This method proposed that the change in potential due to partial discharge can be detected by means of capacitive coupling between the shield layer and an additional foil electrode.

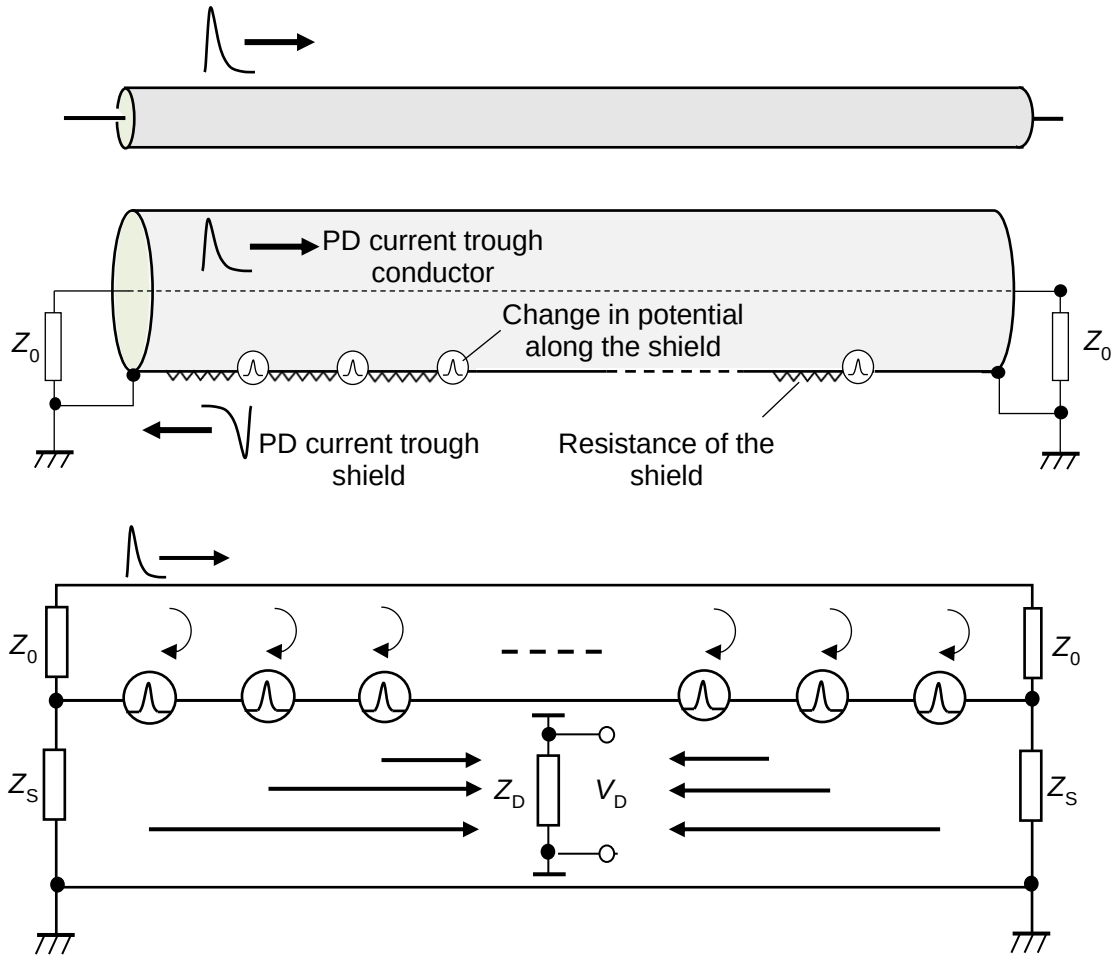

Fig. 3.1 Schematic diagram of the change in potential generated along the shield electrode of the cable line.

3.2.1 Signal Generation

Assuming that the partial discharge is a current source being generated at the near end of the cable line. This current discharge flows through the conductor of the cable and the return (displacement) current flows through the shield electrode of the cable, which in turn may produce a change in potential due to the impedance of the shield electrode itself.

Let us assume that a current discharge with the magnitude of I_0 being generated at the near end of the cable line (x_0=0). At the time t and the distance x from the near end, the instantaneous current discharge can be expressed $I(x,t)$. The result of the Fourier Transform of this current discharge is defined as $I(x,\omega)$. When the discharge is generated, the discharge current flows through a conductor, and the return current flows through the shield electrode of the cable. Subsequently, a small change in potential is generated along the shield electrode.

The change in potential along the shield electrode per unit length is described as shown in equation (3.1).

$$V(x,\omega) = R_s(\omega) \cdot I(x,\omega) \tag{3.1}$$

where $V(x,\omega)$ is the change in potential generated along the shield electrode, and $R_s(\omega)$ is the per unit resistance of the shield electrode. x is the distance from near. This change in potential propagates through the transmission path form between shield electrode ant the ground.

Assuming that the discharge occurs at the magnitude of I_0 with the width of Δt and propagates at the speed c, the change in potential being generated over the differential length $c\Delta t$ is expressed as shown in equation (3.2).

$$V_0(\omega) = R_s(\omega) \cdot I_0(\omega) \cdot c\Delta t \tag{3.2}$$

where $V_0(\omega)$ is the magnitude of a change in potential. At higher frequency, $R_s(\omega)$ is increased significantly due to the skin effect, which eventually increases the change in potential.

3.2.2 Signal Propagation

When the current discharge is being generated, it causes a change in potential propagating through a shield electrode and the region with potential gradient is moving at the speed c in the longitudinal direction through the cable. This propagation has the same propagation characteristic as the signal propagation, which is commonly known to be a coaxial-mode propagation. In the meantime, the potential gradient propagating through the transmission path between the shield electrode of the target and reference cable is moving at speed c_s. This has the same propagation characteristic as the signal propagation, which is known as common-mode propagation. The value of c is 190 m/μs for polyethylene of a communication cable and 160 m/μs for the power cable [13]. The potential gradient

propagates through air insulation of a transmission path formed between shield electrodes of a target and reference cable; thus, the value of c_s is 300 m/μs.

Since the value $c_s > c$, the signal propagating in a common-mode propagation is moving ahead of the signal propagating in coaxial mode. Therefore, the detection signal becomes a dull waveform compared to the signal propagates in coaxial mode propagation.

3.2.3 Signal Detection

The power cable is covered with an anti-corrosion layer; therefore, it is very challenging to get an electrical signal from the cable. In this method, the electrical signal can be acquired by means of capacitive coupling electrode between the shielding layer and aluminum foil pasted onto the plastic jacket.

In order to retain a ground potential, a reference cable with the foil electrode pasted in the same manner as the target cable line is employed. These two electrodes are in connection through a balun (in this particular case, to convert balanced circuit into unbalanced) which leads to an oscilloscope so that the signal can be displayed. In order to correctly measure the potential difference between the two electrodes, it is desirable to convert the balanced connection to the unbalanced connection via the balun.

3.3 Experiment using Mimic Partial Discharge

The experimental study is necessary to confirm the feasibility of the proposed method to be used for partial discharge detection. This section gives details of partial discharge measurement of a communication cable and full-size cable by using the proposed method. In this study, a mimic partial discharge was used to imitate the actual partial discharge signal. This mimic partial discharge signal was directly injected to the conductor of the cable line with which was then detected by capacitive coupling between an additional foil electrode and shield electrode of the cable itself.

3.3.1 Experiment using Communication Cable

3.3.1.1 Cable Specimen

The RG series is high-frequency cables compliant with the U.S. Army and Land Communications Union Specifications JAN-C-17, MIL-C-17, and Defense Agency Specification DSP-C-3102. RG stands for “Radio Guide” and U stands for "Universal". It has characteristics such as large insulation resistance, high withstand voltage, lightweight and easy handling, and it is widely used not only in the United States but also in this country. In this experiment, a coaxial cable lines of RG-58A/U as a mimic transmission line (Fig. 3.2). Table 3.1 shows the properties and structures of RG-58A/U.

Fig. 3.2 A cut-away section of RG-58A/U cable.

Table 3.1Characteristic impedance and structure of RG-58A/U.

Characteristic impedance (20 ° C)	50 Ω
Internal conductor outer diameter and configuration	19 pcs / 0.18 mm Tin-plated annealed copper wire
Insulator outer diameter and configuration	2.9 mm Polyethylene
Outer conductor outer diameter and configuration	3.6 mm Tin-plated annealed copper wire
Sheath outer diameter and configuration	5.0 mm PVC (polyvinyl chloride)

3.3.1.2 Experimental Setup

Fig. 3.3 shows the schematic diagram of a measurement system for partial discharge detection of a long-distance cable line using a capacitive coupling method. In this experiment, the occurrence is produced as a mimic partial discharge by using a line pulsar, and the change in potential can be detected by means of capacitive coupling between foil electrode and shield itself.

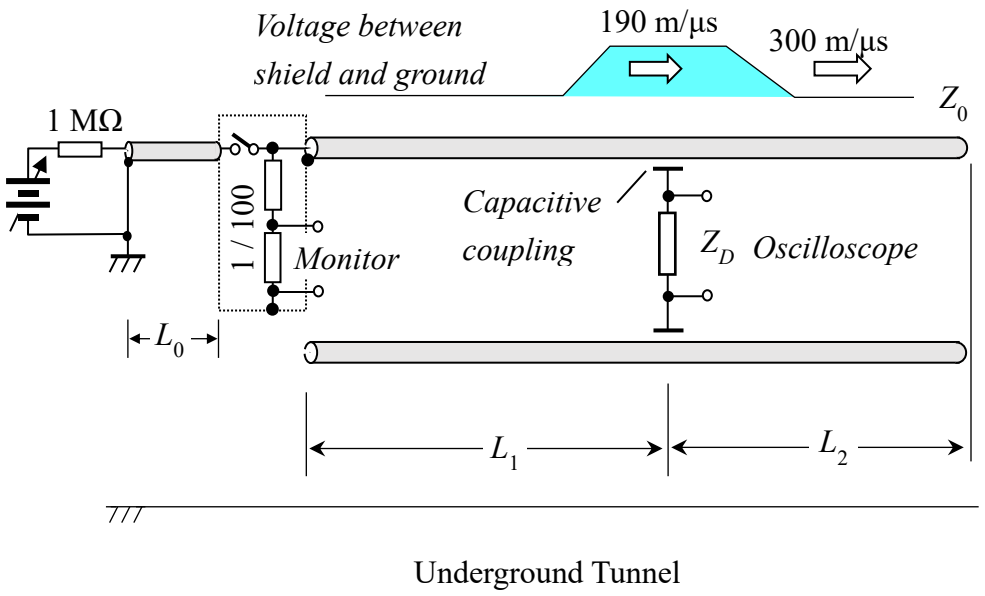

Fig. 3.3 A configuration of measurement system for partial discharge detection.

Fig. 3.4(a) shows the schematic diagram of an injection charge calibration. In this case, a cable with a short length (L_0) and coaxial switch (Sanyu Co., Ltd, rated voltage and current being 12 V and 400 A, respectively) were used to create a mimic partial discharge pulse. The function generator (WAVE FACTORY 2CH1 5 MHz) was employed for controlling the switching frequency of a signal generation. This partial discharge signal was directly injected to the cable line at the rate of 20 per second.

In this experiment, the mimic partial discharge was employed as the partial discharge in the void in the solid material. The signal propagating along the cable was practically measured and ensured that it had an appropriate width as a mimic partial discharge pulse. The width was determined by referring to the literature as 20 ns in pulse width [14]. This corresponds to the time that a surge travels through 4 m, assuming the surge propagation speed as 200 m/μs. Therefore, a 2 m-long cable was chosen to create the line-pulsar.

Considering two different directions of propagation, the discharge intensity being injected to the cable line is calculated as:

$$Q = \frac{C_{L0} V_{DC}}{2} \tag{3.3}$$

where C_{L0} and V_{DC} are the capacitance of the 2 m long and the charging voltage for charge calibration. As expressed in equation (3.3), the charge calibration of the mimic partial discharge can be adjusted by changing the value of V_{DC}.

We carried out an experiment using an RG58A/U long-distance cable line of 100 m in length and 50 Ω characteristic impedance. To retain a ground potential, an identical cable to the target cable was employed as a reference cable. Fig. 3.4(b) shows a schematic diagram of a partial discharge detection circuit by using a capacitive coupling method. The detection circuit composed of aluminum foil electrodes and a balun. Partial discharge activity was detected 50 m away from the near end where partial discharge takes place. The potential difference taken from both electrodes were connected to the oscilloscope through the balun with the ratio of 5:1.

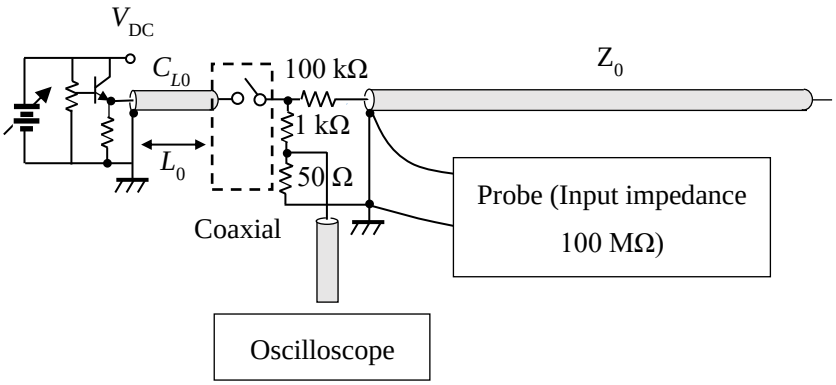

(a) Schematic diagram of charge calibration

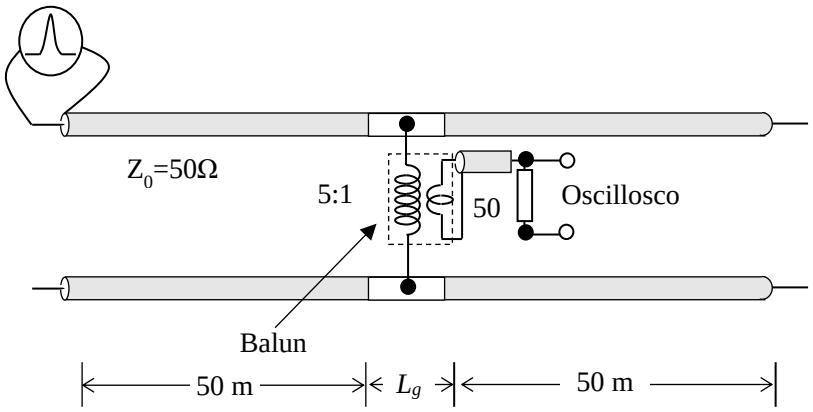

(b) Schematic diagram of partial discharge detection using foil electrode

Fig. 3.4 Schematic diagram of the partial discharge measurement system for long-distance cable lines.

3.3.1.3 Result and Discussion

In order to evaluate whether the detection point voltage is due to the simulated discharge point voltage, we consider the pulse propagation velocity. Considering that the insulator is polyethylene and its relative permittivity is 2.26, and the relative magnetic permeability is 1, then the pulse propagation velocity is calculated below.

$$v = \frac{1}{\sqrt{\varepsilon_r \varepsilon_0 \mu_r \mu_0}} = \frac{1}{\sqrt{2.26 \times 8.854 \times 10^{-12} \times 1 \times 4\pi \times 10^{-7}}} = 200\ (m/\mu s) \qquad (3.4)$$

From the input of the simulated discharge point voltage, it can be seen from Fig. 3.5 that the detection point voltage appears approximately 250 ns later. Since this is equal to the time required to propagate 50 m with the pulse propagation speed shown in the above equation, we can consider that the detection point voltage is due to the simulated discharge point voltage.

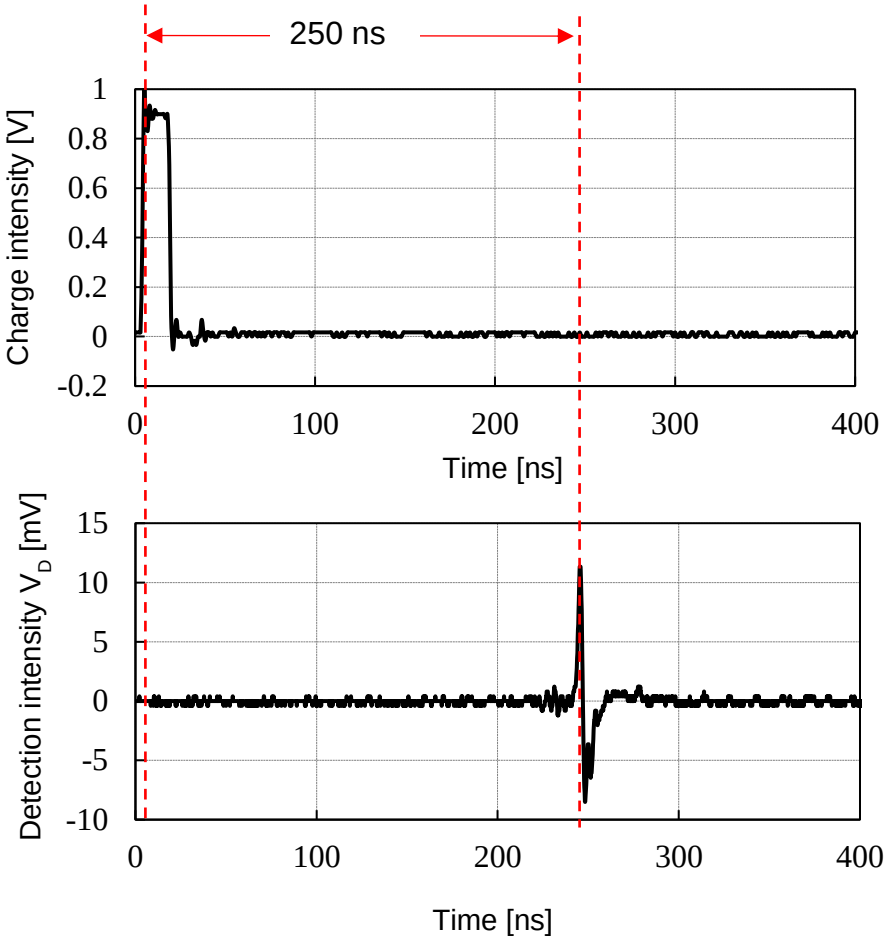

Fig. 3.5 Typical partial discharge detection signal using capacitive coupling method.

(1) The Influence of Capacitive Coupling (C_p)

In the measurement, the change in potential due to the partial discharge propagation through the cable can be detected by the coupling capacitor (C_p) formed between an additional foil electrode and the shield electrode itself. Hence, it is necessary to understand the effect of this capacitor on the detection intensity. Fig. 3.6 shows the configuration model of the C_p that is formed between the cable and an additional foil electrode. In this model, we assume that the shield electrode has a in radius and the foil electrode that is pasted onto the cable has b in radius, the capacitive coupling formed between these two electrodes can be described as follow:

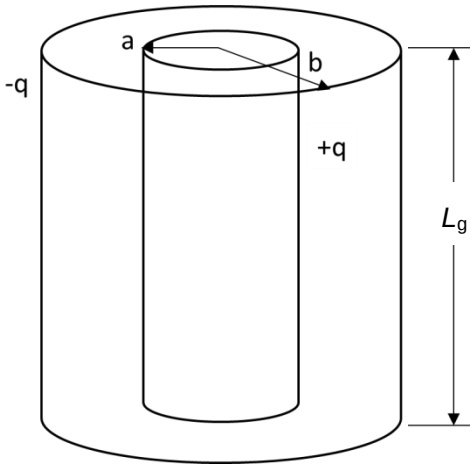

Fig. 3.6 A model of capacitive coupling between the shielding layer and foil electrode.

Consider the Gauss's law the electric field between the inner cylinder and outer cylinder having a volume charge ρ is express as

$$\int_S E \cdot nds = \frac{1}{\varepsilon}\int_V \rho dV \tag{3.5}$$

Thus,

$$E = \frac{q}{2\pi\varepsilon}\cdot\frac{1}{r} \tag{3.6}$$

Hence, the potential V difference between the inner and outer cylinder is expressed as shown in equation (3.7).

$$V = -\int_b^a Edr = -\frac{q}{2\pi\varepsilon}\left[\ln r\right]_b^a = \frac{q}{2\pi\varepsilon}\ln\frac{b}{a} \tag{3.7}$$

Therefore, the capacitance C_p between the foil electrode and the shield electrode of the cable is expressed as

$$C_p = 2\pi\varepsilon \frac{L_g}{\ln\left(\frac{b}{a}\right)} \tag{3.8}$$

where a and b are the radius of the shield electrode of the cable and the radius of the additional foil electrode, respectively. L_F is the length of the foil electrode.

In this method, the change in potential due to the partial discharge propagating along the shield electrode can be detected by C_p. Thus, it is necessary to understand the effect of C_p on the detection intensity by changing the length of the foil electrode (L_F). Table 3.2 shows the value of C_p depending on the L_G (cm). As shown in Table 3.2, the value of C_p is increased with the increase of L_F This suggests that the length of foil electrode may have an effect on detection intensity.

Fig. 3.7 shows the detection intensity depending on the L_F. As shown in Fig. 3.7, the detection intensity is marginally increased with the increase of L_g and shows the saturation tendency when L_F. was 80 cm. This suggested that the L_F does not give a significant change in detection intensity. Although the detection intensity is supposed to be increased at longer L_F, the signal detection intensity may be reduced while passing through foil electrode due to the attenuation coefficient of transmission lines. Thus, the length of foil electrode can be chosen with the condition that L_F must be shorter than the wavelength of the detection signal, otherwise the detection signal would eventually fluctuate.

Table 3.2 Coupling capacitor depending on the foil electrode length.

Foil Electrode Length (mm)	Coupling Capacitor (pF)
20	101
40	203
60	304
80	406
100	508

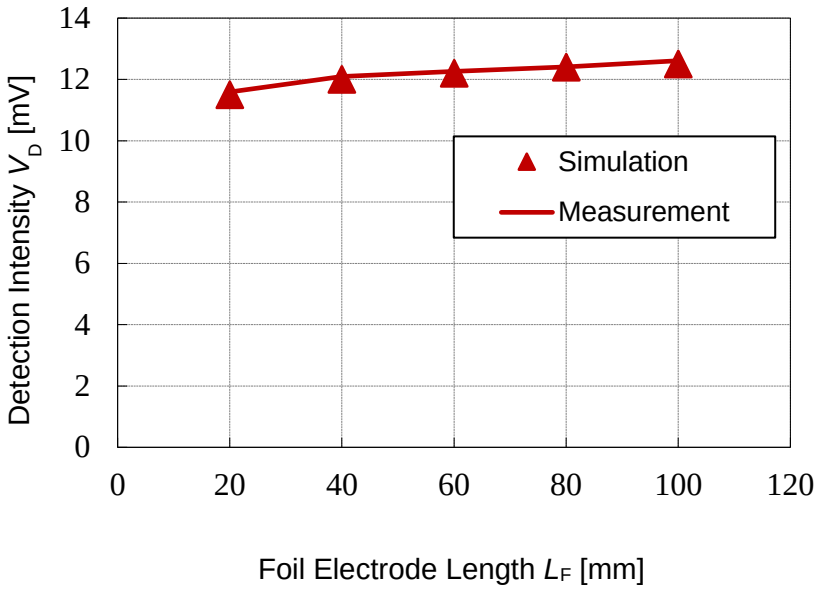

Fig. 3.7 Effect of coupling capacitor on the detection voltage.

(2) Effect of Gap Length (L_G) and Gap Distance (D_G)

When the measurement was performed, a reference cable and target have to be separated between one another in a significant distance D_G which may influence the detection intensity. In order to understand this effect, we studied the change in detection intensity by considering the model shown in Fig. 3.8. This model consists of two parallel lines.

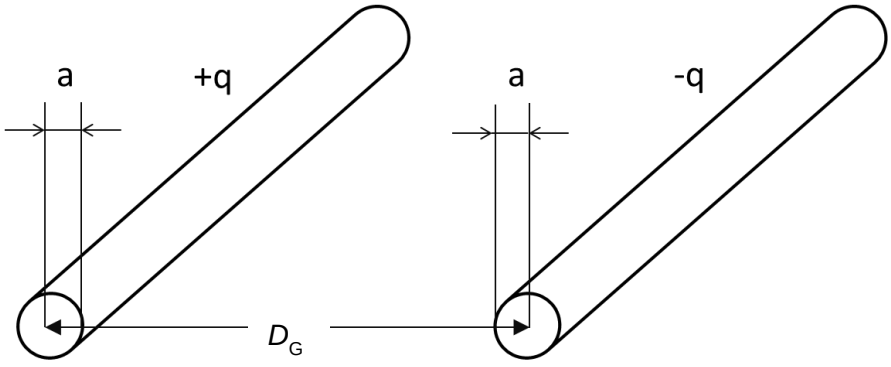

Fig. 3.8 Schematic diagram of a mutual capacitance between the target and reference cable.

The electric field produced by each of the conductors A and B can be obtained in the same manner as in the coaxial cylindrical conductor model in Fig. 3.8. Electric fields E_1 and E_2 at a location r_1 (r_1> a) from the conductor A central axis and r_2 (r_2> a) from the conductor *B* central axis are expressed as follow.

$$E_1 = \frac{q}{2\pi\varepsilon_0 r_1} \tag{3.9}$$

$$E_2 = \frac{-q}{2\pi\varepsilon_0 r_2} \tag{3.10}$$

On a plane perpendicular to the conductors A and B, the potential V_P of a point *P* separated by r_1 from the central axis of the conductor A and r_2 from the central axis of the conductor B is expressed as:

$$V_P = -\int_{\infty}^{r_1} \frac{q}{2\pi\varepsilon_0 r_1} dr_1 + \left(-\int_{\infty}^{r_2} \frac{-q}{2\pi\varepsilon_0 r_1} dr_2 \right) \tag{3.11}$$

Then,

$$V_P = \frac{q}{2\pi\varepsilon_0} \ln \frac{r_2}{r_1} \tag{3.12}$$

Therefore, the surface potential V_A of the conductor A is $r_1 \to a$ and $r_2 \to d - a$

$$V_A = \frac{q}{2\pi\varepsilon_0} \ln \frac{d-a}{d} \tag{3.13}$$

The surface potential V_B of the conductor B is $r_1 \to d - a$ and $r_2 \to a$

$$V_B = \frac{q}{2\pi\varepsilon_0} \ln \frac{d}{d-a} \tag{3.14}$$

Therefore, the potential difference V_{AB} between the conductors AB is

$$V_{AB} = V_A - V_B = \frac{q}{\pi\varepsilon_0} \ln \frac{d-a}{d} \tag{3.15}$$

Therefore, the per unit length capacitance C_{AB} between conductors AB is

$$C_{AB} = \frac{q}{V_{AB}} = \frac{\pi\varepsilon_0}{\ln \frac{D_g - a}{a}} \tag{3.16}$$

We studied the change in detection intensity by changing the length L_G and distance D_G between the target and reference cable. Fig. 3.9 shows the partial discharge detection intensity (V_D) depending on L_G and D_G. As shown in Fig. 3.9, the detection intensity does not significantly change between the $L_G = 40\ cm$ and $L_G = 100\ cm$. Likewise, the detection intensity also does not significantly change although the distance D_G is changed. Therefore, we conclude that the change in L_G and D_G does not give a significant change to the detection intensity. This tendency suggested that these parameters are optional when performing a measurement.

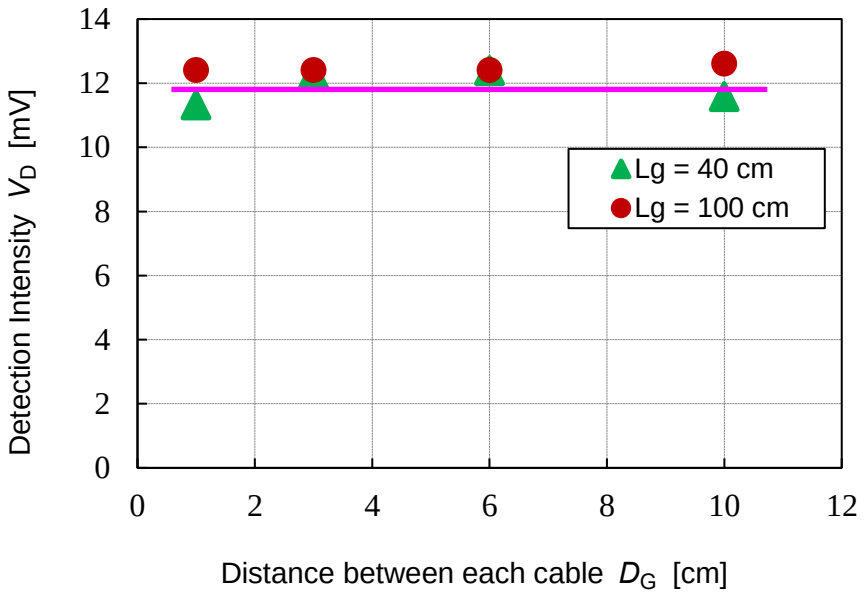

Fig. 3.9 Effect of gap length and gap distance between target and reference cables on detection intensity.

(3) Detection Limit

Fig. 3.10 shows the partial discharge detection waveform and the noise level using an RG58A/U communication cable. The detection limit was determined by adjusting the injection charge calibration, and the respective detection intensity was compared to the noise level. As shown in Fig. 3.10, the signal was compared with the noise level and the sensitivity was finally determined as 400 pC as the detection limit. In this case, we assumed that the detection limit should be twice as high as the noise level, and the sensitivity is supposed to be determined with 6 dB in S/N ratio. We concluded that the limitation of the measurement was about 400 pC, which was far poorer than the measurement method proposed by G. Katsua [10] where the sensitivity was as high as 1 pC. Furthermore, the noise level may be increased in the cable tunnel and the detection limit is expected to be higher than 400 pC. Therefore, the detection sensitivity is even poorer than the measurement at room temperature.

In some cases, partial discharge may take place far from either the insulation joint or the termination leading to a difficulty in detection due to the attenuation after propagation through such a long distance. In this particular case, the proposed method is very advantageous because partial discharge can be detected at the point where partial discharge is being generated. Also, the proposed method has a simple wiring system making it easy to perform a measurement as only an aluminum foil electrode and balun are required. Therefore, we concluded that new partial discharge measurement is feasible at any point of the NJ or the main body, only if a significant reduction in sensitivity compared with the measurement at the insulation joint can be accepted.

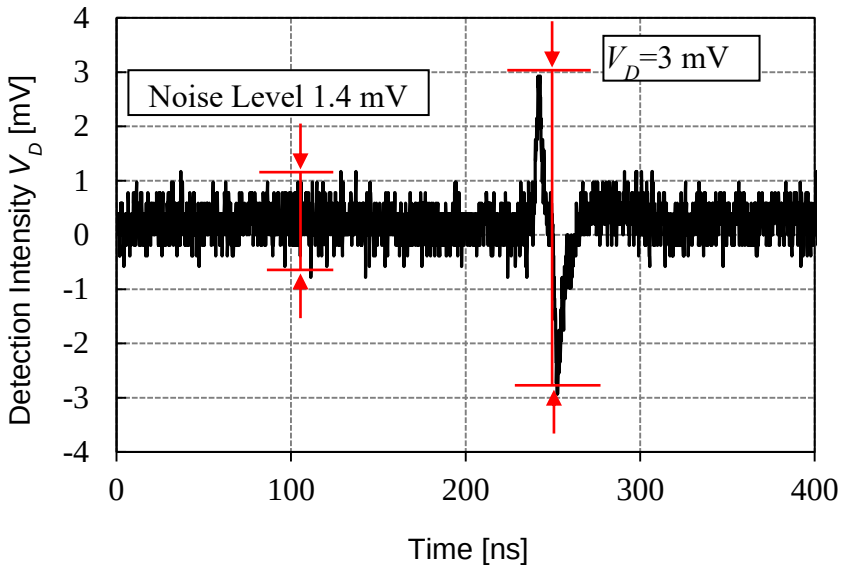

Fig. 3.10 Detection intensity V_D and the noise level: charge calibration 400 pC and *Lg* 20 cm.

3.3.2 Experiment using Full-size Cable

3.3.2.1 Cable Specimen

We performed a partial discharge measurement using a full-size cable lines which were taken off from services. The measurement was conducted in the Central Research Institute of Electric Power Industry (CRIEPI) located in Tokyo. Fig. 3.11 shows the layout of a single core 6.6 kV crosslinked polyethylene (XLPE) cable. A shield electrode of this cable is made of thin copper tape with 28 mm in width and 0.2 mm in thickness. This copper tape was wrapped onto the cable as shown in Fig. 3.11.

Fig. 3.11 Single core 6.6 kV crosslinked (XLPE) cable.

3.3.2.2 Experimental Setup

Fig. 3.12 shows the picture of the on-site partial discharge measurement using a full-size 6.6 kV XLPE cable. In the case, the mimic partial discharge signal and its schematic diagram were described in section 3.3.1. We carried out an experiment using a full-size 6.6 kV XLPE cable line of 200 m in length and 25 Ω characteristic impedance. To retain a ground potential, an identical cable to the target cable was used as a reference cable. The measurement was done by using aluminum foil wrapped onto both target and reference cables. Partial discharge activity was detected 30 m away from the near end where partial discharge takes place. The potential difference taken from both electrodes were connected to the oscilloscope through the balun with the ratio of 5:1.

Fig. 3.12 On-site partial discharge measurement using a 6.6 kV XLPE cable line.

3.3.2.3 Result and Discussion

Fig. 3.13 shows the typical partial discharge measurement using capacitive coupling method. In this particular case, the charging voltage of 5 V was charged to the short cable length (L_0) and the aluminum foil was 1 mm in length. From the input of the simulated discharge point voltage, it can be seen that the detection point voltage appears approximately 150 ns later. Since this is equal to the time required to propagate 30 m with the pulse propagation speed shown in the above equation, we can consider that the detection point voltage is due to the simulated discharge point voltage.

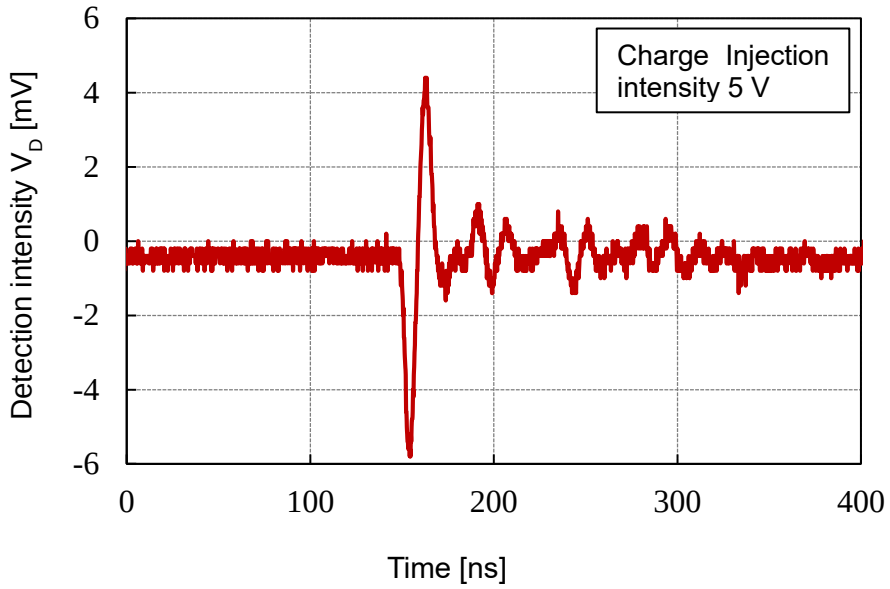

Fig. 3.13 On-site partial discharge detection signal of 6.6 kV XLPE cable.

3.4 Simulation of PD Pulse Propagation

When a partial discharge pulse propagates through a power cable, the pulse properties such as pulse shape, and magnitude change due to the signal attenuation and dispersion. The partial discharge pulses occurred in the power cable network have to travel in a significant distance before being captured at the measurement point. As most of the non-destructive measurement is normally performed at the terminal and in some case at the insulation joint, it is useful to have an idea of what happens with partial discharge signal during the propagation through the cable and at the measurement point.

3.4.1 Theoretical Background

3.4.1.1 Lumped-Element Model and Equivalent Circuit

In the proposed method, a pair of cables are taken as the target and reference cables for the detection of the change in potential by means of capacitive coupling between the shielding layer and an additional foil electrode. In this section, a numerical simulation is performed using a coaxial cable as shown in Fig. 3.14(a) with the same measurement with the measurement configuration using a pair of parallel cables as shown in Fig. 3.14(b).

As the signal has to travel in a significant distance before reaching the detection point, its properties may be changed due to signal attenuation, dispersion, and the time delay. The signal attenuation and dispersion can be determined using the lumped element model of a coaxial cable (Fig. 3.15). The components of the transmission line can be represented by the equivalent electrical circuit which is commonly known as “Lumped element model” [15]. In this model, each symbol represents the functionality of the devices, regardless of the specific shape of the line under consideration. All the components including, source, transmission line components, and the load will be oriented along the x-direction, subdividing it into a small segment each of length Δx.

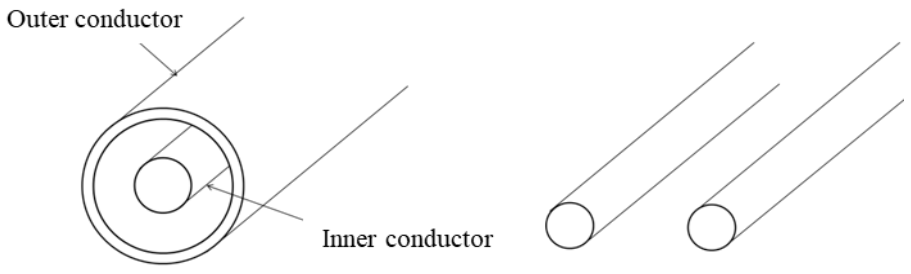

(a) Coaxial cable (b) Parallel double line

Fig. 3.14 Parallel double and coaxial lines (a) and (b) coaxial line parallel double line [21].

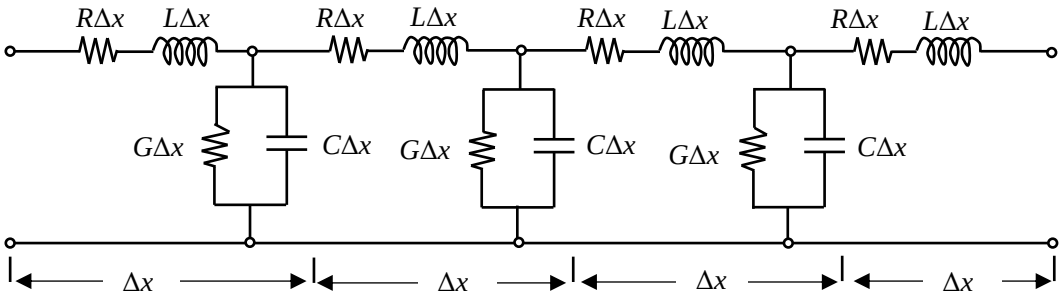

Fig. 3.15 lumped element of uniform line [31].

Where

R: The combined resistance of both conductors per unit length, in Ω/m,

L: the combined inductance of both conductors per unit length, in H/m,

G: The conductance of the insulation medium between the two conductors per unit length, in S/m

C: The capacitance of the two conductors per unit length, in F/m.

The expression of transmission line parameters *R*', *L*', *G*' and *C*' and the details of these parameters are given [15].

3.4.1.2 Transmission-Line Equations

The partial discharge pulse propagation through a cable can be described by using the telegraph equation. Fig. 3.16 shows the equivalent circuit of uniform line. The ohmic losses dissipated in the conductor are represented by resistor R [Ω/m] and the leakage current is caused by conductance G [Sm]. The Fig. 3.16 gives a representation an infinitely small lines section Δx.

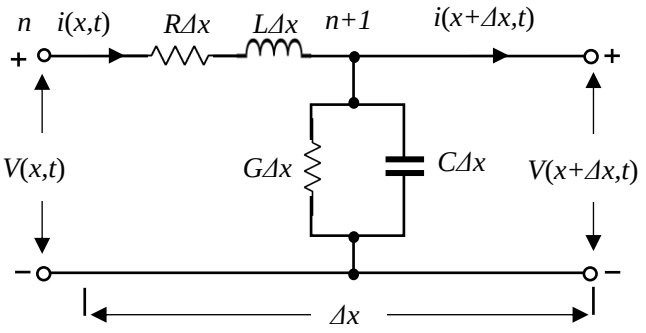

Fig. 3.16 Equivalent circuit of uniform line.

For deriving the Telegraph equation, Kirchhoff's laws are used in the combination with the model of Fig. 3.16. In this model, a small section Δx is considered. Hence, the lump-element including the inductance and resistance of that part are $L\Delta x$, $R\Delta x$, the electrostatic capacitance and the conductance are $C\Delta x$, $G\Delta x$. The quantities $v(x,t)$ and $i(x,t)$ denote the instantaneous voltage and current at the left end of the differential section (node n), and similarly $v(x+\Delta x,t)$ and $i(x+\Delta x,t)$denote the same quantities at node $(n+1)$, located at the right end of section.

We applied Kirchhoff's voltage law accounts for the voltage drop across the series resistance $R\Delta x$ and inductance $L\Delta x$, the voltage equilibrium from this equivalent circuit is:

$$v(x,t)-v(x+\Delta x,t)=R\Delta x\, i(x,t)+L\Delta x\frac{\partial i(x,t)}{\partial t} \tag{3.17}$$

And the current at node (n+1),

$$i(x,t)-i(x+\Delta x,t)=G\Delta x\, v(x+\Delta x,t)+C\Delta x\frac{\partial v(x+\Delta x,t)}{\partial t} \tag{3.18}$$

Substitute equation (3.17), and (3.18) by Δx, then when $\Delta x\rightarrow 0$, we obtain a differential equation

$$-\frac{\partial v(x,t)}{\partial x}=R\,i(x,t)+L\frac{\partial i(x,t)}{\partial t} \tag{3.19}$$

$$-\frac{\partial i(x,t)}{\partial x}=G\,v(x,t)+C\frac{\partial v(x,t)}{\partial t} \tag{3.20}$$

The first order differential equations given by equation (3.19) and (3.20) are the time-domain form of the **transmission-line equations** or otherwise known as the ***telegraph's equations***.

Except for the last section, our primary interest in this chapter is the steady-state conditions. To end this, we shall make use of phasors with cosine reference notation. Thus, we have defined following pair of equations:

$$v(x,t)=\Re\left[\tilde{V}(x)e^{j\omega t}\right] \tag{3.21}$$

$$v(x,t)=\Re\left[\tilde{I}(x)e^{j\omega t}\right] \tag{3.22}$$

where $\tilde{V}(x)$ and $\tilde{I}(x)$ are the phasor quantities of $v(x,t)$and $i(x,t)$, respectively, each of which may be real or complex. Upon substituting equation. (3.21) and (3.22) into equation. (3.19) and (3.20), and utilizing the property that ∂/∂t in the time domain becomes equivalent to multiplication by $j\omega$ in the phasor domain, we obtain the *telegraph's equations* in phase form:

$$-\frac{d\tilde{V}(x)}{dx} = (R + j\omega L)\tilde{I}(x) \tag{3.23}$$

$$-\frac{d\tilde{I}(x)}{dx} = (G + j\omega C)\tilde{V}(x) \tag{3.24}$$

These are the telegrapher's equations in phase form.

3.4.1.3 Wave Propagation on a Transmission Line

The two first-order coupled equations (3.23) and (3.24) can be combined to give two second order uncoupled equations, one for $\tilde{V}(x)$ and another for $\tilde{I}(x)$. The wave equation for $\tilde{V}(x)$ is derived by first differentiating both sides of equation (3.23) with respect to *x*, resulting in

$$\frac{\partial^2\tilde{V}(x)}{\partial x^2} = (R + j\omega L)\frac{\partial\tilde{I}(x)}{\partial x} \tag{3.25}$$

Then substituting equation (3.25) for $\partial\check{I}(x)/\partial x$, equation (3.25) becomes

$$\frac{\partial^2\tilde{V}(x)}{\partial x^2} - (R + j\omega L)(G + j\omega C)\tilde{V}(x) = 0 \tag{3.26}$$

or

$$\frac{\partial^2\tilde{V}(x)}{\partial x^2} - \gamma^2\tilde{V}(x) = 0 \tag{3.27}$$

where

$$\gamma = \sqrt{(R + j\omega L)(G + j\omega C)} \tag{3.28}$$

Applying of the same steps to equation (3.23) and (3.24), in reverse order lead to

$$\frac{\partial^2\tilde{I}(x)}{\partial x^2} - \gamma^2\tilde{I}(x) = 0 \tag{3.29}$$

The second-order differential equations (3.27) and (3.29) are called **wave equations** for $\tilde{V}(x)$ and $\tilde{I}(x)$, respectively, and γ is called the complex propagation constant of the transmission line. As such, γ consists of a real part α, called the attenuation constant of the line with units of Np/m, and an imaginary part β, called the phase constant of the line with units of rad/m. Thus,

$$\gamma = \alpha + j\beta \tag{3.30}$$

with

$$\alpha = \Re e\left(\sqrt{(R + j\omega L)(G + j\omega C)}\right) \tag{3.31}$$

$$\beta = \Im m\left(\sqrt{(R + j\omega L)(G + j\omega C)}\right) \tag{3.32}$$

The square-root solutions of equation (3.31) and (3.32) are chosen to have a positive values for α and β. For positive transmission lines, α is either zero or positive. Most transmission lines, and all those considered in this section, are f the positive type.

The wave equations (3.27) and (3.29) have traveling wave solutions of the following form:

$$\tilde{V}(x) = V_0^+ e^{-\gamma x} + V_0^- e^{\gamma x} \tag{3.33}$$

$$\tilde{I}(x) = I_0^+ e^{-\gamma x} + I_0^- e^{\gamma x} \tag{3.34}$$

The term $e^{-\gamma x}$ represents a wave propagating in the $+x$ direction while the $e^{\gamma x}$ represents a wave propagating in the $-x$ direction. I_0^- and I_0^+, to the voltage wave amplitudes, V_0^- and V_0^+ by using equation (3.33) in equation (3.34) and then solving for the current $\tilde{I}(x)$ to get the result

$$\tilde{I}(x) = \frac{\gamma}{R + j\omega L}\left[V_0^+ e^{-\gamma x} - V_0^- e^{\gamma x}\right] \tag{3.35}$$

Comparison of each term with the corresponding term in equation (3.34) leads us to conclude that

$$\frac{V_0^+}{I_0^+} = Z_0 = \frac{-V_0^-}{I_0^-} \tag{3.36}$$

where

$$Z_0 = \frac{R + j\omega L}{\gamma} = \sqrt{\frac{R + j\omega L}{G + j\omega C}} \tag{3.37}$$

is called the **characteristic impedance** of the line. This Z_0 is equal to the ratio of the voltage amplitude to the current amplitude for each of the traveling waves individually (with an additional minus sign in the of the $-x$ propagating wave), but it is not equal to the ratio if the total voltage $\tilde{V}(x)$ to the total current $\tilde{I}(x)$, unless one of the weaves is absent.

3.4.2 Simulation Approach

3.4.2.1 Time Delay of the Signal

As the partial discharge signal has to travel in a significant distance, the time delay of the signal has to be taken into account. Consider that the partial discharge appeared at the distance x from the measuring point x_{m}, the change in potential propagating along with the shield associated with the time delay $x_{\mathrm{m}} - x/c$ is shown in equation (3.38).

$$V_s(t) = V\left(t - \frac{x_m - x}{c}\right) \tag{3.38}$$

where c (m/μs) is the propagation velocity which takes place in the polyethylene of the cable insulation. x_{m} is the measuring point.

Assuming that the partial discharge signal is being generated over the interval Δx, hence, the time day of each signal in relation to where the partial discharge appeared is illustrated in the equivalent circuit as shown in Fig. 3.17.

3.4.2.2 Partial Discharge Pulse Propagation and Detection

During the propagation of partial discharge pulse through a cable, the signal attenuation and dispersion may take place. Distortion causes a change in pulse shape while the attenuation causes a change in pulse intensity. To analyze the cause of distortion and attenuation, we consider a model shown in Fig. 3.17.

The change in potential propagating along the shield electrode between the differential length x and $x + \Delta x$ is expressed as

$$V_s(\omega)\Delta x = V_0(\omega)e^{-j\beta_s(x_m - x)}\Delta x \tag{3.39}$$

where $V_s(\omega)$ is the change in potential between the differential length x and $x+\Delta x$ and β_{s} ($\beta_s=\omega/c_{\mathrm{s}}$) is the phase constant of a signal propagating through the shield electrode. In this particular case, the attenuation constant is neglected ($\alpha_s=0$). This change in potential propagates along the shield electrode between the target and reference cable toward the measuring point and its polarity depends on the point where the shield voltage appears.

Assuming that the transmission line has an infinite length, thus the total change in potential propagating along the shield electrode being measured at the measuring point x_{m} is expressed as

$$V_m(\omega) = \int_{-\infty}^{x_m} V_0(\omega)e^{-j\beta_s(x_m - x)}dx - \int_{x_m}^{\infty} V_0(\omega)e^{-j\beta_s(x_m - x)}\,dx \tag{3.40}$$

where $V_m(\omega)$ is the total change in potential at the measuring point x_{m}. The first part of the integral

with the positive polarity accounts for the change in potential appearing from the near end to the measuring point. The second part of the integral with the negative polarity accounts for the change in potential appearing from the measuring point to the far end. The factor $e^{-j\beta_s(x_m-x)}$ accounts for the attenuation while propagating along the shield electrode of the cable line. In this particular case, the characteristic impedance of the cable line and the impedance of the detecting impedance are different; therefore, the impedance calibration was also taken into consideration.

Finally, the detection voltage can be defined by means of the voltage divider as shown in equation (3.41).

$$V_D(\omega) = \frac{Z_D}{\frac{2}{j\omega C_p} + Z_D} V_m(\omega) \tag{3.41}$$

where $V_D(\omega)$ is the detection voltage between the target and the referent cable line. C_P is the coupling capacitor between the shield layer and an aluminum foil.

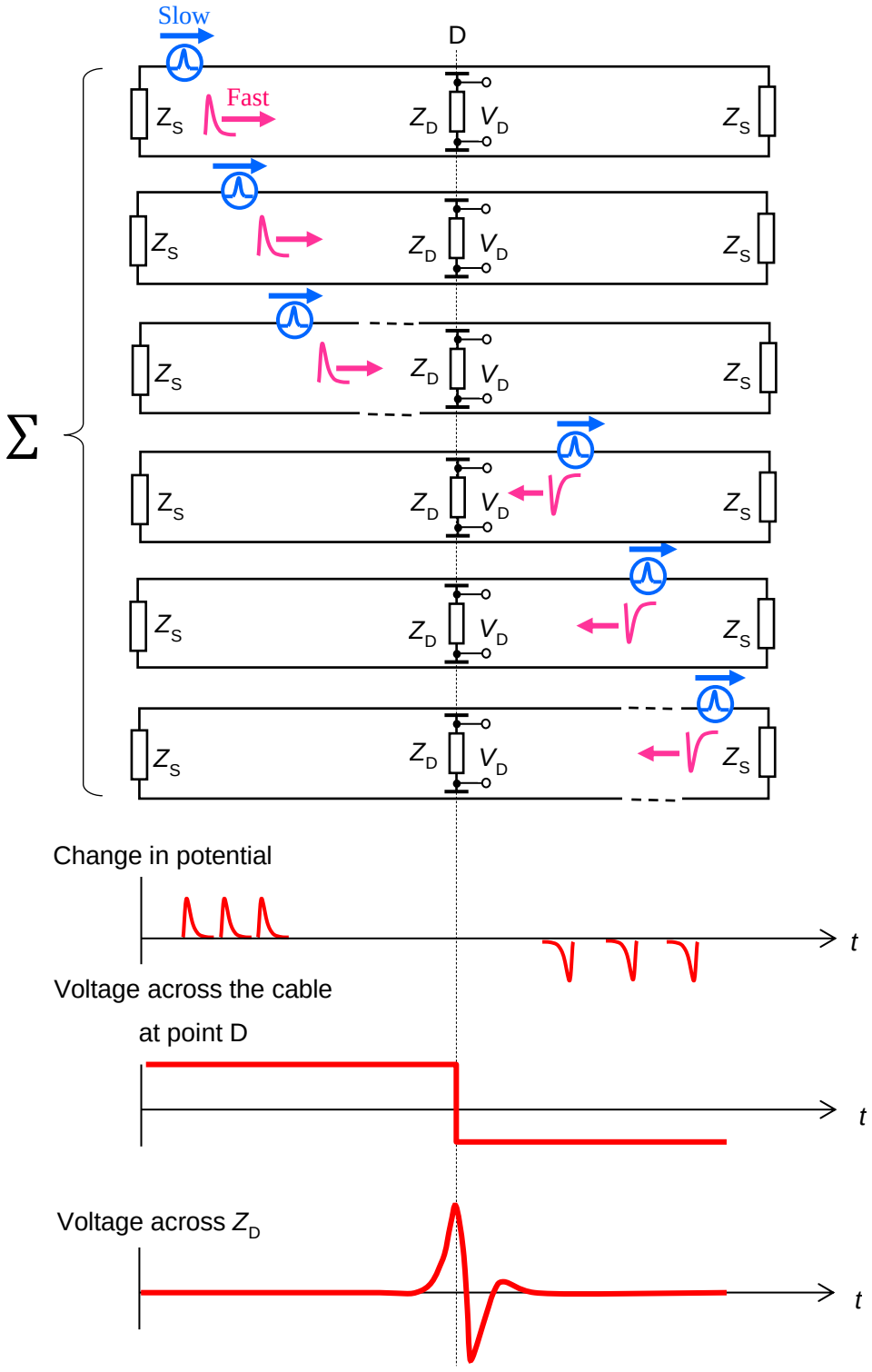

Fig. 3.17 Schematic diagram of a change in potential depending on where the partial discharge occurred.

3.4.3 Simulation using Communication Cable

A numerical simulation was performed in order to explain the partial discharge pulse propagation through the cable. This section gives details of a simulation of partial discharge pulse propagation and detection by using a communication cable. The change in potential along this cable is depending on the shin effect resistance of the shield electrode of the cable itself. This skin effect resistance is to be determined as follow.

3.4.3.1 Skin Effect Resistance

The cable unit DC resistance per length of the shielding layer of a coaxial cable (Fig. 3.18)is expressed as

$$R_{dc} = \frac{1}{n\cos\theta} \cdot \frac{\rho}{\pi(D/2)^2} \tag{3.42}$$

However, D is the wire diameter, θ is knitting angle of the wire, n is the number of wires. Since the AC resistance is influenced by the skin effect, it is greater than the DC resistance. Skin depth resistivity is ρ, magnetic permeability is μ and the angular velocity is ω,

$$d = \sqrt{\frac{2\rho}{\omega\mu}} \tag{3.43}$$

If the skin depth is thinner than the wire diameter, the resistance per cable unit length is approximately shown below

$$R_{ac} = \frac{1}{n\cos\theta} \cdot \frac{\rho}{d} \cdot \frac{1}{\pi(D-d)} \tag{3.44}$$

Copper as the material of the braided wire shielding layer with wire radius 0.2 mm, wire number 64, and the wire braid angle of 45 degrees, DC resistance becomes approximately 12 mΩ / m and it roughly coincides with the measured value. In contrast, AC resistance at 30 MHz is about 52 mΩ / m. The inductance of the shielding layer is considered to be offset because the reverse current flows through the core wire, considering that only the resistance component affects the return current, (3.8) equation's $Z_s(\omega)$ is replaced with $R_{\mathrm{ac}}(\omega)$ as shown below

$$V(\omega) = R_{ac}(\omega) I(\omega) c\Delta t \tag{3.45}$$

The change in potential generated along the shield electrode can be calculated by considering the impedance of the shield electrode itself. A dc per unit resistance of the shield electrode of an RG58A/U

cable is 12 mΩ/m. The resistance of the shield electrode is increased significantly at a higher frequency due to the skin effect. As reported in [16], the shield resistance is approximately 52 mΩ/m at 30 MHz. In this particular case, the current discharge was set to be 20 mA and the change in potential propagated through a coaxial cable at the speed of 200 m/μs. Substituting these parameters into equation (3.44), the change in potential along the shield electrode is 4.2 mV.

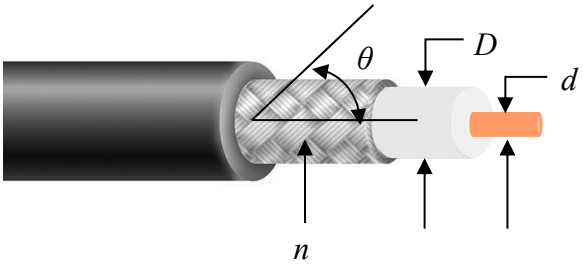

Fig. 3.18 Cut-view of a coaxial cable.

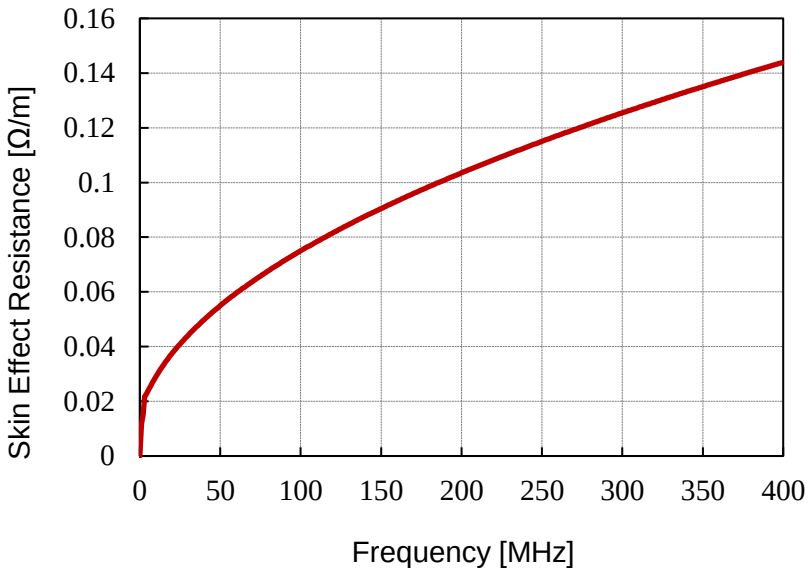

Fig. 3.19 Skin effect resistance of communication depending on frequency.

3.4.3.2 Simulation Result and Discussion

Fig. 3.20 shows the typical waveform of (a) the normalized partial discharge injection pulse waveform and (b) the normalized partial discharge detection waveform in long-distance cable line by using a capacitive coupling electrode. As shown in Fig. 3.20, a normalized injection pulse waveform with a rectangular waveform with a width of 20 ns was employed as a mimic partial discharge signal.

In this particular case, the 2 m long cable was charged to 1 V and the change in potential along the shield electrode of the cable was detected by a foil electrode of 20 cm in length.

Fig. 3.21 shows a normalized partial discharge detection waveform of the simulation and the measurement by using the capacitive coupling electrode. The detection waveform in the simulation was acquired as expressed in equation (3.41), and the measurement waveform was acquired using the detection circuit as shown in Fig. 3.17. As shown in Fig. 3.21, the simulation pulse waveform roughly agreed with the measurement result, although the measurement waveform is slightly sharper than the simulation, because of the high pass filter of the balun.

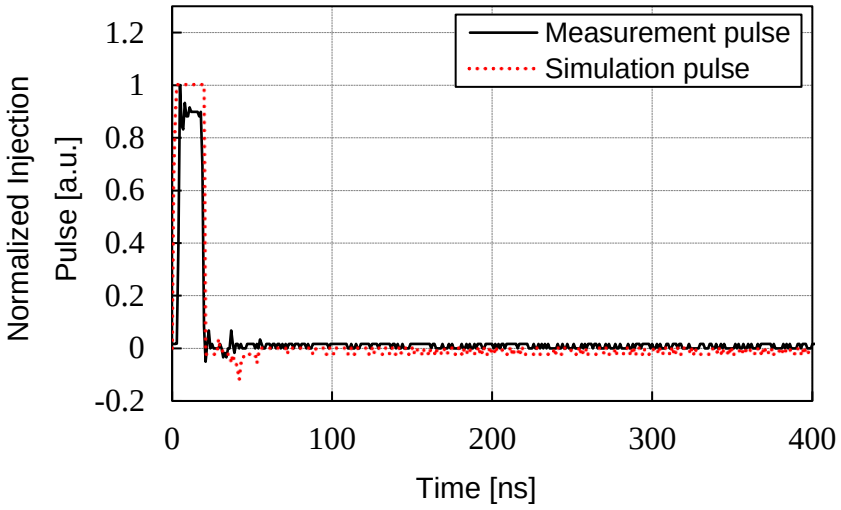

Fig. 3.20 Normalized injection pulse voltage [a.u.].

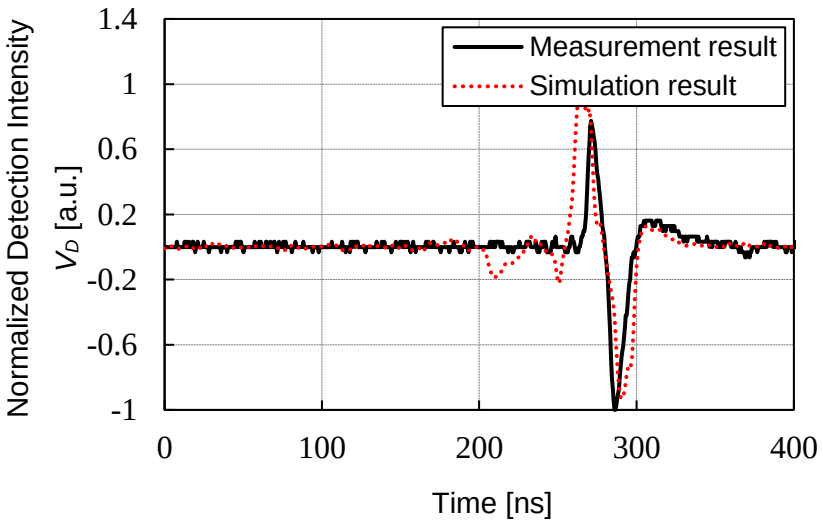

Fig. 3.21 Normalized detection intensity [a.u.].

3.4.4 Simulation using Full-Size Cable

This section provides a numerical simulation of partial discharge pulse propagation through a full-size cable. We studied the detection intensity of partial discharge characteristics for a power cable by the mean of skin effect resistance of the shield electrode of the cable itself.

3.4.4.1 Skin Effect Resistance

Fig. 3.22 shows the cut-view of the copper tape and skin depth of a full-size 6.6 kV XLPE cable. A copper tape with *w* in width and *h* in thickness were wrapped onto the cable in *D* diameter. The per-unit-length *l* of a shield electrode is expressed in equation (3.46).

$$l = \frac{1}{\tan\left(\sin^{-1}\frac{w}{\pi D}\right)} \tag{3.46}$$

Assuming that the contact resistance between the overlapping portions is larger than the resistance of the copper tape, and the copper tape is considered to be a flat conductor. At high frequency, the skin depth is thinner than the thickness of the shield electrode, therefore, the per-unit resistance of a shield electrode per cable length is approximated as:

$$R_{ac}(\omega) = \frac{\rho}{\tan\left(\sin^{-1}\frac{w}{\pi D}\right)} \cdot \frac{1}{2 \cdot \delta(\omega) \cdot w} \tag{3.47}$$

where ρ is the resistivity of the copper tape, and δ(ω) is the skin depth of the copper tape depending on the frequency. As expressed in equation (3.46), the value of $R_{ac}(\omega)$ depends on $\delta(\omega)$ which has a frequency dependency. At higher frequency, the value of this resistance is significantly increased at a higher frequency due to the skin effect (Fig. 3.23).

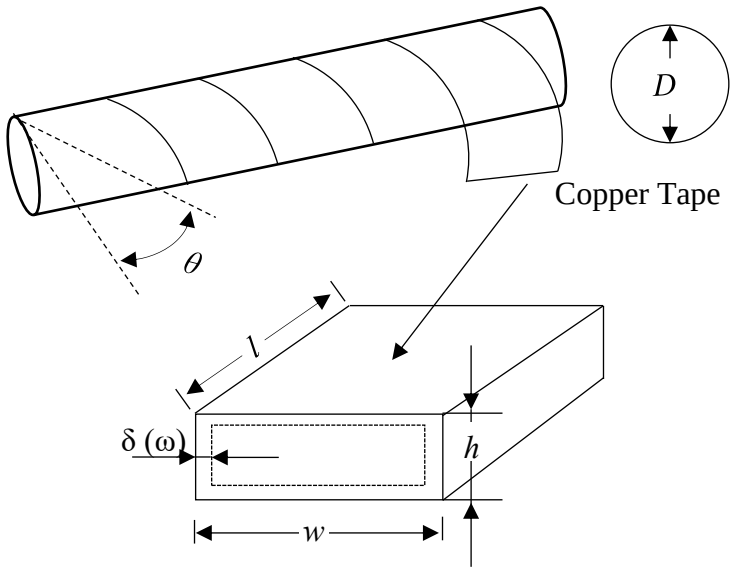

Fig. 3.22 A cut-view of the copper tape and skin depth of a full-size 6.6 XLPE cable.

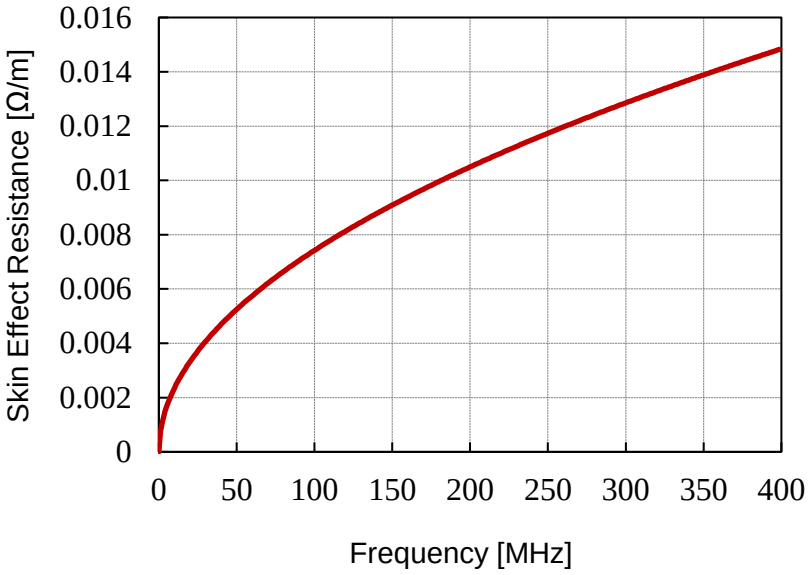

Fig. 3.23 Skin effect resistance of a full-size 6.6 kV XLPE cable depending on the frequency.

3.4.4.2 Simulation Result and Discussion

At 30 MHz, the shield electrode resistance of this cable is approximately 63.72 mΩ/m. In this particular case, a shield electrode of a 6.6 kV XLPE cable made of copper having 24 mm in diameter, 28 mm in width and 0.2 mm thickness was wrapped onto the cable.

In practice, the characteristic impedance of a 6.6 kV XLPE cable is approximately 25 Ω which is two times smaller than the coaxial cable. In such a case, when the same amount of discharge is being generated, the current flowing through a 6.6 kV XLPE is two times larger than the communication cable. Also, the skin effect impedance of a power cable is larger than the communication cable at the same frequency. Therefore, the change in change in potential along the shield electrode of a power cable is even further increased.

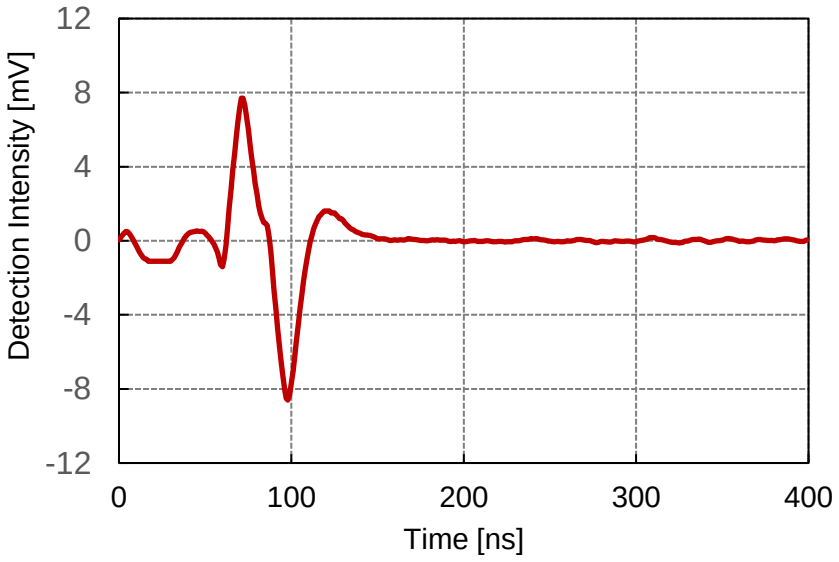

Fig. 3.24 Simulation and experimental result.

3.5 Improvement of Sensitivity and Its Validation

This section discussed the improvement of sensitivity and its validation of the proposed method. In this section, we evaluated the detection sensitivity between the partial discharge detection using a communication cable and a full-size cable. Also, we evaluated our proposed method to the existing partial discharge detection under differential installation conditions.

3.5.1 Detection Sensitivity Evaluation

Fig. 3.25 shows a comparison of detection intensity between communication cable and full-size cable using capacitive coupling method. In this particular case, the intensity of the partial discharge was adjusted by changing the input DC voltage [V] and the respective detection intensity was measured. As shown in Fig. 3.25, the partial discharge detection intensity of a communication has a higher detection intensity compared to the full-sized cable. The simulation results of both cases also show similar tendency to the measurement result.

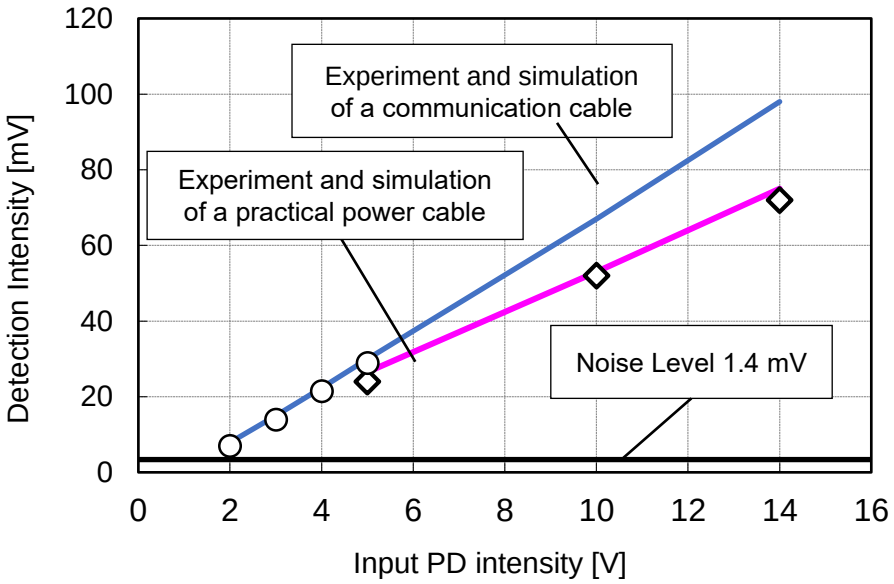

Fig. 3.25 Comparison of detection intensity between communication and full-size cable.

3.5.2 PD Measurement under Differential Installation Conditions

Fig. 3.26 shows a schematic diagram of partial discharge measurement for power cable under different installation conditions (a) terminal (b) insulation joint and main body (normal joint). In this particular case, the discharge current was set to propagate from the near end to the far end, the change in potential along the shield electrode was detected at the main body, insulation joint and terminal.

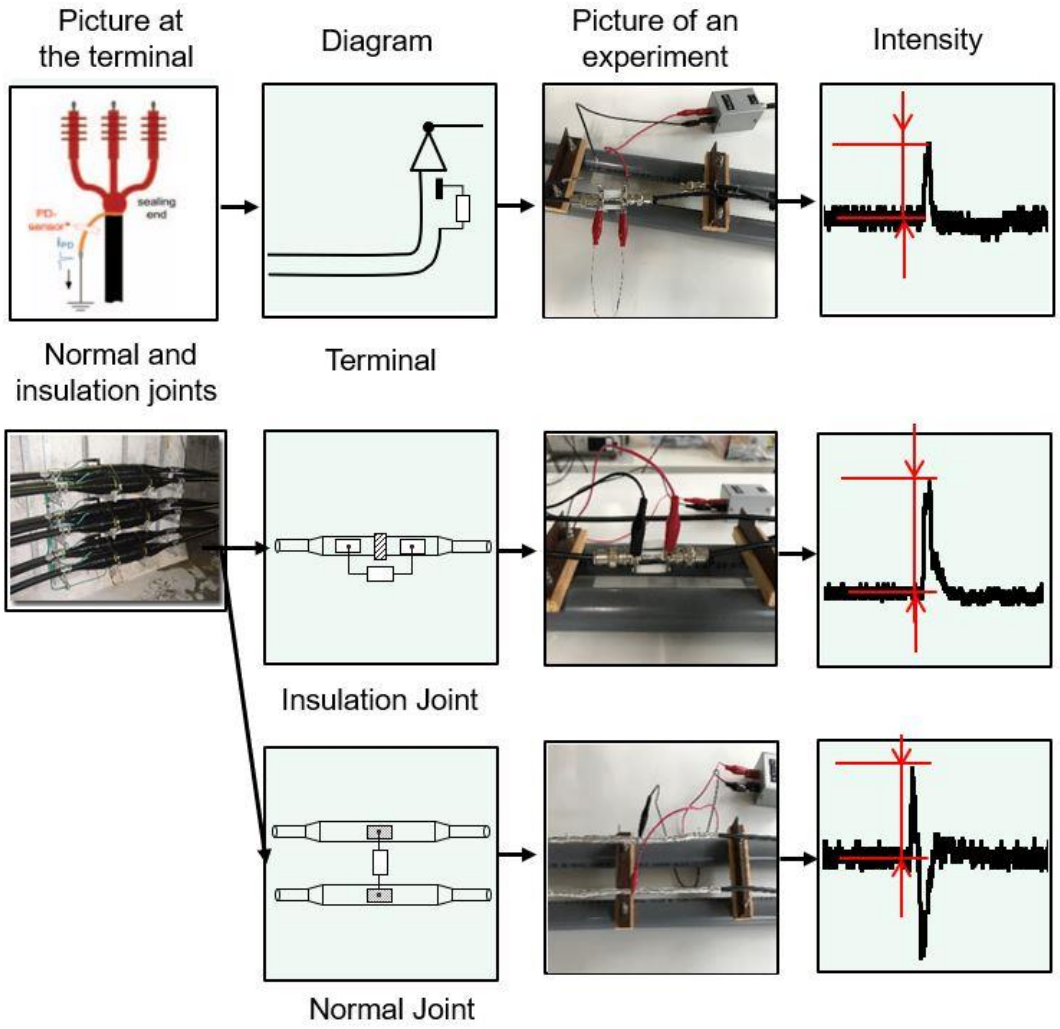

Fig. 3.26 A schematic diagram for partial discharge detection at (a) main body, (b) insulation joint and (c) terminal.

Fig. 3.27 shows the partial discharge detection intensity at the main body, IJ, and terminal depending on the calibration charge. In the measurement, the signal was compared with the noise level, and the detection sensitivity was determined. As shown in Fig. 3.27, the detection sensitivities of partial discharge detection intensity at the main body, terminal, and IJ were 100 pC, 10 pC, 1 pC respectively. In this particular case, we assumed that the detection limit should be twice as high as the noise level the sensitivity is supposed to be determined with 6 dB in S/N ratio. The limitation of the measurement was about 100 pC, which was far poorer than the measurement at IJ (as low as 1 pC [11]).

In some cases, the origin of the partial discharge is likely to be located in some distances away from the terminal or IJ, leading to the difficulty in detection due to attenuation after propagating through a long distance. In such a case, the proposed method is very advantageous, because the partial discharge can be detected at the point where the partial discharge is being generated. Therefore, the partial discharge measurement is feasible at any point of the main body or normal joint (if only a significant reduction in sensitivity compared with the measurement at the IJ can be accepted). Also, the proposed method has a simple system which makes it easy to perform a measurement, because only an aluminum foil electrode and balun are required.

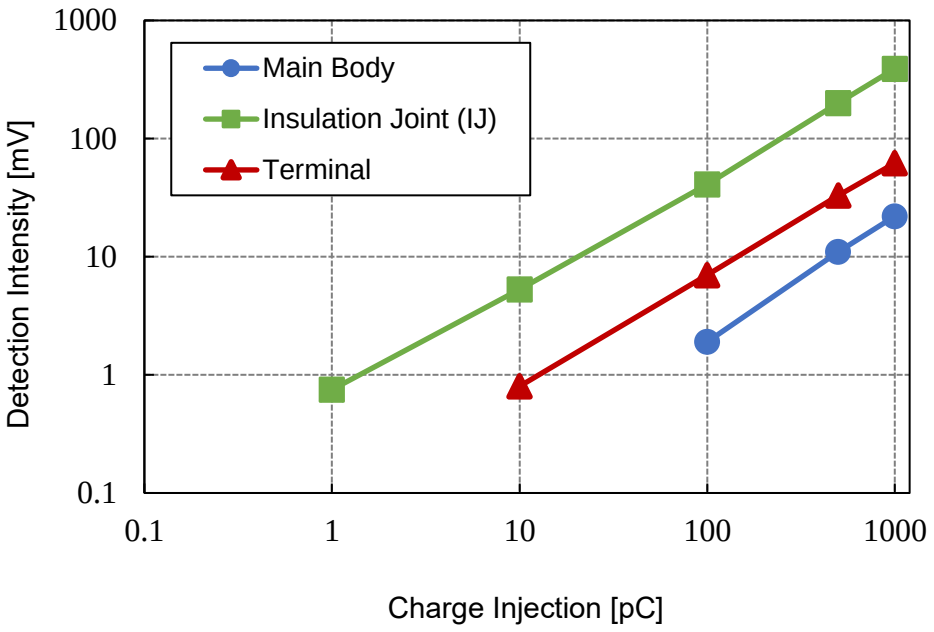

Fig. 3.27 A partial discharge detection intensity at normal part (normal joint), insulation joint (IJ) and terminal depending on the calibration charge (pC).

3.6 PD Monitoring Instrument

3.6.1 General Concept

More than 40 years have passed since the use of cross-linked polyethylene cable, and it is also used for exclusive high-voltage lines of 22 kV class or higher. Some of these are approaching the design life and it is desirable to renew them under appropriate judgement. On the other hand, aside from the request for the low cost of electric power equipment, we want to continue to use what can still be used as much as possible. Partial discharge measurement is performed as a diagnostic method to estimate the soundness of the cable line. Below we will describe the transition and the current situation of partial discharge measurement of continuous vulcanization (CV) cable.

Based on the above background, we decided to design and prototype inexpensive partial discharge monitoring equipment. The concept of the system is shown below.

- It is attached individually to all monitored parts, and it is inexpensive. (Target: system production cost less than 100,000 yen).
- Although high-frequency CT frequently used for the sensing part has high sensitivity, it is expensive (about several hundred thousand yen), so it is necessary to develop an inexpensive detection sensor. The foil electrode method is relatively inexpensive, but measures against surge are necessary. In this research, we aim at designing and prototyping a device that issues an alarm when input is obtained, without considering the sensor part.
- To simplify the configuration as much as possible, to reduce the cost of the electronic circuit of the measurement part as well.
- Operate when a signal that is equal to or greater than the threshold value is detected.
- Partial discharge information such as phase, charge amount, discharge number is unnecessary.
- In consideration of reaction to noise, no storage function is provided. Operate only when partial discharge occurs.
- When the signal is detected, the indicator on the site turned on.

3.6.2 Schematic Diagram and Instrument Prototype

The partial discharge pulse is a single peak pulse with a width of about 20 ns in general. Since it can have both positive and negative polarity, it is normally detected (rectified) and converted into a voltage of one polarity. Even when it is detected by a resonator having an appropriate resonance frequency, the polarity fluctuates between positive and negative. The waveform after detection becomes the envelope curve of the pulse waveform, but if it takes a longer time constant, it becomes a long attenuation signal of the tail. This waveform is amplified and used as a trigger signal. By blinking the light emitting diode with its output, each partial discharge can be visually recognized.

Fig. 3.28 shows the circuit diagram for the prototype and Fig. 3.29 shows the front view of the instrument. As you can see, there is 9 LED on the device which holds three sets of the different threshold value, 0.5 V, 1.0 V and 1.5 V from the left. The first LED from the right shows 10, 1000 and 100 000 of pulse count respectively for each set.

The existing components in the circuit are shown below.

- Detector circuit: a full-wave rectifier circuit. A bias is added to compensate for the onset voltage of the diode.
- Smoothing circuit: smooth the waveform after diode detection. 100 pF is the equivalent gate-source capacitance. The time constant is about 10 μs, but the actual wave tail length is shorter than this.
- Amplifier circuit: when positive voltage is applied to the gate of 2SK241, the output changes to the negative direction. A 500 Ω resistor is used for current feedback. Since the mutual conductance of 2SK241 is about 10 ms, an amplification factor of about 20 times is obtained.
- Pulse stretching circuit: a 555 timer IC is used to output a square wave pulse of about 50 ms per partial discharge pulse. When the voltage at the TR terminal falls below 1/3 of the supply voltage, the trigger operates. The operation level can be adjusted by changing the bias voltage of the TR terminal with a variable resistor.
- Output: the output of the pulse stretching circuit is output to the panel, and the light emitting diode is operated through the control transistor.

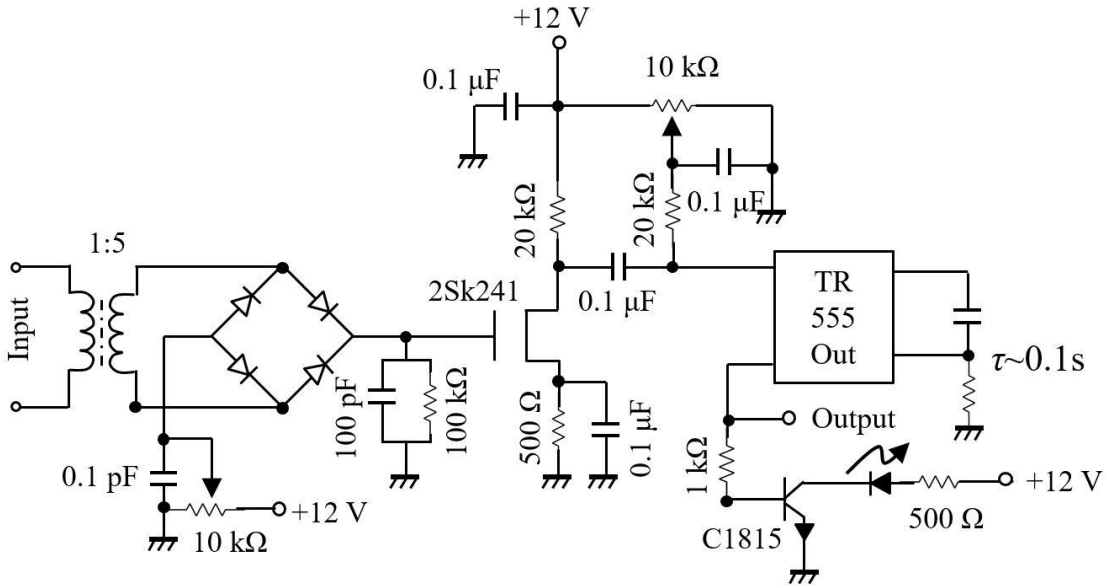

Fig. 3.28 Schematic diagram of the monitoring device.

Fig. 3.29 A monitoring device for partial discharge detection front view of the monitoring device.

3.6.3 Sensitivity Evaluation and On-Site PD Observation

The detection limit of the circuit fabricated this time was about 200 mV in terms of input. Assuming that the time width of the partial discharge pulse is about 20 ns, the current is 50 μA when 1 pC of charge flows during this period. Since the winding ratio of commonly used high-frequency CT is 1: 50 and the load resistance is set to 50 Ω, the current is directly converted to the voltage and a voltage of 50 μV is generated. The detection limit of 200 mV corresponds to 4000 pC. In the case of a foil electrode, if the surge impedance is 20 Ω, the current of 50 μA is converted to a voltage of approximately 1 mV when discharge is occurring at the terminal, so the detection limit of 200 mV corresponds to approximately 200 pC. However, since the voltage amplification factor of the circuit used this time is at most about 20 times, it is considered sufficient to improve this instrument further.

The operation of the partial discharge detection device was conducted in Riemon Substation of Chubu electric power company. The partial discharge detection device was attached to the insulation cylinder EB-G and the operation of the detection device was confirmed (Fig. 3.30). After that, the detection device was left mounted on the EB-G frame for several days and the operation of the cumulative display was checked at the time of removal. The first LED lights up, which means only 10 counts of the pulse was detected. We assume that the first LED lights up because of the switching surge or noise from outside the cable and since it was not continuous, even though the LED lights up the line is considered safe. An oscilloscope was used to confirm the detected pulse, and there was no partial discharge pulse seen except for switching noise.

Fig. 3.30 Riemon branch line at end EB-G.

3.7 Conclusions

We have developed a new diagnostic method that can detect and approach the location of partial discharge site the normal joint or any point along the main body of the cable line by considering the longitudinal cable shield impedance itself. The method assumed that the screen shield is not a perfect conductor and that change in potential would be seen as the partial discharge signal propagates through the cable line. As the partial discharge accompanied by high-frequency components, thus this change in potential is very significant. This change in potential can be detected by newly proposed capacitive coupling between an additional foil electrode and the cable shield electrode itself.

Experiments of communication and full-sized 6.6 kV XLPE cables were performed using mimic partial discharge to confirm the feasibility of the proposed method. Also, the numerical simulation of partial discharge current pulse propagation through the cables was performed by considering the skin effect of the cable shield impedance. After, the detection sensitivity of the proposed method was evaluated using partial discharge measurement under differential installation conditions. Finally, the detail of a simple partial discharge monitoring device was successfully developed.

Under the specific conditions described in this paper, our conclusions are as follows:

(a) It was confirmed that the new partial discharge measurement method is feasible at the NJ or any point along the main body of the communication cable line. In the experiment, the signal was compared with the noise level and the sensitivity was finally determined as 400 pC as the detection limit. We assumed that the detection limit should be twice as high as the noise level the sensitivity is supposed to be determined with 6 dB in S/N ratio.

(b) We have conducted using a full-size 6.6 kV XLPE cable and a significant partial discharge intensity was detected. This suggested that the proposed method is feasible for applying to the full-size cable, although there was a reduction in detection intensity.

(c) Numerical simulation using communication and full-size 6.6 kV XLPE cable were performed in the same manner to the actual measurement systems. The results showed that the simulation and experiment have similar waveform and intensity.

(d) The detection sensitivity of the proposed method was evaluated based on the existing partial discharge detection methods under the differential installation conditions. It was suggested that the detection limit of the proposed method was approximately 30 times lower than the insulation joint.

(e) A simple partial discharge monitoring device was successfully developed, and its performance was satisfactory in term of low cost and its versatility. Since the voltage amplification factor of the circuit used this time is at most about 20 times, it is considered sufficient to further improve this instrument.

References

[1] T. Okamoto; M. Kanegami; N. Hozumi; M. Ikeda: "Partial Discharge Endurance Life of Polymer Insulating Materials at High Temperature", Electrical Engineering Japan, Vol. 126, No. 1, pp.15-22, Jan 1999.

[2] C. Mayoux, C. Laurent: "Contribution of Partial Discharges to Electrical Breakdown of Solid Insulating Materials", *IEEE Trans. Dielectr. Electr. Insul*, Vol. 2, No. 4, pp.641-652, Aug 1995.

[3] H. Ohno, G. Katsuta, R.Sakaguchi, Y.Ebinuma, N. Sakai, A.Nagaoka: "Influence of defects on insulating properties of XLPE cable", *Proceedings of the 3rd International Conference on Properties and Applications of Dielectric Materials*, Vol. 1, pp.485-489, Jul 1991.

[4] M. G. Danikas: "Small Partial Discharges and their Role in Insulation Deterioration", *IEEE Trans. Dielectr. Electr. Insul*, Vol. 4, No. 6, pp.863-867, Dec 1997.

[5] S.A. Boggs: "Partial Discharge-Part III: Cavity-Induced PD in Solid Dielectrics", *IEEE Trans. Electr. Insul*, Vol. 6, No. 6, pp.11-20, Nov./Dec 1990.

[6] S. Gutiérrez, I. Sancho, L. Fontán and J. De Nó: "Effect of protrusions in HVDC cables", *IEEE Trans. Dielectr. Electr. Insul*, Vol. 19, No. 5, pp.1774-1781, Oct 2012.

[7] Y. Iwashita, T. Kurihara, T. Takahashi, and T. Okamoto: "Partial Discharge Characteristics of Oil Impregnated Insulation System with an Oil Gap under Continuous AC Voltage Application", *Conference Proceeding of ISEIM*, pp.212-215, Jun 2014.

[8] M. M. Yaacob, M. A. Alsaedi, J. R. Rashed, A. M. Dakhil, S. F. Atyah, "Review on partial discharge detection techniques related to high voltage power equipment using different sensors", *Photonic Sensors*, Vol. 4, No. 4, pp. 325-337, Sep 2014.

[9] G. Chen, J. Tao, Y. Ma, H. FU, Y. Liu, Z. Zhou, C. Huang, C. Guo, "On-site Portable Partial Discharge Detection Applied to Power Cables Using HFCT and UHF methods", *WSEAS Transactions on Circuits and Systems*, Vol. 15, pp. 83-90, 2016.

[10] G. Katsuta, A. Toya, et al: "Development of a new detection method of partial discharge for Extra-High voltage cross-linked polyethylene insulated cable lines", *IEEE Trans. Power Delivery*, Vol. 7, No. 3, pp. 1068-1079, Jul 1992.

[11] E. F. Vance: "Shielding Effectiveness of Braided Wire Shields", *IEEE Trans. Electromagn. Compat*., Vol. EMC-17, No. 2, pp. 71-77, Apr 1975.

[12] S. A. Schelkunoff: "The Electromagnetic Theory of Coaxial Transmission Lines and Cylindrical Shields", *Bell System Tech. J*., Vol. 13, pp. 532-579, Oct, 1934.

[13] R. Papazyan, R. Eriksson, "Calibration for time domain propagation constant measurements on power cables", *IEEE Trans. Instrum. Meas.*, Vol. 52, No. 2, pp. 415-418, Apr. 2003.

[14] S. Boggs, A. Pathak and P. Walker: “Partial discharge XXII: high frequency attenuation in shielded solid dielectric power cable and implication thereof for PD location”, *IEEE Electr. Insul. Mag*., Vol. 12, No. 1, pp. 9-16, Jan./Feb1996.

[15] T. F. Ulaby and U. Ravaioli, Fundamentals of Applied Electromagnetics. New Jersey, USA:

Pearson, 2004, Ch. 2: Transmission Lines, pp. 40-100, 2015.

[16] R. Nhet, N.S. Mustafa, T. Kawashima, Y. Murakami, N. Hozumi "Development of Partial Discharge Measuring Method for Long-Distance Cable Line", *IEEJ Transaction on Fundamentals and Materials*, Vol.14, No.7, pp.996-1001, Jul 2019.

Chapter 4: Diagnostic Method for Water Tree Ageing XLPE Cable

4.1 Introduction

Insulation parts of underground cables deteriorate with time, which leads to failure. This problem is caused by many reasons, particularly “water tree degradation” [1][2]. Water trees have a shape of a tree and will evolve in a place where water and electric field concentration exist [3][4]. Water tree degradation influences the dielectric performance of XLPE cable, such as its breakdown strength [5]. Therefore, a diagnosis method for water tree degradation is necessary.

Several techniques have been developed to measure water tree degradation. The detail of these methods is described in chapter 2 (section 2.5.2). Among these methods, the residual charge method has been widely used to measure water tree degradation [6]. Gaining some enlightenment for residual charge method [7], Kurihara et al. developed a residual charge method using pulse voltage application. The measurement principle of this method is similar to the conventional residual charge that water-tree. In this method, the pulse voltages are used for rapid charge accumulation and also the release of the residual charge instead of DC and AC voltages; which provides a major improvement compared to the conventional residual charge method in term of light weight and low operating cost. However, the obtained result can only show the degree of degradation making it difficult to identify the degradation points in the cable.

We propose to detect water tree degradation by applying biasing (poling) and probing pulse voltages. The water tree is once poled to create stable space charge in the vicinity of a water tree, and the response to the probing pulse is compared with the response to the same pulse without the space charge. The principal of this method is similar to the conventional residual charge in the point that water-tree is poled by DC to form the space charge. However, the pulse voltage is used to release the deeply trapped charge instead of AC application. We believe that using only pulse and DC voltage sources, compact and light equipment will be realized.

4.2 Measurement Principle

Principle of the measurement is shown in Fig. 4.1. A bias voltage is applied to the conductor as the first step. This bias voltage is defined as "poling bias". In this particular case, as the poling bias is negative, and the water tree is generated from the shield side, the tip of the water tree is poled positive.

After removing the poling bias, the "depolarizing pulse", its polarity being opposite to that of the poling bias, is applied. The pulse voltage propagates along the cable, generating subsequent echoes depending on mismatching at such as joints, bending spots, and the terminal. At the same time, the charge, trapped at the water tree during the poling process, is released and generates an echo. As a result, the acquired echo signal is composed of those relevant and non-relevant to the degradation.

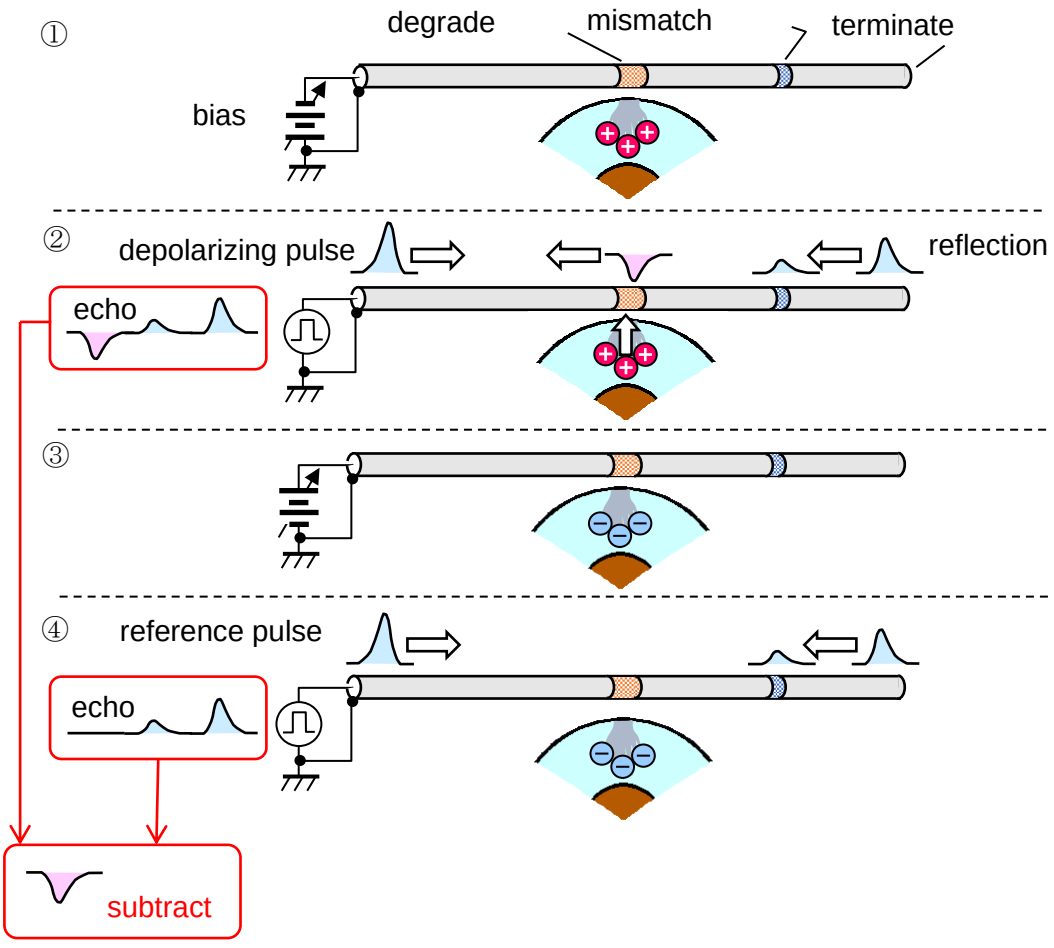

Fig. 4.1 Measurement principle of the charge radar method.

In order to discriminate the degradation signal, a depolarizing bias voltage with the opposite polarity (positive in this case) is applied. This bias voltage removes the charge at the water tree and may give the charge with opposite polarity (negative in this case). Finally, the "reference pulse", its polarity is the same as that of the depolarizing pulse, is applied, and the echo signal is acquired again. At this time, as the water tree is poled negative, charges are not released by the reference pulse. Consequently, only echoes by mismatching are detected. The responses to the depolarizing pulse and reference pulse are compared to cancel the echoes by mismatching, and degradation signal is finally extracted.

The responses to the depolarizing pulse and reference pulse are compared to cancel the echoes by mismatching, and degradation signal is finally extracted. It could be understood that the non-linear response at the water tree region depends on the biasing prior to the pulse application, whereas linear response due to normal mismatching such as bending, jointing and terminating does not change as long as the transmitted pulse shape is identical. One can also understand such as "a non-linear mismatching takes place where water trees are existent and detected by canceling linear mismatching".

4.3 Experimental Using Communication Cable with Water Tree

4.3.1 Sample preparation

A coaxial communication cable (RG-58A/U) of 50 Ω in characteristic impedance was employed as the specimen. The thickness of its insulation layer was about 1 mm. 5 m of the cable was subjected to the degradation process. After removing the jacket and shield layers, a spiral knife cut, approximately 1 mm in pitch and 0.3 mm in depth, was made around the insulation layer. The cable core was soaked with 1 mol/l of saline solution, and an AC voltage of 1 kHz, 5 kV (rms) was applied between the conductor and saline solution for 4 days. After this ageing process, it was found that a large number of water trees, about 0.5 mm in average length, were generated from the tip of the knife cut. The cross section of the cable core is shown in Fig. 4.2.

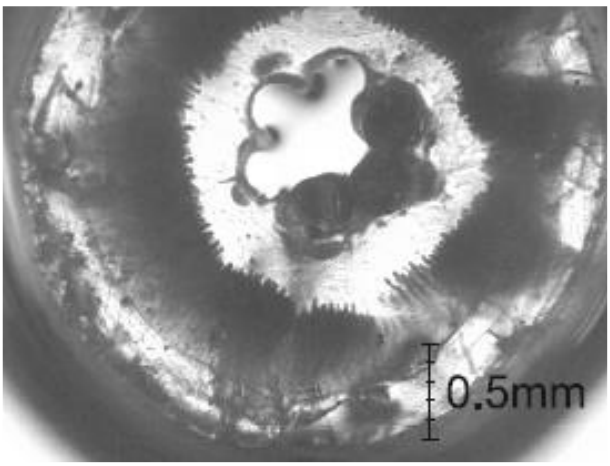

Fig. 4.2 A cut view of the measured sample.

4.3.2 Experimental Setup and Pulse Propagation

Fig. 4.3 shows the circuit for measurement using a high-frequency current transformer (CT) for detecting the signal. A target cable and a reference cable are coupled to the CT in the same manner, the direction of the coupling being opposite together. These cables are connected in parallel, and the bias and pulse voltages are applied to these cables. When a pulse voltage is applied, a large surge current, as well as reflection current, flows into or out of the cables, both of which may be detected as a large signal. However, as two cables are oppositely coupled to the CT, these signals are cancelled. On the other hand, the signal attributed to the degradation comes back from only the target cable; the signal is not cancelled. The degradation signal can thus be detected with a high S / N ratio.

A reference cable, which is non-degraded and the same length as the target cable, was employed in this experiment. This reference cable is supposed to arise no degradation signal because it is a new one. However even the cable is degraded with water trees, the degradation signal would not arise when the poling bias voltage has not been applied. Therefore, a degraded cable can also be used as the reference cable. So, if one phase of a cable line is chosen as a target of diagnosis, one phase of the rest can be employed as the reference, not depending on if it is degraded or not.

In the measurement, a water tree degraded cable with 5 m in length was inserted in the middle of the non-degraded 400-m-long cable. The total length was therefore 405 m, the degraded span being 200 - 205 m from the terminal.

Bias and pulse voltages were applied using the sequence shown in Fig. 4.4. The poling bias was applied to the target cable; subsequently, a depolarizing pulse was applied and reflection signal (target signal) was acquired. Afterward, the depolarizing bias was applied to the target cable with the same manner as the poling bias but for its polarity. The reference pulse was then applied to acquire the reference signal. The reference signal was subtracted from the target signal to obtain the degradation signal. In order to upgrade the S/N ratio, the sequence was repeated for several times (up to 20 times) and the obtained signals were averaged in the time domain.

After charging a capacitor with high voltage, the semiconductor switch, its rated voltage and current being 12 kV and 400 A respectively, was closed for 0.5 μs to generate a high voltage pulse. As no matching is taken at the far end comes back to the near end. As the cable as long as 400 m, the pulse comes back 4 μs later, assuming that the pulse propagation speed is 200 m/μs. Because the semiconductor switch is open at this moment, the pulse is not affected by the switching circuit and propagates to the other cable (i.e., reflection from the target cable propagates to the reference cable, and *vice versa*.

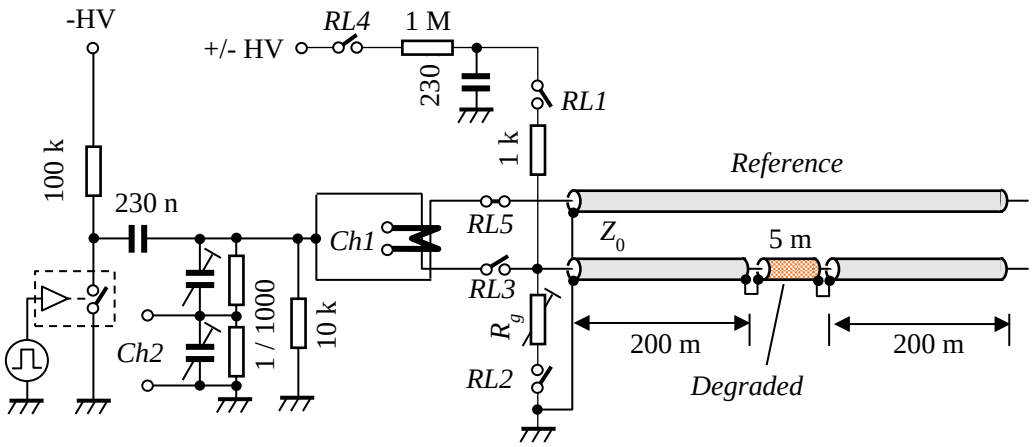

Fig. 4.3 Measurement system for residual charge method under pulse voltage applications.

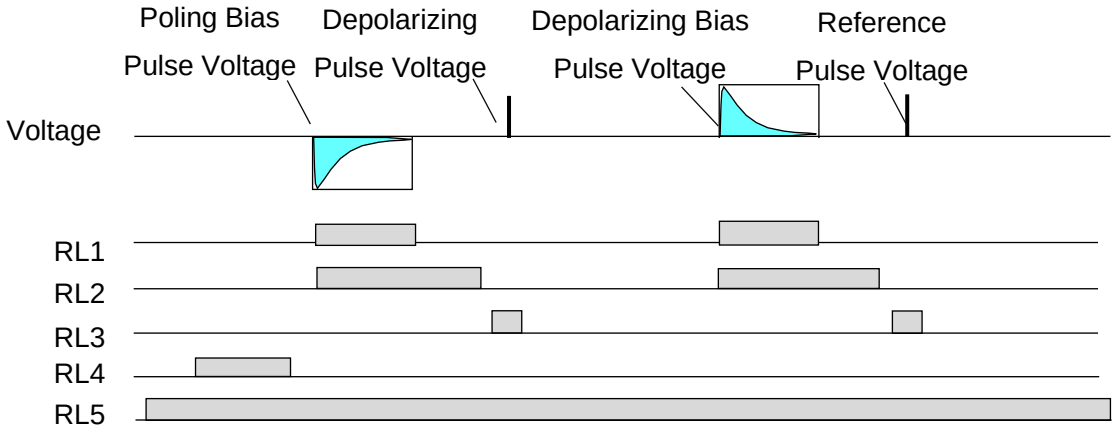

Fig. 4.4 Schematic diagrams of sequence of applied pulse voltage and DC bias voltage.

Let us assume that the degradation is located at one point, and released charge by a pulse of Δt in width is q. A current source of $q/\Delta t$ appears at the degraded point. This brings current pulses propagating towards the opposite direction, each intensity being $q/2\Delta t$. As a current pulse is coupled with twice at the CT, a current pulse equivalent to the $q/\Delta t$ in intensity was finally detected. Assuming that the released charge intensity is as much as 10 nC, a current pulse of 20 mA in intensity expected to be detected by 0.5 μs-wide pulse voltage.

Let the depolarizing current at time t, and distance x_m from the near end terminal be $i_d(x_d,t)$. This current component arises the waves propagate to both directions. The current wave $i_p(x,t)$ that propagates to the near end can be described as

$$i_p(x,t) = \frac{1}{2}\int_x^l i_d\left(x_d, t - \frac{x_d - x}{c}\right) dx_d \tag{4.1}$$

where x is the distance from the near end. The detected current at near end $(x=0)$ is

$$i_p(x,t) = \frac{1}{2}\int_x^l i_d\left(x_d, t - \frac{x_d}{c}\right) dx_d \tag{4.2}$$

The integration of i_p along time is corresponded to the total released charge due to the depolarizing,

$$Q = 2\int_0^\infty i_p(x,t)dt = 2\int_0^\infty \int_x^l i_d\left(x_d, t - \frac{x_d}{c}\right) dx_d dt \tag{4.3}$$

In case, the degradation is localized at one point, the detected current at the near end is represented as

$$i_p(0,t) = \frac{1}{2} i_d\left(x_d, t - \frac{x_d}{c}\right) \tag{4.4}$$

Hence

$$Q = 2\int_0^\infty i_p(0,t)\,dt = 2\int_0^\infty i_d\left(x_d, t - \frac{x_d}{c}\right) dt \tag{4.5}$$

is corresponded to the released charge due to depolarizing at the degraded point.

4.3.3 Experimental Results

Fig. 4.5 shows a typical result of the measurement. A voltage pulse of 6 kV is applied. The pulse propagates to the far end, be reflected, and comes back to the near end (waveform (a)). There is a time-lag of about 4 μs between the transmitted and reflected pulses. The reflected pulses from both target and reference cables are overlapped at the near end, so the reflected pulse voltage looks larger in spite of the expected attenuation after propagating thorough 800 m. Waveforms (b) and (c) are the current responses to the depolarizing and reference pulses, respectively. These two waveforms look very similar; however, the waveform (d) appears when the waveform (c) is subtracted from the waveform (b). In the waveform (d), a clear peak, of which rising point is 2.1 μs behind the first pulse in waveform (a), is seen (at 4.8 μs in the time axis). As the surge propagation speed through such a communication cable is as fast as 200 m/μs, this delay time corresponds to 210 m in the distance, which briefly coincides the distance to the degraded point.

Although it is not of practical importance, it may be interesting that the second peak appears with a delay of about 2.2 μs from the first. The degradation signal propagates towards the far end as well. This signal is superposed to the high voltage pulse, which also propagates towards the far end. These waveform components are reflected at the far end, and come back to the near end. During this propagation, a high voltage pulse is applied to the degradation point again. A degradation signal may be produced again at this moment. This would be the reason why the second peak is as high as the first, in spite that a substantial attenuation for the second is expected.

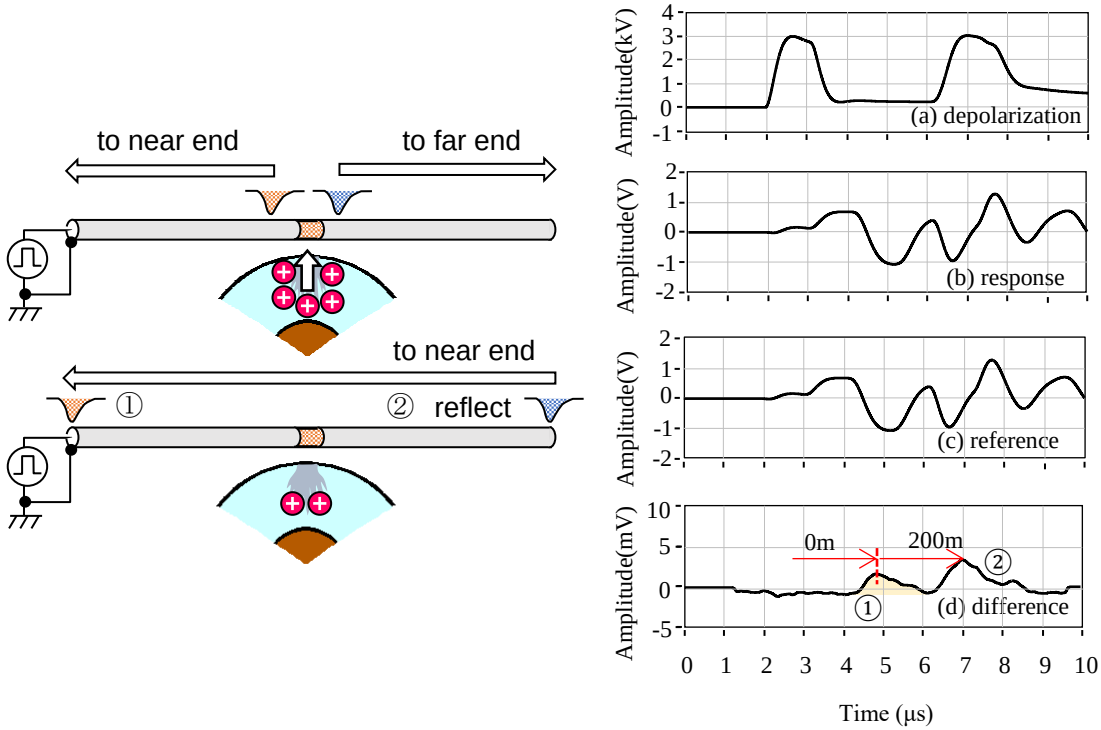

Fig. 4.5 A typical measurement result of charge radar method: bias -3 kV, 2 ms, pulse: +3 kV, 1 μs.

4.3.3.1 Correction Waveform

As the CT has specific frequency dependence, the waveform shown in Fig. 4.5(d) would be distorted. This distortion can be corrected if the transfer function of the measurement system is known. In order to clarify the transfer function of the measurement system, a non-degraded 400 m long cable, which was identical to the target cable, was applied with a 2 μs-width pulse voltage. Both voltage and current waveforms were recorded. The current response, measured by the CT, was converted to a voltage by the termination resistance with 50 Ω. As the pulse voltage was reflected at the far end, two peaks appeared. The response corresponding to the first peak was the rush current to the equivalent resistance of 50 Ω, the resistance being the same as the characteristic impedance of the cable. So, the current is able to be calculated by dividing the pulse voltage by 50 Ω. This part of the response and corresponding voltage waveform were extracted by using an appropriate window function.

Assume that the reference cable is semi-infinitive in length, and the current response to the applied voltage $v_{ref}(t)$ is $i_{ref}(t)$, and that the transfer function of the measurement system (from the current transformer to the measurement equipment) $h(t)$, the detected current waveform is represented as

$$i'(t) = \int_{-\infty}^{\infty} h(t) i'(t-\tau) d\tau \tag{4.6}$$

This waveform can be measured. The impedance of the cable can be recognized as a lumped impedance corresponding to the characteristic impedance Z_0. Therefore, if the applied voltage waveform is known, the "true" current waveform can be calculated as

$$i(t) = \frac{v(t)}{Z_0} \tag{4.7}$$

The transfer function of the measurement system can be represented in the frequency domain as

$$H(\omega) = \frac{I'(\omega)}{I(\omega)} \tag{4.8}$$

where $I_{ref}'(\omega)$, $H(\omega)$, and $I_{ref}(\omega)$, are Fourier transform of the corresponding functions. If $H(\omega)$ is known by the experiment with the reference cable, the waveform for the cable with degradation (target cable) can be corrected in the frequency domain that

$$I(\omega) = \frac{I'(\omega)}{H(\omega)} \tag{4.9}$$

Inverse Fourier transform of $I(\omega)$, gives the corrected waveform in the time domain.

Fig. 4.7 shows the result of this deconvolution process. Two well-defined peaks with negative polarity appear in the corrected waveform, the position of peaks corresponding to about 200 m and 400 m, respectively. As the poling bias voltage was negative, the polarity of the peak is negative as well. One at 200 m in the equivalent distance is the direct signal, and the other at 400 m is the signal due to reflection at the far end. The charge intensity can be calculated by integrating the waveform. In this particular case, it was as much as 14.4 nC. The half width of the peak is corresponding to about 50 m, suggesting that a sufficient resolution is realized. The second peak at 400 m may disturb the diagnosis when the degradation point is close to the far end. This may be removed if the far end is terminated by an appropriate terminator, or brought behind if an appropriate delay line is connected to the far end.

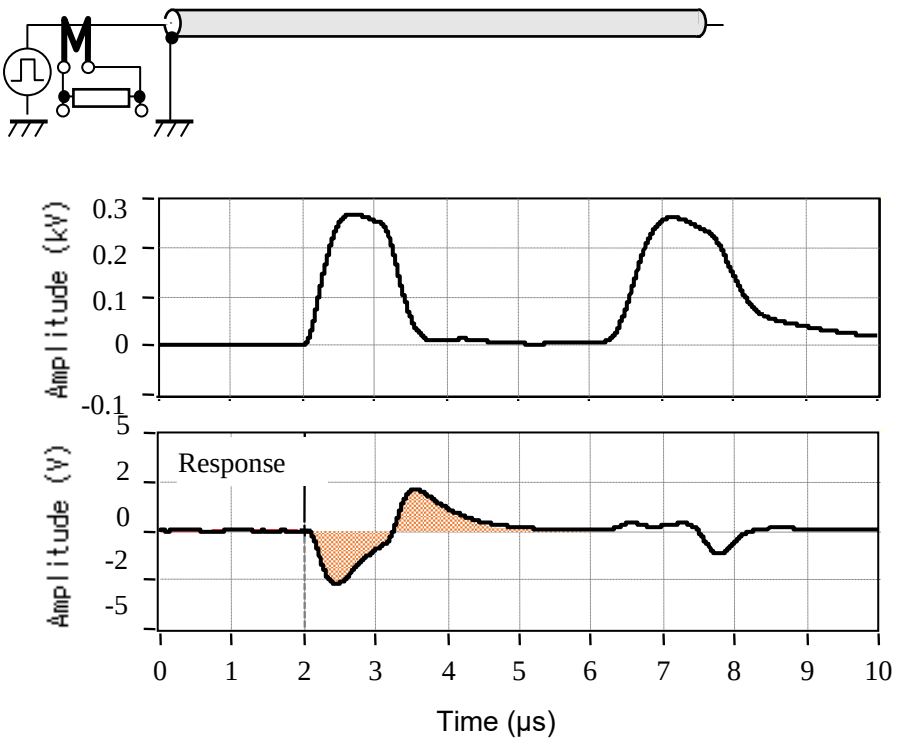

Fig. 4.6 Measurement of the impulse response of the system. The 400 m-long cable is used as a requirement resister with 50 Ω.

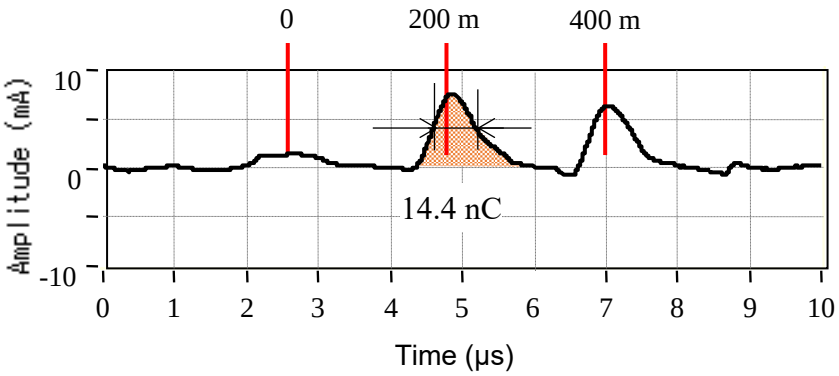

Fig. 4.7 Correction waveform after deconvolution process.

4.3.3.2 Result by changing with multiple location degradation

In the previous case study, only one local degradation was inserted in the middle of the non-degraded 400-m-long cable. In practice, multiple local degradations may exist in the insulation of cable. Thus, we conducted a position test using charge radar method. In this particular case, water tree degraded cables with 2 m, 3 m, and 5 in length were inserted in the near end and middle of the non-degraded 400-m-long cable as shown in Fig. 4.8. The total length of the cable including degraded and non-degraded is 405. The measurement sequence was performed in the same manner to the previous case and the pulse responses were recorded.

Fig. 4.8 shows the result of the position of the degraded cable and pulse responses of a charge radar method. In this experiment, the terminal of cables was left open, hence the pulse response composes of the degraded signal and the reflection signal. The pulse propagates to the far end, be reflected, and comes back to the near end. Waveform (a) shows the result of the measurement of degraded cable with 5 m in length inserted at the near end of the cable. As shown in waveform (a), a first clear peak appears at 0 μs in the time axis. The second peak, of which the rising point is 4.2 μs behind the first peak, is seen (at 7 μs in the time axis). Waveform (b) shows the result of the measurement result of degraded cable with 5 m in length inserted in the middle of the cable. As shown in waveform (d), a clear peak, of which rising point is 2.1 μs behind the first pulse in waveform (a), is seen (at 4.8 μs in the time axis). As the surge propagation speed through such a communication cable is as fast as 200 m/μs, this delay time corresponds to 210 m in the distance, which briefly coincides the distance to the degraded point. Waveform (c) shows the result of the measurement of degraded cables with 2 m in length inserted at the near end and 3 m inserted in the middle of the cable. This waveform has 3 peaks. The first clear peak is the echo signal of the degraded cable inserted at the near end of the cable. and the second clear peak is the echo signal of the degraded cable inserted in the middle of the cable. The third clear peak is the reflection signal.

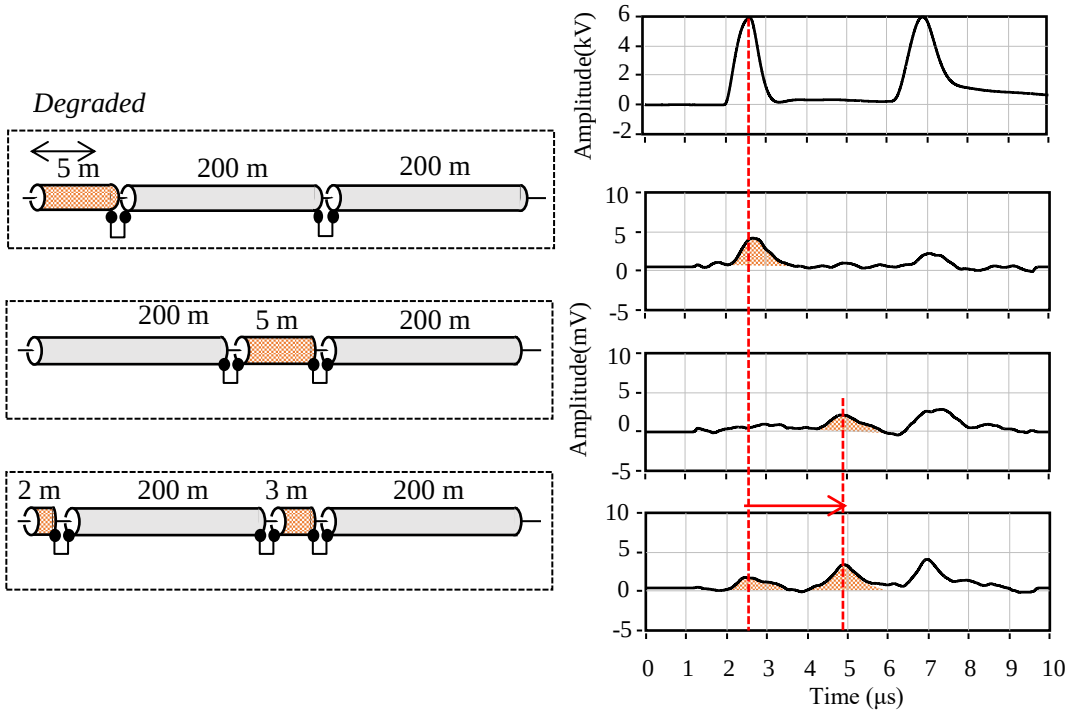

Fig. 4.8 Result by changing the degradation location.

4.3.3.3 Signal intensity under the influence of pulse and bias voltage

We studied the influence of bias and pulse voltages on the release charge intensity. In this particular case, the degraded cable with 5 m in length was inserted in the middle of the non-degraded 400-m-long cable. The sequences of the measurement were the same as the previous case, however, the bias and pulse high were changed accordingly.

Fig. 4.9 shows the signal intensity depending on the depolarizing pulse voltages. As shown inFig. 4.9, the signal intensity increased with the increase of pulse high. Fig. 4.10 shows the residual charge with depolarizing pulse voltages on bias voltages. It was suggested the amount of residual charge is high with higher depolarizing pulse. On the other hand, the amount of residual charge with different bias voltage show a similar tendency. Fig. 4.11 shows the residual charge with bias voltages on depolarizing pulse voltages. In this particular case, it shows a similar tendency, which is higher bias voltage and higher depolarizing pulse voltage provide a higher residual charge amount. From this result, it still not clear whether or not the charge can be released by such a sharp pulse voltage (as sharp as 1μs). Thus, the release mechanism of the residual charge is investigated in chapter 6.

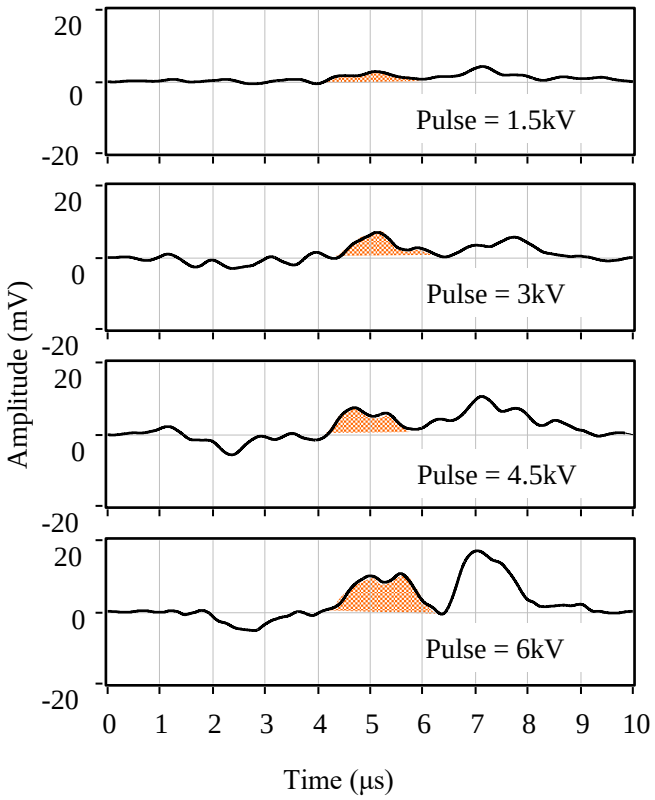

Fig. 4.9 Signal of signal intensity with pulse voltage.

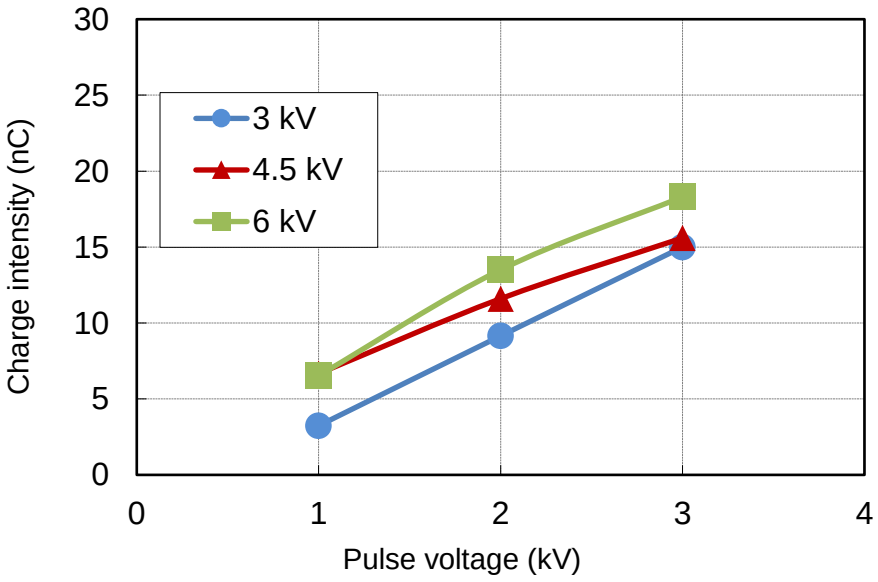

Fig. 4.10 Residual charge with pulse voltage on bias voltage.

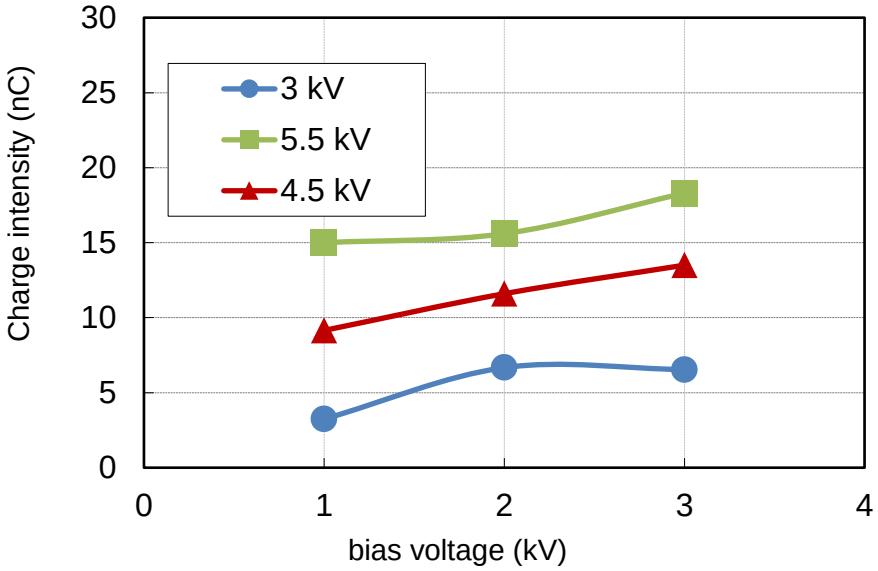

Fig. 4.11 Residual charge with bias voltage on pulse voltage.

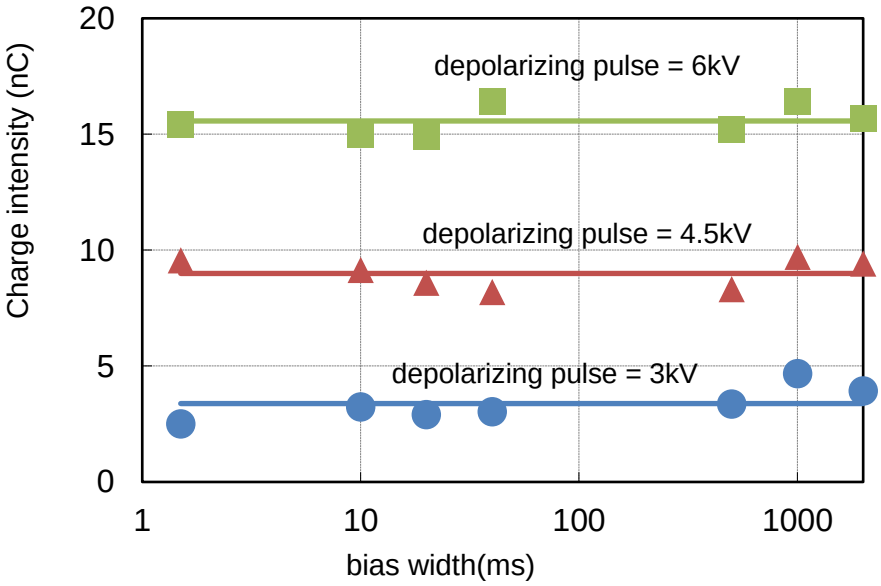

Fig. 4.12 Residual charge with bias width.

4.4 Assessment of Charge Behavior using PEA Method

4.4.1 Measurement Principle

Pulse ElectroAcoustic (PEA) method was developed by prof. T. Takada et al [8] to measure the distribution of space charges in dielectric materials. Since then it has become one of the most widely used technique by the researchers from industry and academics, partly because it has the advantages of relatively simple experimental arrangement and comparatively easy interpretation of the experimental results. The measurement principle of this method is shown in Fig. 4.13 and the basic principle is as follow:

Consider a sheet sample with thickness d and space charge distribution $\rho(x)$. When a pulse electric field $e_p(t)$ is externally applied to the sample and it induces a perturbation force that causes a slight movement of charge in its position. This movement generates an acoustic wave $p(t)$ as shown in equation (1) that is proportional to the charge distribution $\rho(x)$ in the sample. A piezoelectric transducer (sensor) attached beneath the lower electrode converts the acoustic waves into electrical signals $q(t)$as shown in equation (2), which after amplification, can be monitored by a high-speed digital oscilloscope. The amplitude of the signals is related to the charge density, and the delay is associated with the distance from the charges to the lower electrode. Thus, the spatial distribution of the space charges can be measured.

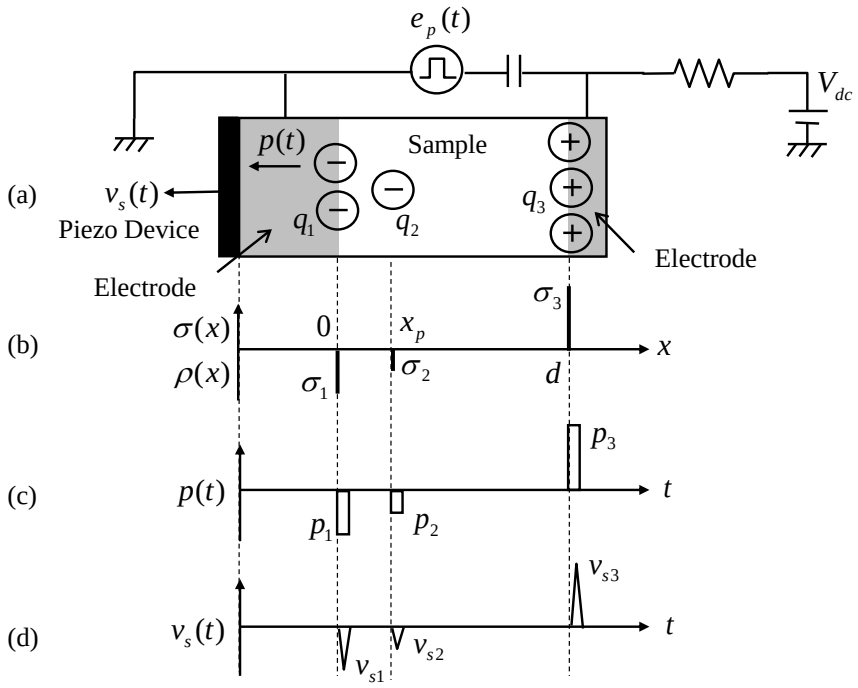

Fig. 4.13 PEA measurement principle [18].

$$p(t)=\frac{Z_{Al}}{Z_{sa}+Z_{Al}}\times\left[\sigma(0)e(t)+u_{sa}\int_{-\infty}^{+\infty}\rho(\tau)e_p(t-\tau)d\tau+\sigma(d)e\left(t-\frac{r}{u_{sa}}\right)\right] \quad (4.10)$$

$$q(t)=p(t)=\frac{2Z_p}{Z_{Al}+Z_p}\frac{u_p}{b}\int_{-\infty}^{+\infty}h(\tau)p(t-\tau)d\tau \quad (4.11)$$

4.4.2 Signal Processing (Deconvolution)

The output signal $v_s(t)$of the PEA method can be described as the convolution of the charge distribution $\rho(x)$, the impulse response of the detection unit (a piezoelectric device and an amplifier) $h(t)$, and the pulsed electric field $e_p(t)$. By Fourier transformation, the output signal $Vs(f)$is described by the values $R(f)$, $H(f)$ and $Ep(f)$ in equation (4.12).

$$V_s(f)=H(f)\times P(f)=K\times H(f)\times R(f)\times E_p(f) \quad (4.12)$$

where *K* is the sensitivity factor of the measurement system, $R(f)$, $H(f)$ and $Ep(f)$ represent the Fourier transformed charge distribution, the impulse response of the detection system and the pulse electric field, respectively.

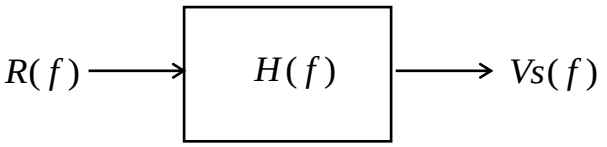

$$Vs(f)=H(f)\times P(f)$$

f : Frequency
$R(f)$: Fourier transform of space charge distribution *r* (*t*)
$H(f)$: Fourier transform of the instrument response *h* (*t*)
$Vs(f)$: Fourier transform of the measurement signal v_s (*t*)

Fig. 4.14 Space charge distribution and response from equipment.

From equation (4.12), it is obvious that the output signal is determined by the convolution of the transfer function $H(f)$ and the applied electric field $Ep(f)$. Assuming that the output signal is an impulse, corresponding to the space charge distribution itself, $Vs1(f)$ in the equation (4.13) is, therefore, a constant.

$$V_{s1}(f)=K\times H(f)\times\sigma_1\times E_p(f) \quad (4.13)$$

It becomes. The amount of charge $\sigma_1$on the sample interface can be set to an arbitrary value by applying a DC voltage V_{dc} to the sample in which no space charge is formed. A signal obtained at this time is defined as a reference waveform. At this time, assuming that the thickness of the sample is d, the charge amount $\sigma_1$is

$$\sigma_1 = \frac{\varepsilon_0 \varepsilon_r V_{dc}}{d} \tag{4.14}$$

Since the measurement signal is discretized, when converting $\sigma_1$to volume charge density, let the sampling interval be τ,

$$\rho(0) = \frac{\sigma_1}{V_{dc} \cdot \tau} \tag{4.15}$$

where $\rho(0)$ is the space charge density at the position $x = 0$ with respect to the lower electrode, and in the discrete Fourier transform is equal to an impulse of height $\rho(0)$. Therefore, equation (4.16) is

$$V_{s1}(f) = K \times H(f) \times \rho(0) \times E_p(f) \tag{4.16}$$

It becomes. From equation (4.13) and equation (4.16), the space charge distribution $R(f)$ for the charged charge is

$$R(f) = \rho(0) \times \frac{V_s(f)}{V_{s1}(f)} \tag{4.17}$$

It becomes $R(f)$. The space charge distribution $r(x)$ is obtained by inverse Fourier transform of this $R(f)$ and replacing the time t with the position x by the sound velocity of the sample. Furthermore, the electric field/potential distribution can be calculated from the electric field distribution. Assuming that the charge distribution in a plane is uniform on a plane in a parallel plate sample, Poisson's equation can be expressed in one dimension, and the electric field/potential distribution can be calculated from the charge distribution as follows:

$$E(x) = \int \frac{\rho(x)dx}{\varepsilon_0 \varepsilon_r} \tag{4.18}$$

$$V(x) = \int E(x)dx \tag{4.19}$$

4.4.3 Sample and Experimental Setup

In this experiment, a thin crosslinked polyethylene sheet with 850 μm in thickness was employed as a specimen. On side of the sample contained a water tree with 250 μm in length. This water tree degradation was produced by applying 8.5 kVrms, 400 Hz to a small water tank which mounted on the roughed side of the sample for 300 hours.

Fig. 4.15 shows the typical PEA experimental setup. The space charge measurement was performed under the DC stress voltage application at 4 kV, 5 kV, or 6 kV for 600 s. Afterward, the sample was subjected to a short-circuit condition for several seconds. Subsequently, a probing pulse voltage with a width of about 20 ns was applied to the sample. The measurement was taken in the interval of 1 s to 1200 s. The parameters used in this experiment is given in Table 4.1. The experiment was carried out at room temperature.

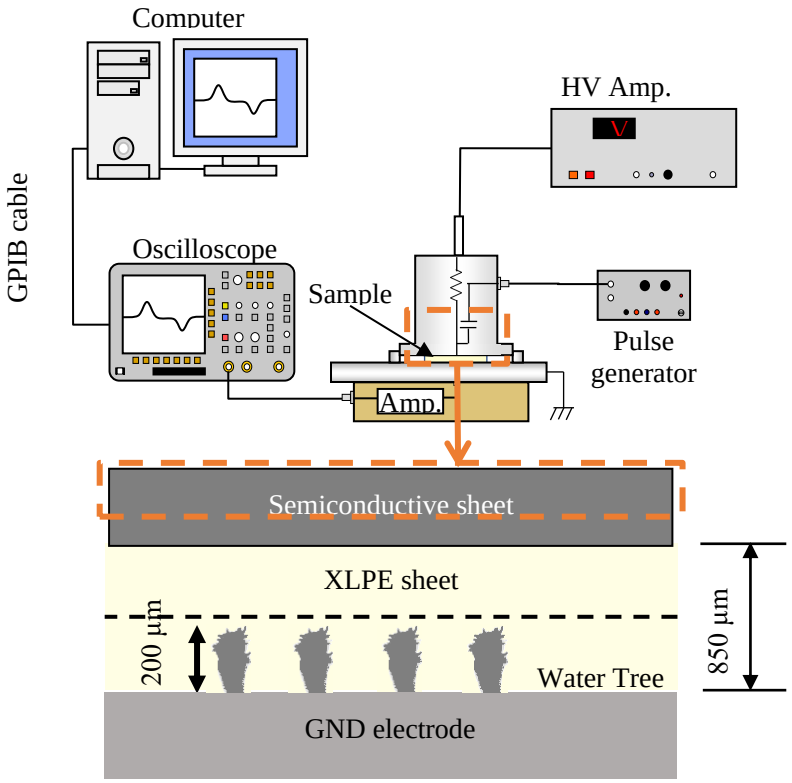

Fig. 4.15 Experimental Setup for typical PEA measurement system.

Table 4.1 Measurement sample and measurement conditions

Sample	Unit
Permittivity	2.4
Thickness	850 μm
V_{dc}	4, 5, 6 kV
Pulse voltage	2 kV
Pulse width	20 ns
Pulse interval	26 ms

4.4.4 Space Charge under DC Voltage and Short-Circuit Condition

Fig. 4.16 shows a typical result of a space charge measurement using the PEA method. As shown in Fig. 4.16, the space charge distribution did not significantly change shortly after the application of DC voltage, and this tendency can be also confirmed after a short-circuited condition.

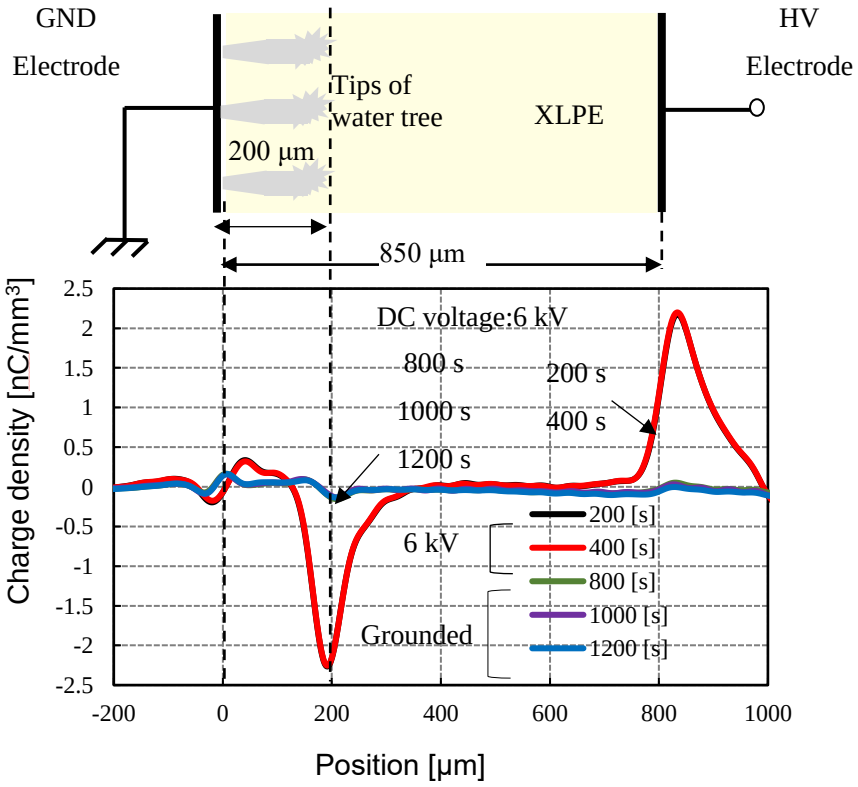

Fig. 4.16 Typical result of space charge measurement using PEA method.

Fig. 4.17 shows the charge density at the tips of water trees under the DC voltages and short-circuiting condition. As shown in Fig. 4.17, the space charge decayed rapidly after the short-circuiting, and a certain space charge remained at the vicinity of water tree tips as a residual charge which would stay for a longer period of time depending on the depth of the trapping layers.

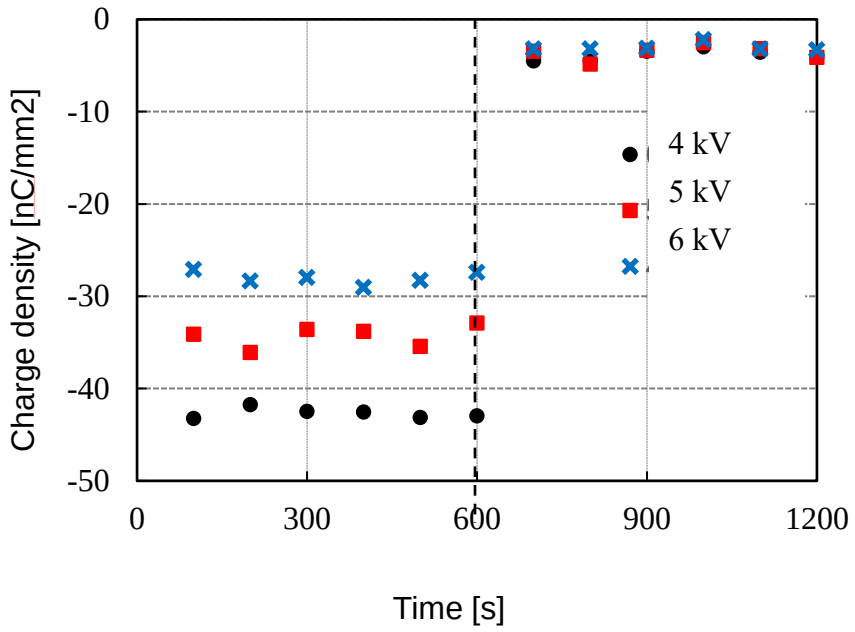

Fig. 4.17 Charge density at water tree tips under DC voltages and short-circuiting condition.

4.4.5 Space Charge under 1 μs Pulse Voltages

Fig. 4.18 shows the modified PEA experimental setup. We modified the PEA measurement system by adding a pulse impulse generator to the system. The sequences of the measurement system are shown in Fig. 4.19. In this particular case, 6 kV of DC voltage application was applied to the sample which contained a water tree for 600 s. After, the sample was subjected to 200 s short-circuiting. Afterward, the sample was subjected to a short-circuit condition for 200 seconds. Subsequently, a depolarizing pulse voltage with a width of about 1 μs was applied to the sample. The measurement was taken in the interval of 1 s to 1200 s. The experiment was carried out at room temperature.

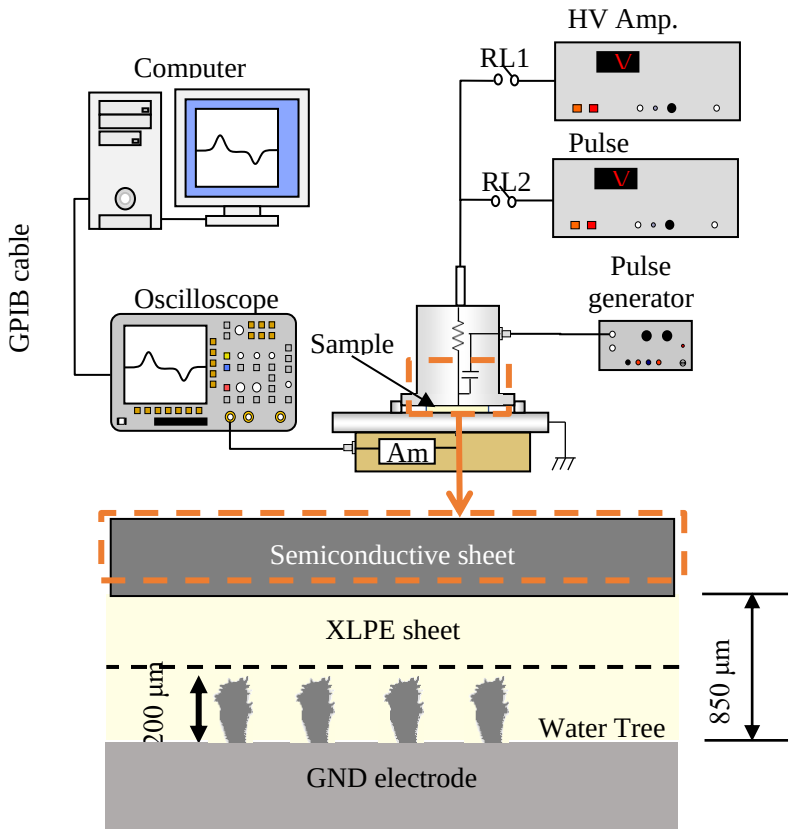

Fig. 4.18 Modified PEA measurement system including 1 µs depolarizing pulse voltage.

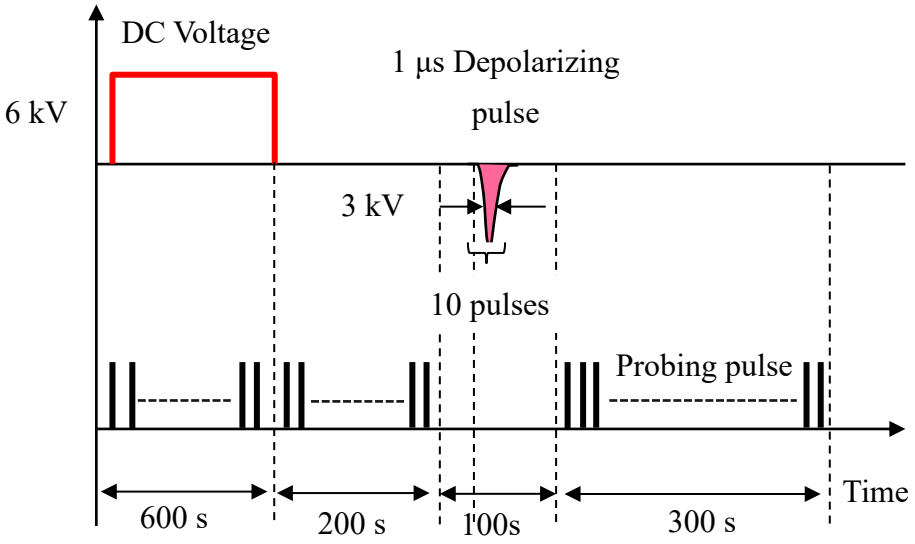

Fig. 4.19 Sequence of the measurement system for space charge measurement.

As shown in Fig. 4.20, it took as much as 10 seconds until the space charge became stable, which is a very short time after short-circuiting. It was also revealed that the depolarizing pulse voltages with the width of 1 μs did not affect space charge condition in the vicinity of the water tree. The reduction around 800 and 900 seconds (in the time axis) appeared because the poling bias pulse voltage was not applied.

Since the charge amount before and after the application of depolarizing pulse voltage remained the same, it is suggested that the decay of charge amount should depend on the short-circuiting time after polarization and the time constant (τ) in which its value can be extracted by considering the conductivity and permittivity of the water tree. Assuming that the charge transport is as quick as 20 μs, and the depolarizing pulse voltages were applied at the interval of 1 s, it is obvious that the measurement results included the effect of charge decay because it takes at least 24 s to complete the measurement. This reason is explained in the next section.

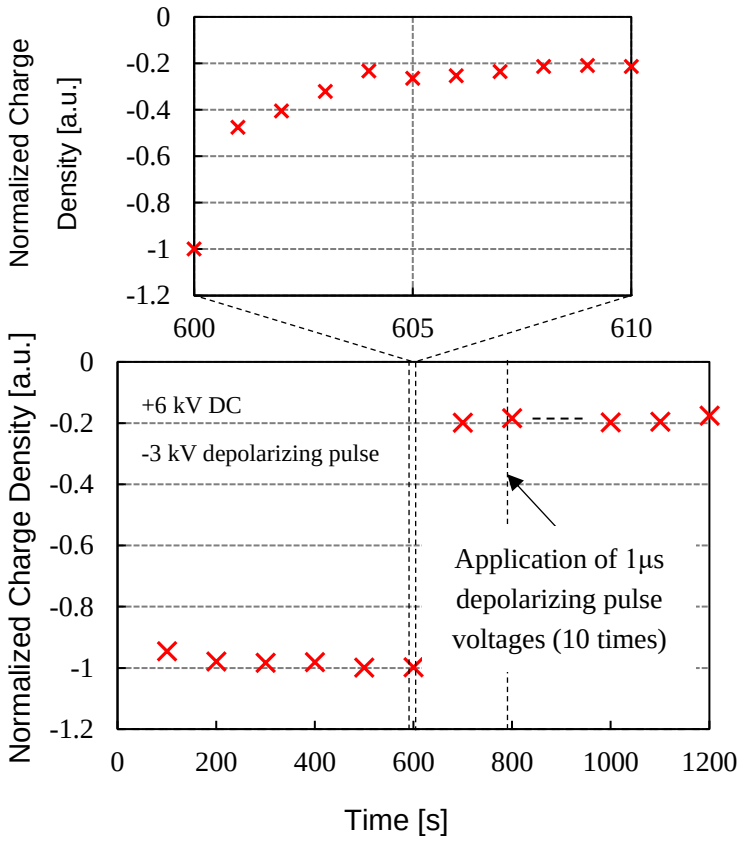

Fig. 4.20 Normalized charge density at water tree tips under a +6 kV DC voltage and 1μs depolarizing pulse voltages.

4.5 Charge Behavior under Different Time Intervals

4.5.1 Measurement Procedure

In the measurement, a water tree degraded cable of 5 m in length was inserted into the middle of a non-degraded 400 m long cable. The total length was therefore 405 m, and the degraded span being 200-205 m from the terminal near the pulse generator. Fig. 4.21 shows the sequences of the applied pulse voltages of the Charge Radar method. The sequences of the bias and depolarizing pulse voltages are explained as follows:

A 3 kV poling bias pulse voltage was applied to the target cable for 2 ms. Subsequently, a depolarizing pulse voltage with 1 μs in width was applied 24 shots with 1 s or 5 μs of the time interval between each pulse voltage and a reflection signal (target signal) was acquired.

In order to discriminate the degradation signal, a 3 kV depolarizing bias pulse voltage was applied to the target cable in the same manner as the poling bias pulse voltage with opposite polarity. The bias pulse voltage removes the charge at the water tree and may give the charge with opposite polarity (negative in this case). The reference pulse voltage was then applied in the same manner as a depolarizing pulse voltage to acquire the reference signal. A reference signal was subtracted from the target signal to obtain the degradation signal.

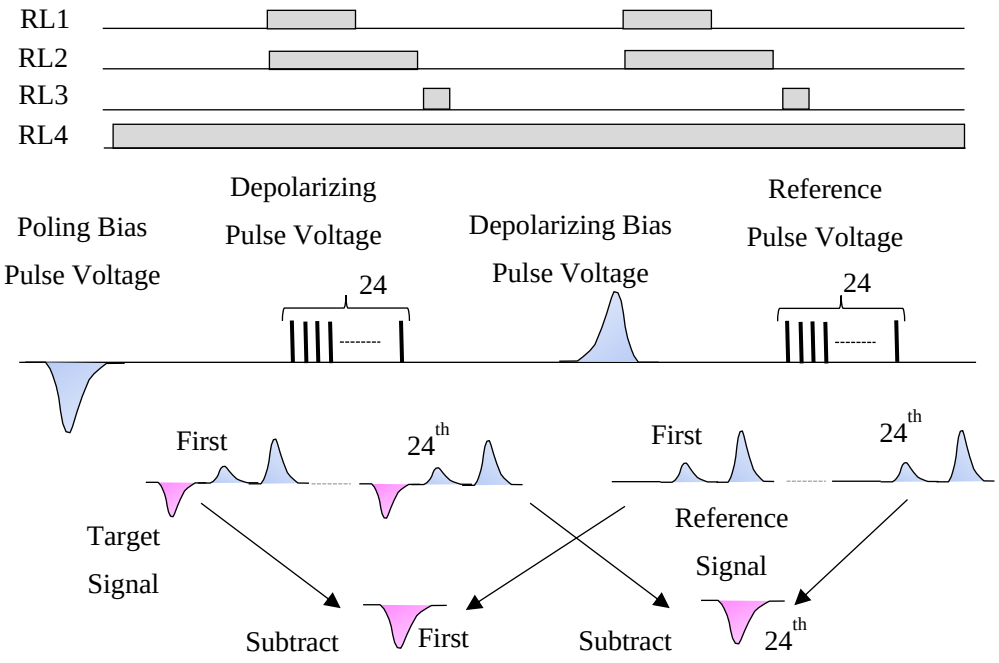

Fig. 4.21 Measurement system for residual charge method under pulse voltage applications.

4.5.2 Decay of Space Charge under Different Time Interval

Fig. 4.22 shows the decay of normalized residual charge intensity under pulse voltage applications with 5 μs time interval. As exhibited in Fig. 4.22, there was no change in the reduction of charge amount although 24 pulse voltages were applied to the cable sample. This tendency suggested that the number of pulses did not give a significant change to the reduction of charge amount.

Fig. 4.23 shows the decay of the normalized space charge under pulse voltage applications with 1 s of the time interval. As shown in Fig. 4.23, the space charge was significantly decayed when the time interval between each pulse is long enough. Thus, we firmly believe that the space charge was detrapped by the thermoelectric effect. This effect will be explained in the next section.

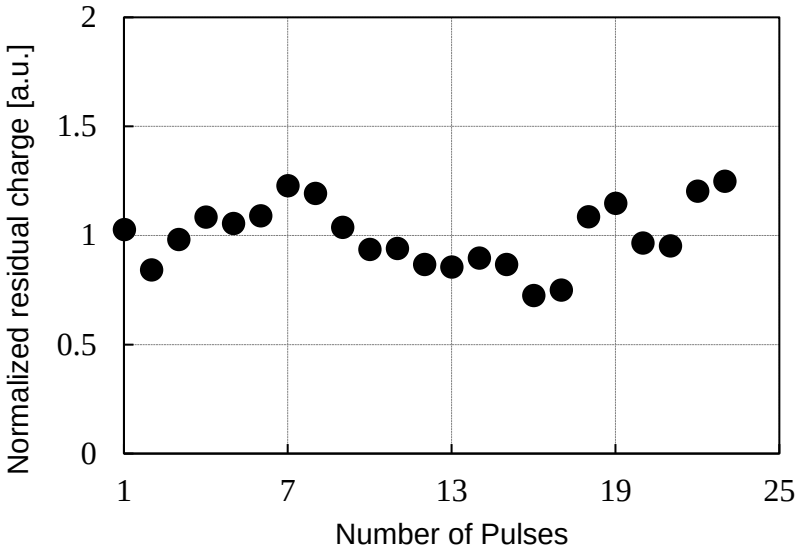

Fig. 4.22 Correlation between number of pulses and the amount of residual charge (pulse interval 5 μs).

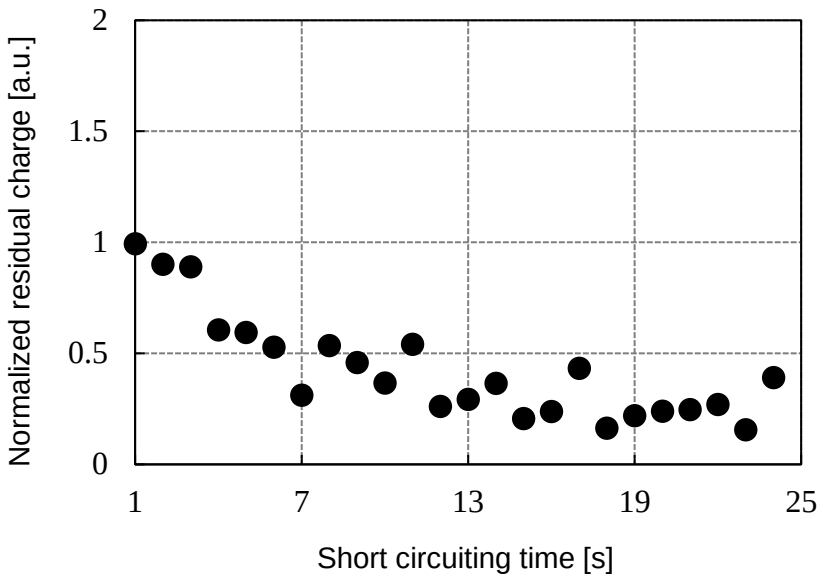

Fig. 4.23 Correlation between number of pulses and the amount of residual charge (pulse interval 1 s).

4.6 Simulation by Multi-Layers Dielectric Model

4.6.1 Equivalent Model

Fig. 4.24 shows a schematic diagram for explaining the multi-layers dielectric material model of a water tree [9]. The model consists of a water tree degradation layer, a residual charge trapped layer, and XLPE. The numerical simulation was performed based on the Maxwell-Wagner model of dielectrics shown in Fig. 4.24.

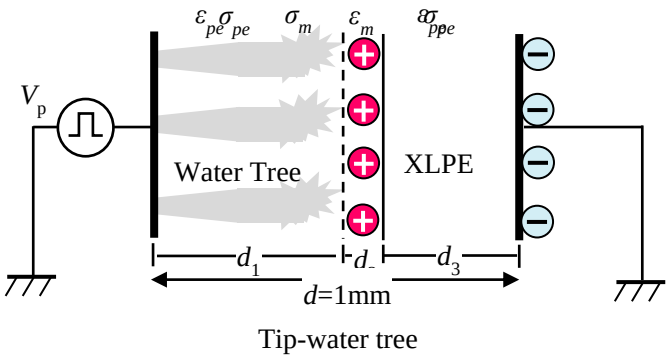

Fig. 4.24 Multi-layers dielectric model for simulation.

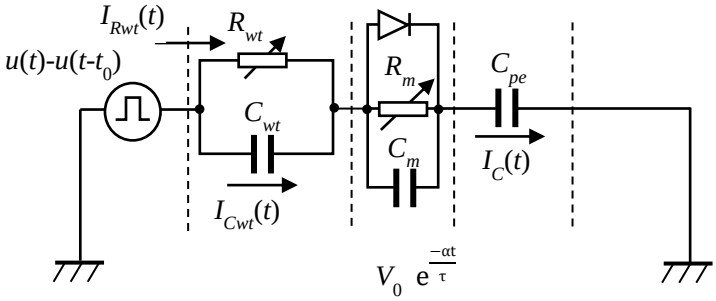

Fig. 4.25 Equivalent circuit for numerical simulation.

Based on an equivalent circuit exhibited in Fig. 4.25, the current through a water tree degradation layer is expressed as shown in equation (6.1). The integration of $I_{\mathrm{Rwt}t}$ over time t corresponded to the total released charge Q_{wt} due to the depolarizing pulse voltage.

$$I_{R_{wt}}(t)=\frac{C_m}{\tau}\left[V\left(e^{\frac{-t}{\tau}}+e^{-\frac{t-t_0}{\tau}}\right)+\frac{V_0}{1-\alpha t}\left(e^{\frac{-t}{\tau}}-\alpha\tau e^{-\alpha t}\right)\right] \tag{4.20}$$

$$Q_{wt}=\int_0^t I_{R_{wt}}(t)dt \tag{4.21}$$

where $\tau=R_{\mathrm{wt}}\left(C_{\mathrm{wt}}+C_{\mathrm{m}}C_{\mathrm{pe}}/\left(C_{\mathrm{m}}+C_{\mathrm{pe}}\right)\right)$ is the time constant and $C_{\mathrm{wt}}, C_{\mathrm{pe}}, C_{\mathrm{m}}$, R_{wt} and R_{m} represent the capacitance, and resistance of water tree degradation, tip of water tree, and XLPE, respectively. V and V_0 are the amplitude of the depolarizing pulse and the voltage of the residual charge, respectively. α is attenuation constant.

The values of the resistances and capacitances of a water tree degradation layer were extracted by considering the conductivity and permittivity of a water tree. The value of the permittivity $\varepsilon_{\mathrm{wt}}$ is $4\varepsilon_0$ at the frequency of 1 kHz [9], and the value of the conductivity of the water tree is shown in equation (4.22).

$$\sigma_{wt}=\sigma_0\exp\left(-\frac{E_{wt}}{kT}\right) \tag{4.22}$$

where σ_{wt}, E_{wt} are respectively the conductivity and an electric field at the water tree degradation layer. σ_0, k, and T are constant, Boltzmann constant, and temperature, respectively. The residual charge which is trapped at the tip of the water tree is represented as shown in equation (4.23).

$$Q_m=Q_0\exp\left(\frac{-At}{\tau}\right) \tag{4.23}$$

where Q_0 is the initial value of a residual charge at the tip of a water tree. In equation (6.14), and an acceleration factor A is introduced to the reduction of residual charge. The trapping and de-trapping processes of this residual charge accumulated at the tip of the water tree are explained based on the Pool-Frenkel emission process [19]. An acceleration factor due to the applied electric field is shown in equation (4.24).

$$A=\frac{1}{T'}\int_0^t \exp\left[\frac{\sqrt{\frac{e^3\left|F_0\left[u(t)-u(t-t_0)\right]\right|}{\pi\varepsilon}}}{2kT}\right]dt \tag{4.24}$$

where e, and F_0 are the elementary charge (e=1.602×10^{-19} C), and an amplitude of the applied electric field, respectively.

Since the residual charge that causes the deterioration signal flows toward the water tree layer, it is necessary to calculate the current flowing to the water tree layer. In particular, the degradation signal

waveform was calculated by performing a simulation with the application interval of the pulse voltage simulating only the current flowing in the resistance component being 5 μs. In addition, conditions such as each conductivity, dielectric constant, and thickness of the sample are shown in Table 4.2.

Table 4.2 Parameters for simulation.

Parameter	Unit
DC bias voltage V	3 kV
Pulse voltage: V_{pulse}	1 kV
Relative permittivity: ε_0	8.85×10^{-12} F/m
Dielectric constant in water tree: ε_{wt}	16 F/m[4]
Dielectric constant in insulation: ε_{pol}	2.125 F/m[4]
Boltzmann constant: k	1.38×10^{-23} J/K
Conductivity of R_1: σ_0	25×10^{-6} S/m (300 K)
Length of water tree: d_1	0.5 mm
Length of capturing residual charge: d_2	1 nm
Length of insulation: d_3	0.5 mm

4.6.2 Simulation Results

Fig. 4.26 shows the decay of the space charge under pulse voltage application under 5 μs of time interval between each pulse voltages. As shown in Fig. 4.26the amount of space charge does not significantly change under pulse voltages applications. Although the pulse voltage used in this simulation was a square waveform, the result still shows a similar tendency to the experimental result.

On the other, Fig. 4.27 shows a different tendency. The charge amount decayed significantly under the same number of pulse voltages. This tendency suggested that the number of pulses did not give a significant change to the reduction of charge amount. Fig. 4.27 also shows the comparison of the reduction of charge amount under the different intensity of the pulse voltage by the mean of an acceleration factor A. As shown in Fig. 4.27, the reduction tendency of the charge amount is the same regardless of a higher acceleration factor. Even though the reduction of charge amount had been expected to be accelerated fast under higher depolarizing pulse voltage, the pulse was very short (as short as 1μs) so that the trapped charge may not respond to the electric field generated by the pulse

voltage. Therefore, it was suggested that the reduction in charge amount may depend on the short-circuiting time after polarization. This reason is discussed in the next section.

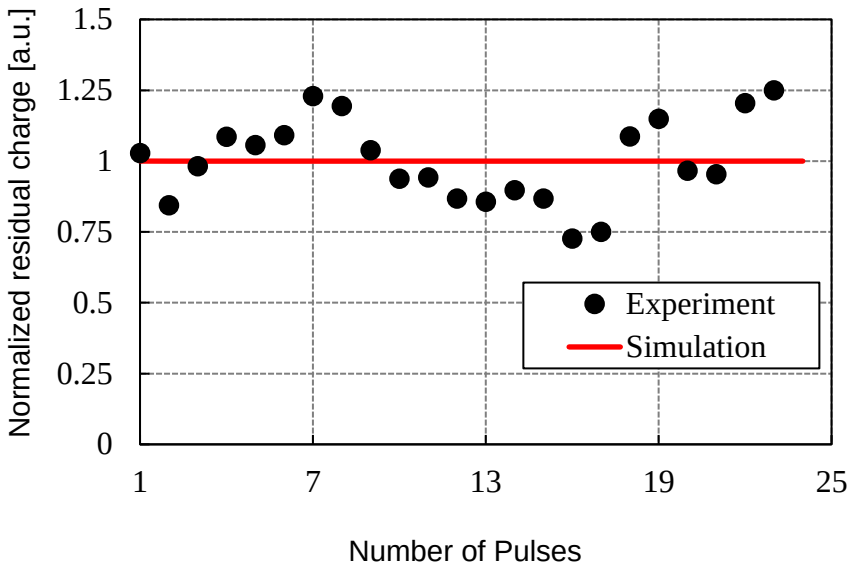

Fig. 4.26 Reduction of normalized charge amount depending on the number of pulse voltage applications and the time interval. 5 μs (α=5 10-10, τ=20μs, and A=1.3).

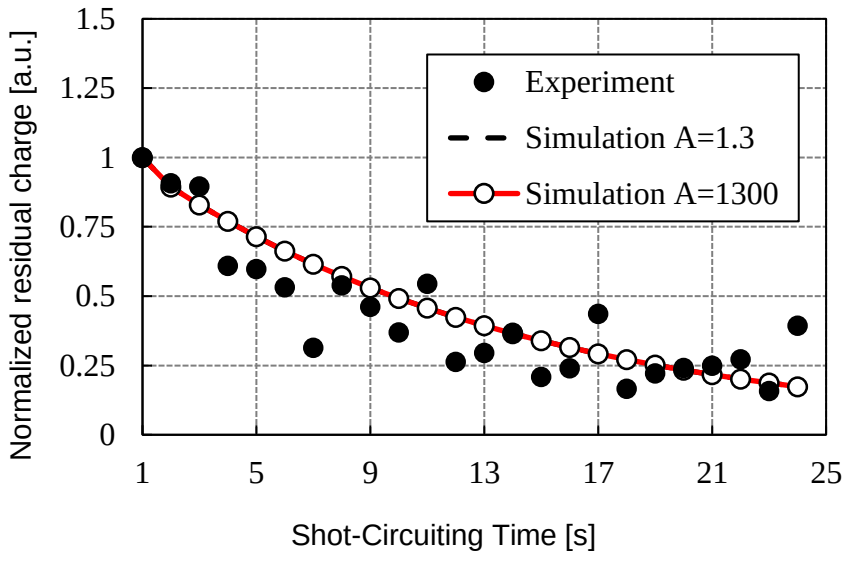

Fig. 4.27 Reduction of normalized charge amount depending on the number of pulse voltage applications and the time interval of 1 s (α=5 10^{-10}, τ=20μs).

4.6.3 Influence of Short-Circuit Time on Degradation Signal

Fig. 4.28 shows the decay of the space charge depending on the short-circuiting time. As shown in Fig. 4.28, the space charge significantly decayed significantly from 0 to 30 s. After 30 s, the amount of space remained a residual charge which would last for a long period of time. This tendency was also confirmed by the PEA measurement. Therefore, the amount of space charge collected by the was released by the thermoelectric effect.

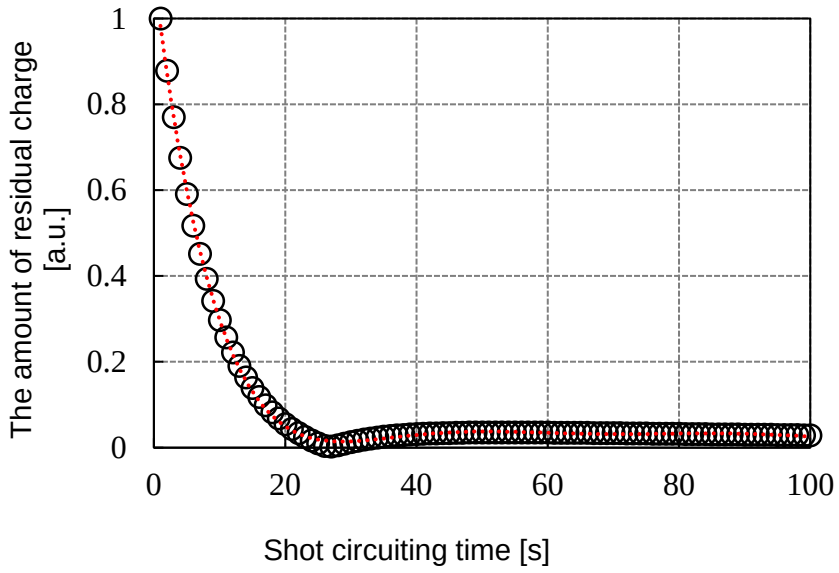

Fig. 4.28 Correlation between the amounts of residual charge and number of pulses.

4.7 Mechanism for Signal Generation of Residual Charge Under Pulse Voltages

These results suggest the following items: (a) the residual charge does not decay by applying the pulse voltage, and (b) the presence or absence of the residual charge affects the obtained signal. We proposed a model satisfying these two points. Fig. 4.29 shows the schematic image of a charge behavior at the water tree interface.

The charge at the boundary between a water tree degradation layer and an XLPE layer (Q_s) can be approximated by the product of the capacitance of XLPE (C_{pe}) and the applied pulse voltage (V_P Vp) as in the following equation (4.25).

$$Q_s = C_{pe} \mathrm{V}_p \left(1 - e^{\frac{-t}{\tau_s}} \right) \tag{4.25}$$

where τ_s is the time constant of the insulation system including the water tree degradation and XLPE layers. As illustrated in Fig. 4.20, the residual charge remains at the tips of the water trees even after short-circuiting with a longer time than τ_s.

Assuming the system as a single relaxation system, the amount of space charge is Q_{r-} or Q_{r+} after short-circuiting, and its polarity depends on the applied voltages. The residual charge decay over the passing time ($t \gg \tau_s$) becomes $Q_{r-}e^{-\left(\frac{1}{\tau_s}+\frac{1}{\tau_r}\right)t}$ or $Q_{r+}e^{-\left(\frac{1}{\tau_s}+\frac{1}{\tau_r}\right)t}$. τr is the time constant of the tips of water trees.

The responses of the charges Q_{tgt} and Q_{ref} at tips of water trees, whose initial values are $-Q_{r-}$ and $+Q_{r+}$, respectively, by applying a pulse voltage, are expressed in equations (4.26) and (4.27). These responses of the charges Q_{tgt} and Q_{ref} are shown in Fig. 4.30.

$$Q_{tgt} = C_{pe} V_p \left(1 - e^{\frac{-t}{\tau_s}} \right) - Q_{r-} e^{-\left(\frac{1}{\tau_s}+\frac{1}{\tau_r}\right)\cdot t} \tag{4.26}$$

$$Q_{ref} = C_{pe} V_p \left(1 - e^{\frac{-t}{\tau_s}} \right) + Q_{r+} e^{-\left(\frac{1}{\tau_s}+\frac{1}{\tau_r}\right)\cdot t} \tag{4.27}$$

The current responses to the depolarizing pulse and reference pulse voltages are expressed in equations (4.28) and (4.29).

$$i_{tgt} = \frac{1}{\tau_s} C_{pe} V_p \cdot e^{\frac{-t}{\tau_s}} + Q_{r-} \left(\frac{1}{\tau_s} + \frac{1}{\tau_r} \right) e^{-\left(\frac{1}{\tau_s}+\frac{1}{\tau_r}\right)\cdot t} \tag{4.28}$$

$$i_{ref} = \frac{1}{\tau_s} C_{pe} V_p \cdot e^{\frac{-t}{\tau_s}} - Q_{r+} \left(\frac{1}{\tau_s} + \frac{1}{\tau_r} \right) e^{-\left(\frac{1}{\tau_s} + \frac{1}{\tau_r} \right) \cdot t} \tag{4.29}$$

By subtracting the current responses between depolarizing and reference pulse voltages, the current response related to the water tree degradation can be expressed as shown in equation (4.30).

$$i_{sub} = \left(Q_{r+} + Q_{r-} \right) \left(\frac{1}{\tau_s} + \frac{1}{\tau_r} \right) e^{-\left(\frac{1}{\tau_s} + \frac{1}{\tau_r} \right) \cdot t} \tag{4.30}$$

Since the residual charge is not released by the pulse voltage applications, $\tau_r >> \tau_s$, and the equation (4.31) can be approximated to the following equation

$$i_{sub} = \left(Q_{r+} + Q_{r-} \right) \left(\frac{1}{\tau_s} \right) e^{-\frac{t}{\tau_s}} \tag{4.31}$$

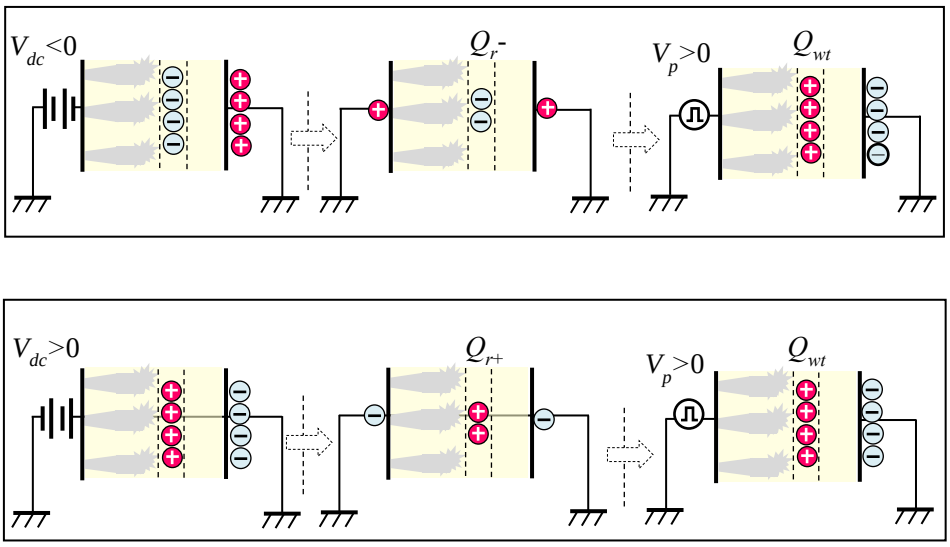

Fig. 4.29 Schematic image of the charge behavior at the water tree interface with applying voltage pattern.

The decay of the above transition currents over time *t* is demonstrated in Fig. 4.31. By considering the above transition currents, it could be explained that the current response related to water tree degradation can be detected even if no change in residual charge amount takes place by applying the short pulse voltage.

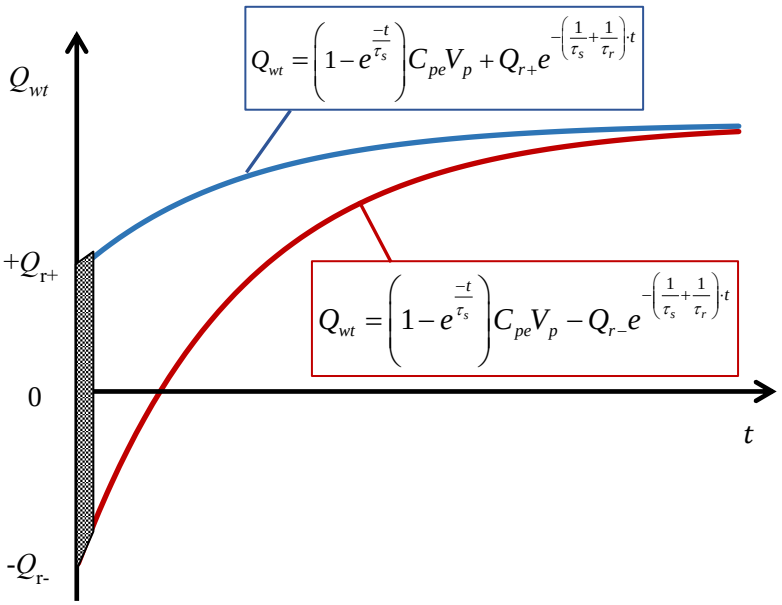

Fig. 4.30 Charge behavior at the water tree interface.

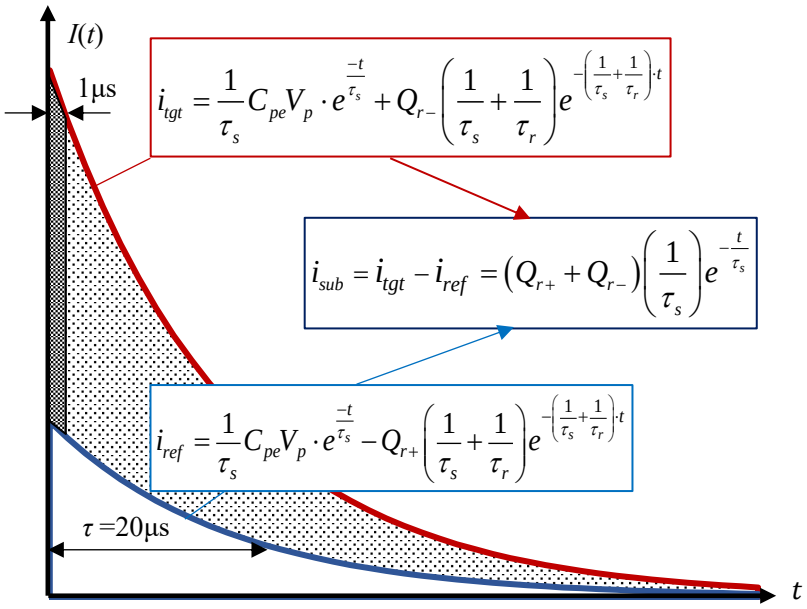

Fig. 4.31 Schematic image of the charge behavior and current transition at the water tree.

4.8 Conclusions

A new method for locating water tree degradation in power cables was successfully developed. In principle, a depolarizing pulse voltage is applied following the poling bias voltage. As the pulse voltage propagates through the cable with a certain speed, the delay time of the response can be correlated to the distance from the near end terminal. In order to suppress the response from the non-degraded part, several noises canceling techniques were employed. A communication coaxial cable was artificially degraded with water trees. A 5 m-long degraded cable was inserted in the middle of a 400 m-long non-degraded cable. A measurement circuit with a high voltage semiconductor switch and a high-frequency current transformer was assembled. The response was corrected considering the frequency dependence of the measurement system. A result of these measurements and correcting process, the degraded part was successfully located with a resolution of about 50 m.

The responses to high voltage pulse voltages were investigated in order to clarify the charge behavior with which the signal of newly proposed charge radar method is detected. Under the specific conditions described in this paper, the conclusions are as follows:

(1) The assessment of charge behavior in water tree degradation using pulse voltages under different time interval (1 s and 5 μs) and pulse number was investigated. It was suggested, the space charge was significantly detected when the time interval was as long as 1 s. On the other hand, almost no space was detected when the time interval as short as 5 μs.

(2) Space charge measurement using the pulsed electroacoustic method exhibited that a significant space charge is accumulated in the vicinity of the water tree tips under DC biasing voltage, and that a part of the charge remains even after several minutes of short-circuiting condition.

(3) The reduction curve of the intensity of the pulse response under the short-circuiting condition suggested that the decay time of the charge under the short-circuiting condition is as much as 10 of seconds.

(4) Both the pulse response after applying several numbers of depolarizing pulse voltages and the space charge distribution before and after the application of a depolarizing pulse voltage suggested that the application of pulse voltage with the opposite polarity (to the bias voltage) does not significantly change the condition of space charge, if the pulse width is as short as 1 μs.

(5) It was suggested that the degradation signal is based on the difference in a transient current through the water trees depending on the polarity of the bias pulse voltage applied prior to the pulse voltage.

References

[1] Y. Ikeda, and T. Tanaka, “Possibility of Deterioration Diagnosis of XLPE Cable with Water Trees by Residual Electric Charge,” *IEEJ Transaction on Power and Energy*, vol.107, no.9, pp.465-465, Sep 1987(in Japanese).

[2] M. T. Shaw and S. H. Shaw, “Water Treeing in Solid Dielectric,” *IEEE Trans. Dielectr. Electr. Insul.*, Vol. E1-19, No.5, pp. 419-452, Oct 1984.

[3] R.Patsch, and J. Jung, “Water Trees in Cables: generation and detection,” *IEEE Proc-Sci, Meas. Tecnhol*. Vol.146, No.5, pp. 253-259, Sep 1999.

[4] R. Ross, “Inception and propagation mechanism of water treeing,” *IEEE Trans. Dielectr. Electr. Insul*, Vol. 5, No.5, pp. 660-680, Oct 1980.

[5] L.A. Dissado, and J.C. Fothergill, “Treeing degradation in Polymers,” *Electrical degradation and breakdown*, G.C. Stevens, Eds. London, UK, pp. 75-113.

[6] Y. Ikeda, and T. Tanaka, “Diagnosis Method for Water Tree Aging of XLPE cables-Development of Residual Charge Measuring Device,” CRIEPI, *Yokosuka Engineering Laboratory, Japan, Tech. Report W86008*, July 1986 (in Japanese).

[7] T. Kurihara, T. Okamoto, N. Hozumi et al., "Evaluation of relationship between residual charge signal and AC breakdown strength of water-tree degraded 22 to 77 kV classes XLPE cables removed from service using pulsed voltages", *IEEE Trans. Dielectr. Electr. Insul.*, vol. 24, pp. 656-665, Mar. 2017.

[8] T. Takada, T. Maneo, H. Kushibe, "An electric stress an electric stress-pulse technique for the measurement of charges in a plastic plate irradiated by an electron beam", *IEEE Trans. Dielectr. Electr. Insul.*, Vol. EI-22, pp. 497-501, Aug. 1987.

[9] T. Toyoda, S. Mukai, Y. Ohki, Y. Li, and T. Maeno, " Estimation of Conductivity and Permittivity of water trees in PE from space charge distribution measurement ", *IEEE Trans. Dielectr. Electr. Insul.*, Vol. 8, No.1, pp. 111-116, Mar. 2001.

Chapter 5: Conclusion and Future Work

5.1 Summary

We have proposed diagnostic techniques for newly installed and also degraded cables. These methods can approach or locate the defect and/or degradation with high precision, low cost and short time. For the defects at the early stage (or aged as well) can be detected by partial discharge detection by means of passive measurement. On the other hand, at the aged stage can be detected by means of active measurement. After a series of studies, the following are the conclusions:

(1) We have developed a new diagnostic method that can detect and approach the location of partial discharge site the normal joint or any point along the main body of the cable line by considering the longitudinal cable shield impedance itself. The method assumed that the screen shield is not a perfect conductor and that change in potential would be seen as the partial discharge signal propagates through the cable line. As the partial discharge accompanied by high-frequency components, thus this change in potential is very significant. This change in potential can be detected by newly proposed capacitive coupling between an additional foil electrode and the cable shield electrode itself.

Experiments of communication and full-sized 6.6 kV XLPE cables were performed using mimic partial discharge to confirm the feasibility of the proposed method. Also, the numerical simulation of partial discharge current pulse propagation through the cables was performed by considering the skin effect of the cable shield impedance. After, the detection sensitivity of the proposed method was evaluated using partial discharge measurement under differential installation conditions. Finally, the detail of a simple partial discharge monitoring device was successfully developed.

Under the specific conditions described in this paper, our conclusions are as follows:

(a) It was confirmed that the new partial discharge measurement method is feasible at the NJ or any point along the main body of the communication cable line. In the experiment, the signal was compared with the noise level and the sensitivity was finally determined as 400 pC as the detection limit. We assumed that the detection limit should be twice as high as the noise level the sensitivity is supposed to be determined with 6 dB in S/N ratio.

(b) We have conducted using a full-size 6.6 kV XLPE cable and a significant partial discharge intensity was detected. This suggested that the proposed method is feasible for applying to the full-size cable, although there was a reduction in detection intensity.

(c) Numerical simulation using communication and full-size 6.6 kV XLPE cable were performed in the same manner to the actual measurement systems. The results showed that the simulation and experiment have similar waveform and intensity.

(d) The detection sensitivity of the proposed method was evaluated based on the existing partial discharge detection methods under the differential installation conditions. It was suggested that the detection limit of the proposed method was approximately 30 times lower than the insulation joint.

(e) A simple partial discharge monitoring device was successfully developed and its performance was satisfactory in term of low cost and its versatility. Since the voltage amplification factor of the circuit used this time is at most about 20 times, it is considered sufficient to improve this instrument further.

(2) A new method for locating water tree degradation in power cables was successfully developed. In principle, a depolarizing pulse voltage is applied following the poling bias voltage. As the pulse voltage propagates through the cable with a certain speed, the delay time of the response can be correlated to the distance from the near end terminal. In order to suppress the response from the non-degraded part, several noises canceling techniques were employed. A communication coaxial cable was artificially degraded with water trees. A 5 m-long degraded cable was inserted in the middle of a 400 m-long non-degraded cable. A measurement circuit with a high voltage semiconductor switch and a high-frequency current transformer was assembled. The response was corrected considering the frequency dependence of the measurement system. A result of these measurements and correcting process, the degraded part was successfully located with a resolution of about 50 m.

The responses to high voltage pulse voltages were investigated in order to clarify the charge behavior with which the signal of newly proposed charge radar method is detected. Under the specific conditions described in this paper, the conclusions are as follows:

(a) The assessment of charge behavior in water tree degradation using pulse voltages under different time interval (1 s and 5 μs) and pulse number was investigated. It was suggested, the space charge was significantly detected when the time interval was as long as 1 s. On the other hand, almost no space was detected when the time interval as short as 5 μs.

(b) Space charge measurement using the pulsed electroacoustic method exhibited that a significant space charge is accumulated in the vicinity of the water tree tips under DC biasing voltage and that a part of the charge remains even after several minutes of short-circuiting condition.

(c) The reduction curve of the intensity of the pulse response under the short-circuiting condition suggested that the decay time of the charge under the short-circuiting condition is as much as 10 of seconds.

(d) Both the pulse response after applying several numbers of depolarizing pulse voltages and the space charge distribution before and after the application of a depolarizing pulse voltage suggested that the application of pulse voltage with the opposite polarity (to the bias voltage) does not significantly change the condition of space charge, if the pulse width is as short as 1 μs.

(e) It was suggested that the degradation signal is based on the difference in a transient current through the water trees depending on the polarity of the bias pulse voltage applied prior to the pulse voltage.

5.2 Future Works

In this research work, two components of study were performed. First, the development of partial discharge detection of a long-distance cable line and a fabrication of simple and cheap partial discharge monitoring device. Although the device has been fabricated and tested in the practical cable line, there is still a room for improvement. Second, we have proposed the diagnostic method for water tree of a degraded XLPE cable by employing bias and depolarizing pulse voltage. The method has been successfully detected a water tree degraded of a communication cable, yet this method has not been tested with full-size cable. Based on this background, we proposed future works as follow:

5.2.1 Future Prospect of PD Monitoring Instrument

In chapter 3 (section 3.6), we have fabricated a monitoring device that can be applied to detect a partial discharge pulse in cable lines. As the cable line is practically long, this monitoring device should be placed as much as possible to get a good detection sensitivity. This would make the cable maintenance become difficult and cost a lot of money.

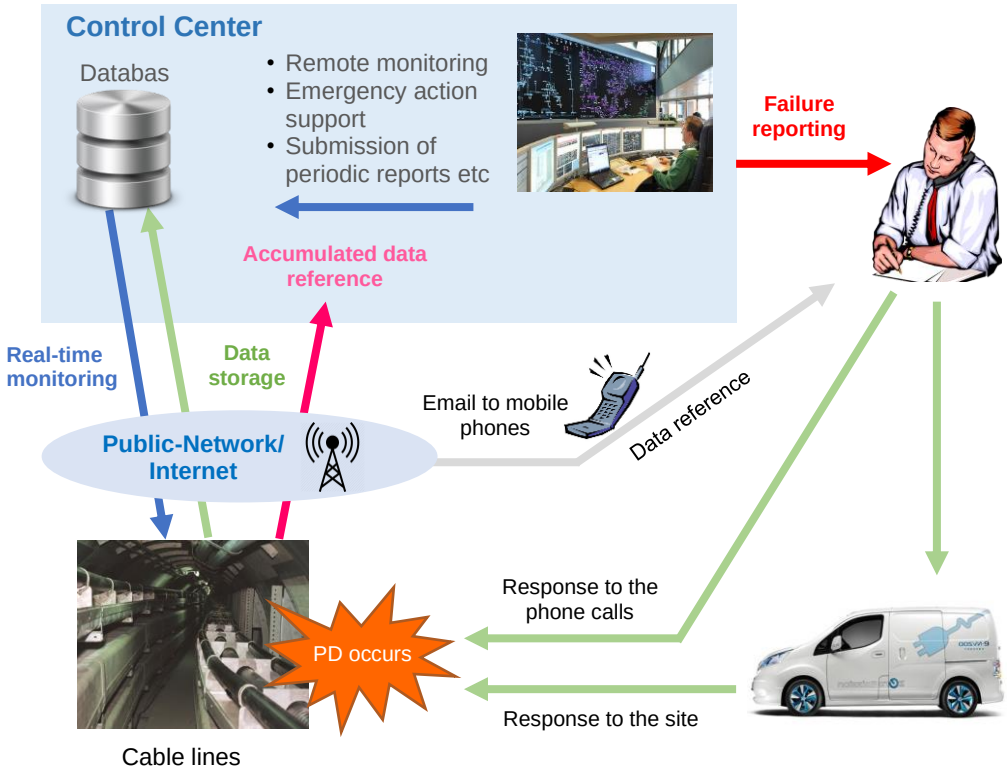

Fig. 5.1 Proposed a remote partial discharge monitoring using internet network.

We propose to develop a remote partial discharge motoring system using an internet network for real-time monitoring. The basic conception of this real-time partial discharge monitoring is shown in Fig. 5.1. The devices will be installed along the cable lines for observing the partial discharge activity. The data collected from each monitoring device is monitored and analyzed in real time by using internet data transfer. When there is a significant partial discharge takes place in the cable line, the power utilities can take a countermeasure if necessary.

5.2.2 Fabrication of Measurement Systems for Water Tree Detection

In chapter 4, we have successfully established a measurement system for water tree detection by employing bias and pulse voltages. However, this measurement system has a low rate voltage (several kilovolts) which cannot be applied for the commercial transmission and distribution cables. In addition, the equipment becomes large and heavy making it difficult for bringing to the site.

In the next phase of study, we aim to fabricate a measurement system that can be applied to a wide range of cable namely 6.6 V class cable, 22 kV class, and 66 kV and 77 kV. The concept of this measurement system is similar to the measurement system of residual charge method (Fig. 5.2). In this particular case, the measurement system should be put in the van so that it can be taken the site easily.

Fig. 5.2 proposed measurement system for water tree detection of a full-size cable equipped in a van [4][5].

References

[1] P. Mulroy, A. Hutado, D. Badezt, "On-line partial discharge monitoring system for distribution network", *IEEE Int. Conf. Cond. Monit. Diagnosis*, pp. 542-545, Sep 2012.

[2] X. He, G. Xie, and Y. Jiang, "Online partial discharge detection and location system using wireless sensor network," *Energy Procedia*, Vol. 12, pp. 420–428, Jan. 2011.

[3] B. A. Lloyd, S. R. Campbell, G. C. Stone, "Continuous On-Line Partial Discharge Monitoring of Generator Stator Windings", *IEEE Trans E.C.*, Vol. 14, pp. 1131-1137, Dec 1999.

[4] T. Tsujimoto, M. Nakade, Y. Yagi, K. Adachi, H. Tanaka, Egasakicho, Tsurumi-ku, Yokohama, Kanagawa, Yawata-kaigandori, Ichihara, Chiba, Higashi-shinagawa, Shinagawa-ku, "Development of ON-SITE Diagnostic for XLPE Cable by Harmonics in AC Loss Current," *Proceedings of the 7th International Conference on Properties and Applications of Dielectric Materiais*, Nagoya, pp 73-76, Jun 2003.

[5] Meiden Engineering, 'Life expectancy diagnsis', Cable deterioration diagnosis [Online].Available: https://www.meidensha.com/mec/service/serv_08/index.html. [Accessed: June. 28, 2019].

Acknowledgements

I would like to take this opportunity to express my profound gratitude and deep regards to my beloved persons for their excellent guidance, monitoring and constant encouragement throughout this thesis without them this thesis could not have been written. It is a great pleasure for me to acknowledge the assistance and contributions of many individuals in making this dissertation a success.

First and foremost, I would like to express my profound gratitude to my enthusiastic supervisor, professor Naohiro Hozumi, who is always to happy and willing to have me solve the confusions and direct me to approach the final result of the thesis. On top of that, professor Hozumi s an easy going and open mined person who is also a good friend to me. Without his encouragement, I would not finish this final work in my PhD degree study.

Secondly, I would like to thank to associate professor Yoshinobu Murakami and assistant professor Tomohiro Kawashima and to all the professors in Toyohashi University of Technology for their ideas, feedback during the process in doing this dissertation.

Special mention goes to Mr. Ryota Yamane, Mr. Shosuke Morita, Mr. Hiroyuki Futami, Ms. Nur Sabihah Binti Mustafa, Mr. Akiyama, Mr. Masahiko Hori, Mr. Edo Bagus Prastika, Mr. Matsui Takuto, Mr. Thein Min Aung, Mr. Totoh Abdul Matin and all the members of Hozumi laboratory who gave a lot of cooperation and helped in carrying out this research.

Furthermore, I would like to show my gratitude to Dr. Norikazu Fuse, Dr. Takashi Kurihara, and Dr. Tsuguhiro Takahashi of Central Research Institute of Electric Power Industry (CRIEPI) for providing an opportunity to conduct an onsite measurement in their institute.

Similar, profound gratitude goes to Ms. Takenaga Chihiro, who has been a genuinely dedicated coordinator of Japan International Cooperation Agency (JICA) program. She is always patient to me out with questions in term of administration and rules.

Lastly, I wish to express my sincere gratitude to my family for their encouragement and moral support during my time in Toyohashi University of Technology.

Publications

Publications related to this thesis

Reviewed articles

1. R. Nhet, N.S. Mustafa, T. Kawashima, Y. Murakami, N. Hozumi, “Partial Discharge Measurement for Power Cable under Different Installation Conditions and Fabrication of Simple Monitoring Device”, AIP Conference Proceedings, Tokyo, Japan, pp.020012-1-020012-8 (2018).

(Chapter 3, Section 3.6-3.7)

2. R. Nhet, N.S. Mustafa, T. Kawashima, Y. Murakami, N. Hozumi “Development of Partial Discharge Measuring Method for Long-Distance Cable Line”, IEEJ Transaction on Fundamentals and Materials, Vol.14, No.7, pp. 996-1001 (2019).

(Chapter 3, Section 3.1-3.3, 3.5)

3. R. Nhet, R. Yamane, H. Futami, T. Kawashima, Y. Murakami, N. Hozumi “Assessment of Charge Behavior in Water Tree Degraded Cables under Pulse Voltages”, IEEJ Transaction on Fundamentals and Materials, Vol.14, No.8, pp. 1126-1132 (2019).

(Chapter 4, Section 4.2-4.7)

International conferences

1. R. Nhet, N.S. Mustafa, H. Futami, T. Kawashima, Y. Murakami, N. Hozumi, T. Takahashi, "Development of the New Partial Discharge Measuring Method and Device for Long Power Cable Using Foil Electrode", 8th International Symposium on Electrical Insulating Materials, Toyohashi, Japan, No.P1-12, pp.347-350 (2017).

(Chapter 3, Section 3.1-3.3, 3.5)

2. R. Nhet, H. Futami, T. Kawashima, Y. Murakami, N. Hozumi, T. Kurihara, T. Okamoto, "Study On Charge Dynamics in Water-Tree XLPE Insulation for Deterioration Diagnosis", 8th International Symposium on Electrical Insulating Materials, Toyohashi, Japan, No.P1-11, pp.343-346 (2017).

(Chapter 4, 4.2-4.3)

3. H. Futami, R. Nhet, T. Kawashima, Y. Murakami, N. Hozumi, T. Kurihara, T. Okamoto, K. Miyajima "Study on short time charge behavior in pulsed residual charge method for water tree diagnostics of XLPE cables," 8th International Symposium on Electrical Insulating Materials, Toyohashi, Japan, No.V2-20, pp.559-562 (2017).

Domestic conferences

1. Binti Mustafa Nur Sabihah，Nhet Ra，二見 啓之，穂積 直裕，「活線状態における電力ケーブル線路の部分放電測定法」, 平成 29 年電気学会全国大会 講演論文集, No.7, pp.161 (2017).

2. Nur Sabihah Binti Mustafa，Nhet Ra，二見啓之，川島朋裕，村上義信，穂積直裕，「箔電極を用いた電力ケーブル線路の活線部分放電測定法」，電気学会研究会資料 誘電･絶縁材料/電線・ケーブル合同研究会，No.DEI-17-088/EWC-17-027 (2017).

3. 二見啓之，Nhet Ra，川島朋裕，村上義信，穂積直裕，栗原隆史，岡本達希，宮島和久，内田克己，「水トリー劣化診断のためのパルス式残留電荷法における短時間電荷挙動の検討」，平成 29 年電気学会全国大会 講演論文集，No.7，pp.164 (2017).

3. 二見啓之，Nhet Ra，森田翔亮，村上義信，穂積直裕，「水トリー劣化ケーブル中の電荷挙動のパルス応答解析」，平成 29 年度電気・電子・情報関係学会東海支部連合大会講演論文集， CD-ROM，No.L3-2 (2017).

5. 二見啓之，Nhet Ra，川島朋裕，村上義信，穂積直裕，「パルス電圧による水トリー劣化ケーブル中の電荷挙動の解析」，電気学会研究会資料 誘電･絶縁材料/電線・ケーブル合同研究会，No.DEI-17-089，EWC-17-028 (2017).

6. 山根涼太，ニアトラ，川島朋裕，村上義信，穂積直裕，「電荷レーダ法における信号発生メカニズムに関する検討」，電気学会研究会資料 誘電･絶縁材料/電線・ケーブル合同研究会，No.DEI-18-085，EWC-18-017 (2018).

Others

1. R. Nhet, T. Kawashima, N. Hozumi, Y. Murakami, U. Khayam, Suwarno “Simulation of Partial Discharge Induced Electromagnetic Wave in Power Transformer”, EPI International Journal of Engineering, Vol.1, No.1, pp. 54-59, Vol.1, No.1, pp.54-59 (2018).

2. T. Kawashima, R. Nhet, Y. Yamashita, Y. Murakami, N. Hozumi, M. Nagao “Nonlinear distortion of AC dissipation current waveform and space charge in EVA film”, IEEJ Transaction on Fundamentals and Materials, Vol.138, No.7, pp. 948-952 (2018).

3. R. Nhet, U. Khayam, "Partial discharge measurement of 4 types of electrodes configuration in air insulation using high frequency current transformer sensor," 2015 Joint International Conference on Electric Vehicular Technology and Industrial, Mechanical, Electrical and Chemical Engineering (ICEVT & IMECE), Surakarta, Indonesia, 4D1-4, pp.100-105 (2015).

4. R. Nhet, U. Khayam, "Measurement of partial discharge in needle-plane electrode using RC detector, HFCT, and antenna sensors," 2015 Joint International Conference on Electric Vehicular Technology and Industrial, Mechanical, Electrical and Chemical Engineering (ICEVT & IMECE), Surakarta, Indonesia, 4D1-5, pp.106-111 (2015).

5. H. Futami, R. Nhet, T. Kawashima, Y. Murakami, N. Hozumi, T. Kurihara, T. Okamoto, K. Miyajima "Study on short time charge behavior in pulsed residual charge method for water tree diagnostics of XLPE cables," 8th International Symposium on Electrical Insulating Materials, Toyohashi, Japan, No.V2-20, pp.559-562 (2017).

I have gained agreements with all of coauthors about using the above thesis to apply for Academic Degree.

Nhet Ra
ニアト ラ